An assessment of the use of the ABSORB bioresorbable vascular scaffold in the treatment of 'false' coronary bifurcations

Rajiv Rampat

A thesis submitted for the degree of Doctor of Medicine to the Brighton and Sussex Medical School

September 2017

Abstract

Introduction

The use of a bioresorbable scaffold has potential advantages when used to treat coronary bifurcation disease. We investigated the influence of sizing strategy on the performance of the ABSORB bioresorbable vascular scaffold (BVS) in this setting. In addition, we evaluated the effect of elective BVS implantation on coronary microvasculature and inflammation. Finally the role of wall shear stress (WSS) in coronary bifurcation disease was reviewed and a novel method for determining WSS with the ABSORB BVS described.

Methods

The ABC-1 trial (Absorb in Bifurcation Coronary study) was a pilot trial which enrolled thirty-eight patients with 'false' coronary bifurcation lesions (Medina X,X,O classification) undergoing elective percutaneous coronary intervention (PCI). Patients were randomised in randomly permutated blocks of varying lengths to receive a BVS based either on the proximal or distal reference vessel diameter. Peripheral arterial blood samples were drawn before the procedure. Optical coherence tomography (OCT) imaging and pressure wire studies were performed before and after BVS implantation. Nine months after the index procedure, seventeen patients returned for blood sampling, intracoronary imaging and physiological assessment. Microvascular resistance was assessed using the Index of Microcirculatory Resistance (IMR). Serum concentrations of IL-6, CRP, sCD40L and MCP-1 were measured before scaffold implantation and at 9 month follow-up using enzyme-linked immunosorbent assays (ELISA). Wall shear stress distribution was calculated in two cases (1 in each randomisation arm) using the principles of Computational Fluid Dynamics (CFD).

Results

37 patients were recruited in the study out of whom 19 were randomised to a proximal sizing strategy and 18 to a distal one. Procedural complication rates were 89.4% and 94.4% respectively (p=0.58). In the distal-sizing arm, there was a greater incidence of significant strut malapposition (defined as a malapposition

distance >300 μm) at the proximal end of the scaffold (2.3% versus 0.8%, p=0.023). The incidence of distal edge dissections was numerically greater in the proximal-sizing group but was not statistically significant (31.3% vs 11.8%, p=0.17). At follow up, there were fewer uncovered struts (1.1% v 7.2%, p=0.001) in the distal cohort.

PCI was accompanied by an immediate reduction in IMR of 8.6 (p=0.02). Mean CFR improved by 0.9 from pre to postprocedural levels (p=0.02). At follow up, FFR remained significant lower compared to pre-procedural values (0.92 v 0.78, p=0.001). In contrast, there was no significant improvement in CFR or IMR at follow up compared to preprocedural values (p=0.58 and p=0.30 respectively).

The changes in the median levels of inflammatory markers from baseline to follow up were as follows: CRP (1 to 2.1, p=0.53), IL-6 (1.1 to 1, p=0.81), MCP-1 (47.2 to 36.4, p=0.06) and sCD40L (82.6 to 80.6, p=0.53). The Spearman correlation coefficients between baseline marker levels and neoinitimal burden along with the corresponding p value were as follows: CRP (0.30, p=0.34); IL-6 (0.49, p=0.10), MCP-1 (-0.22, p=0.48); sCD40L (0, p=0.99). Similarly, the coefficients and p values between follow up levels and neointimal burden were as follows: CRP (0.41, p=0.19); IL-6 (0.52, p=0.08), MCP-1 (-0.77, p=0.81); sCD40L (-0.06, p=0.86).

Conclusion

The provisional approach with a modified ‘PSP’ strategy is safe and feasible when using the ABSORB BVS in bifurcations. Both proximal and distal sizing strategies have similar procedural complication rates. While a proximal sizing strategy is associated with less significant malapposition immediately after implantation, there are fewer uncovered struts with a distal sizing strategy at medium term follow up. Scaffold implantation does not appear to adversely affect the coronary microcirculation. Levels of preprocedural inflammatory mediators did not correlate with the amount of neointimal coverage detected on OCT at 9 months. In addition, there was no significant change between baseline and follow up levels of inflammatory biomarkers after elective BVS implantation.. Finally, computational flow modelling can be used to assess the haemodynamic impact of different bifurcation stenting strategies with the ABSORB BVS.

Contents

List of tables

List of figures

List of abbreviations

3-D:	Three-dimensional
ABC-1:	Absorb bifurcation coronary study
ACC:	American college of cardiology
ACS:	Acute coronary syndrome
ACT:	Activated clotting time
AHA:	American heart association
ARC:	Academic research consortium
BMI:	Body mass index
BMS:	Bare metal stent
BSUH:	Brighton and Sussex University Hospitals
BVS:	Bioresorbable vascular scaffold
CABG:	Coronary artery bypass grafting
CAD:	Coronary artery disease
CCR:	CC chemokine receptor
CCS:	Canadian cardiovascular society
CD:	Clusters of differentiation
CFD:	Computational fluid dynamics
CFR:	Coronary flow reserve
CRF:	Case report form
CRP:	C reactive protein
CT:	Computerised tomography scan
CTO:	Chronic total occlusion
D1:	First diagonal artery
DAPT:	Dual antiplatelet treatment
DES:	Drug eluting stent
DS:	Diameter stenosis
EBC:	European Bifurcation Club
EC:	Endothelial cell
ECG:	Electrocardiogram
ECM:	Extracellular matrix
eGFR:	Estimated glomerular filtration rate
EI:	Eccentricity Index
ELISA:	Enzyme-linked immunosorbent assay
ESC:	European Society of Cardiology

FFR:	Fractional flow reserve
FGF:	Fibroblast growth factor
FIM:	First in man
FKBI:	Final kissing balloon inflation
Fup:	Follow up
GP:	General practitioner
HRA:	Health research authority
IL:	Interleukin
IMR:	Index of microcirculatory resistance
ISA:	Incomplete strut apposition
ISR:	In stent/scaffold restenosis
IV:	Intravenous
IVUS:	Intravascular ultrasound
LAD:	Left anterior descending artery
LAISA:	Late acquired incomplete strut apposition
LBBB:	Left bundle branch block
LCx:	Left circumflex artery
LDL:	Low density lipoprotein
LMS:	Left main stem
LVEF:	Left ventricular ejection fraction
MACE:	Major adverse cardiac event
MCP:	Monocyte chemotactic protein
MeLA:	Mean luminal area
MeLD:	Mean luminal diameter
MI:	Myocardial infarction
MLA:	Minimum luminal area
MLD:	Minimum luminal diameter
MMP:	Matrix metalloproteinase
MRI:	Magnetic Resonance Imaging
MV:	Main vessel
NASB:	Non apposed side branch strut
NC:	Non compliant
NIA:	Neointimal area
NIT:	Neointimal thickness
OCT:	Optical coherence tomography
Pa:	Aortic pressure
PAI:	Plasminogen Activator Inhibitor

PCI: Percutaneous coronary intervention

Pd: Coronary distal pressure

PDLLA: Poly-D-L-lactide polymer

PDGF: Platelet derived growth factor

PLLA: Poly-L-lactide polymer

PMI: Periprocedural myocardial infarction

POBA: Plain old balloon angioplasty

POT: Proximal optimisation technique

PS: Provisional strategy

PTCA: Percutaneous transluminal coronary angioplasty

Pv: Coronary venous pressure

PVD: Peripheral vascular disease

Pw: Coronary wedge pressure

QCA: Quantitative coronary angiography

RCA: Right coronary artery

RCT: Randomised controlled trial

REC: Research ethics committee

RVD: Reference vessel diameter

SA: Scaffold area

SAE: Serious adverse event

SB: Side branch

SBO: Side branch occlusion

ST: Scaffold thrombosis

STEMI: ST-elevation myocardial infarction

TAWSS: Time averaged wall shear stress

TIA: Transient ischaemic attack

TLR: Target lesion revascularisation

TGF: Transforming growth factor

TIMI: Thrombolysis in myocardial infarction

Tmn: Mean transit time

TNF: Tumour necrosis factor

TV-MI: Target vessel myocardial infarction

TVR: Target vessel revascularisation

VLST: Very late scaffold thrombosis

VSMC: Vascular smooth muscle cell

WBC: White blood cell

WSS: Wall shear stress

Acknowledgements

I would like to thank my supervisors, Dr James Cockburn and Professor Hildick-Smith for their invaluable support and guidance throughout the course of this project. Their ability to pursue both their extensive clinical and research interests while maintaining a fantastic sense of humour is a source of inspiration.

I am extremely grateful to all the people who helped me with this project over the past two years: Susanna Migliori, Dr Claudio Chiastra and Prof. Gabriele Dubini from Polictecnico di Milano for their contribution to the computational flow modelling aspect of this project; Dr Stephen Bremner for his advice on statistics; Dr William Wilkinson for allowing me to sit in on his lectures on vector calculus; Prof. Sergei Sazhin and Dr Andreas Papoutsakis for allowing me to attend their lectures on Computational Fluid Dynamics; Prof. Kevin Davies for his academic support; Prof. Pietro Ghezzi, for his advice on the chapter on inflammation and Dr Manuela Mengozzi for her kind patience when teaching me how to perform ELISA tests.

I would like to acknowledge the patients who firstly took part in this study and then kindly gave up their time to return for a follow up coronary angiogram. This study was performed in the cardiac catheterisation laboratory at Royal Sussex County Hospital, Brighton. I would like to extend my thanks to all the lab staff who were involved in the study. I am also heavily indebted to the research staff in the Clinical and Investigations Research Unit at RSCH for their help in the practicalities of running a trial.

I would also like to thank my parents whose sacrifices throughout my life have put me where I am today.

Finally, my deepest gratitude goes to my wife, Radhika, who single-handedly looked after our two young children, Aryana and Rohan, while pursuing her ophthalmology training in London during the weekdays when I stayed over in Brighton. Her unwavering support is the reason why this thesis is complete today.

Declaration

I declare that the research contained in this thesis, unless otherwise formally indicated within the text, is the original work of the author. The thesis has not been previously submitted to this or any other university for a degree, and does not incorporate any material already submitted for a degree

Rajiv Rampat

September 2017

1 Introduction

1.1 Percutaneous coronary intervention

1.1.1 Evolution of PCI

Coronary artery disease is the leading cause of mortality and morbidity in the western world[1]. Percutaneous treatment of coronary stenosis was pioneered by Andreas Gruntzig back in 1977 when he performed the first coronary balloon angioplasty also known nowadays as 'plain old balloon angioplasty or POBA[2]. This mode of treatment was rapidly embraced by cardiologists worldwide and spawned the field of interventional cardiology. While POBA treatment revolutionised the treatment of coronary atherosclerosis, early studies showed that occlusive dissections and elastic recoil of the coronary artery occurred in proportion of patients sometimes with fatal consequences[3]. An endoluminal prosthesis was needed to firstly treat the iatrogenic dissections and secondly to provide sufficient radial force to prevent elastic recoil of the arterial wall. This led to the second revolution in the interventional field namely the introduction of bare metal stents (BMS). The first-in-human coronary stent was implanted in 1986[4]. At first, it seemed that splinting of the artery with a metal cage addressed the shortcomings of balloon angioplasty. However a new problem soon arose in the form of excessive neointimal proliferation causing restenosis. The degree of tissue growth caused by the body's reaction to the metal stent was in fact higher than the one induced by barotrauma from POBA[5]. This provided the impetus for the third revolution namely the creation of drug eluting stents (DES). Antiproliferative agents were added to the metal platforms with the aim of inhibiting tissue growth within the stent. In 2001, the results of the First In Man (FIM) study confirmed the anti-restenotic efficacy of sirolimus eluting stents with no angiographic restenosis or major adverse events present at 1 year[6]. The dramatic reduction in restenosis rates with DES led to the global adoption of this technology and it remains to this day the standard of care for the percutaneous treatment of coronary disease[7]. But interfering with vessel healing came at a price. At the European Society of Cardiology (ESC) meeting in 2006, a late increase in mortality was reported with DES[8]. Late stent thrombosis occurs in a small subset of patients due to several factors including presumed delayed re-endothelialisation caused by the antiproliferative drugs[9]. Several iterations of DES including the use

of thinner struts[10] have since reduced complication rates but the issue of restenosis and thrombosis are still problematic.

1.1.2 Bioresorbable technology

In parallel with the evolution of metal stents, another therapeutic concept known as vascular restoration therapy has been developing. The aim of this treatment modality is simple – to allow the vessel to return to its native state once the need for arterial support expires. Data from the balloon angioplasty era suggests that the lumen stabilises around 3 months after intervention[11] though there is still no consensus on the exact duration of mechanical support required. A device that provides support when required and disappears thereafter is a particularly tantalising option with many theoretical advantages. Complete resorption of a stent would allow for repeat percutaneous intervention without the need to overload the artery with multiple layers of metal. It would also permit future surgical grafting of the artery if required. With no permanent implant in situ, the length of antiplatelet treatment could potentially be curtailed, thus reducing bleeding risk.

The first coronary biodegradable scaffold to be tested in an animal model was implanted in the early 1980s[12]. Radial strength was maintained for the first month after implant and biodegradation was complete by 9 months. However concerns about radial strength loss, biocompatibility of the degradation products and swelling of the stent due to diffusion of water into it, hampered its development. The first fully degradable human coronary stent (Igaki-Tamai) was implanted in 1998[13]. It was made of poly-L-lactic acid and had restenosis rates comparable to contemporary bare metal stents. Widespread use was hampered by the concerns about the mode of deployment. The stent required a thermal balloon for the PLLA to self-expand. This was concerning in the light of experimental evidence that high temperatures within an artery could induce arterial wall necrosis, exaggerate the neointimal response and increase platelet adhesion resulting in higher thrombosis rates[12]. While a higher rate of stent thrombosis was not observed in clinical practice, it was enough to discourage widespread acceptance of this stent. Other materials have been investigated. The first metallic bioabsorbable stent was a magnesium alloy stent which was completed degraded over only 2 months[14].

However, radial support was lost much earlier. Thus, the stent was unable to counteract negative remodelling of the artery. Similar to bare metal stents, it did not contain an antiproliferative agent. The above factors resulted in a restenosis rate of almost 50% at 4 months. The REVA device was a poly-carbonate scaffold with no antiproliferative drug coating. The resorption process of the carbonate polymer imparted good radial support for the first 3 months without significant vessel shrinkage. However, the device was prone to focal mechanical issues such as polymer embrittlement which led to an excessively high TLR of 66.7% by 6 months[15].

The high iterative revascularisation rates of these earlier 'bare' devices shifted the focus to the development of a drug-eluting bioresorbable stent. The ABSORB bioresorbable vascular scaffold (BVS) is coated with everolimus as the anti-proliferative agent and is the first of this line of devices to obtain Conformité Européene (CE) mark approval. It was first implanted in Auckland in 2006[16]. The initial version (BVS 1.0) of the scaffold consisted of out of phase hoops joined together at the site of the straight connectors. The device had to be kept refrigerated below -20 degrees to maintain polymer stability. The BVS 1.0 was evaluated in the ABSORB Cohort A study which enrolled 30 patients[17]. It showed a late luminal loss of 0.44mm at 6 months which was comparable to DES. However acute and late recoil were higher suggesting that the polymer strength was inferior to contemporary DES. This led to the iteration in design aimed at improving the mechanical support provided by the platform. The second version (BVS 1.1) was evaluated in the ABSORB Cohort B study comprising 101 patients. Patients underwent serial invasive imaging at various time points over a 5 year period. The device showed outcomes comparable with metal stents with low incidence of restenosis and adverse cardiac event[18]. There were no cases of scaffold thrombosis. However it needs to be pointed out that the scaffold was used in relatively simple lesions in the ABSORB B study. Promising results in early phase studies do not necessarily guarantee success in a real world setting especially with more complex lesion subsets. This was indeed the case with the early generation drug-eluting stents. The pivotal RAVEL study[19], which evaluated the first generation Cypher DES in relatively low risk lesions, did not have any

cases of stent thrombosis but subsequent trials revealed a higher rate of very late ST compared to BMS[20].

Nonetheless, the encouraging results of ABSORB B paved the way for an extensive clinical programme with both industry sponsored and independent investigator led studies. To date, the ABSORB BVS has been studied in more than 24,000 patients.

1.2 The ABSORB BVS

1.2.1 Material

The ABSORB bioresorbable vascular scaffold consists of a semi-crystalline poly-L-lactide (PLLA) backbone and an amorphous coating made up of a 1:1 mixture of poly-D,L-lactide polymer (PDLLA) and 100 μg/cm^2 of the antiproliferative drug everolimus[21]. The scaffold is composed of in phase sinusoidal hoops linked to each other by thinner straight connectors (Figure 1). It has a crossing profile of 1.4mm and a lower radial strength compared to metal. The weaker mechanical property of the scaffold is compensated by having thicker struts. With a thickness of 157μm, they are almost twice the size of contemporary drug eluting stents. The scaffold is radiolucent. The tip of each end has radiopaque markers in order to allow visualisation during fluoroscopy and those markers are the only remnant of scaffolding after completion of bioresorption. Elution of the everolimus is controlled by the PDLLA coating with 80% of the drug being released within the first 30 days. The pharmacokinetics of the antiproliferative drug is similar to that of the Xience V drug eluting stent.

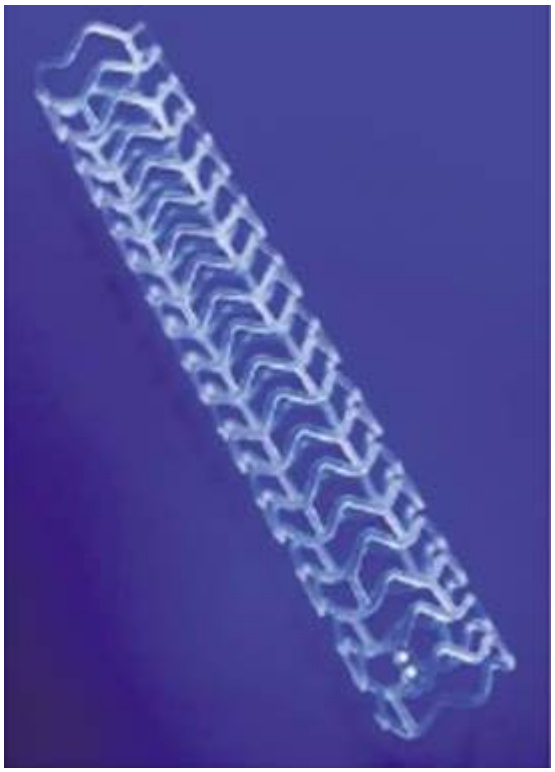

Figure 1: Image of the ABSORB BVS 3.0x18mm scaffold (Reproduced from Oberhauser et al.)[22]

1.2.2 Kinetics of bioresorption

The polylactide polymer degrades by hydrolysis (Figure 2). During this process, the polylactide ester bonds are cleaved by water molecules as shown in the diagram below. The degradation happens over three phases[22]. First water molecules diffuse into the scaffold and start hydrolysing the less dense amorphous regions of the polymer. This causes the polymer to lose weight but not strength as the tie chains which determine radial strength are essentially intact. In the second phase, hydrolysis extends to the amorphous tie chains binding the crystalline structure and at this point, the device begins to lose radial strength. Structural discontinuities start appearing at this stage. In the third and final phase, extensive hydrolysis results in monomer subunits and isomers of lactic acid. These hydrophilic components are able to diffuse out of the scaffold. Phagocytosis by macrophages and enzymatic degradation via the Kreb's cycle completes the resorption process. The final products are carbon dioxide and water which are excreted through the lungs and kidneys. The interior of the scaffold is replaced by a matrix of cellular infiltrate and proteoglycan.

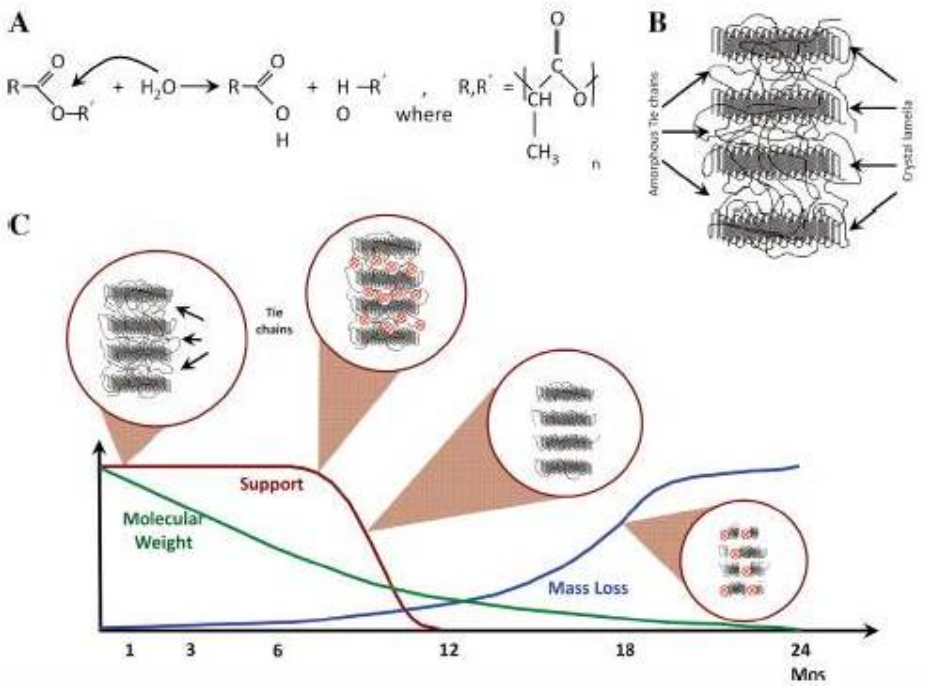

Figure 2: Resorption process of the ABSORB BVS. A - Reaction equation demonstrating hydrolysis of ester bonds during bioresorption. B - Structure of polylactide polymer with crystalline lamellae linked by amorphous tie chains. C - Change in structural and mechanical properties of the ABSORB scaffold with bioresorption (Reproduced from Onuma et al.)[23]

1.2.3 Technique of implantation

Over the recent years, it has become apparent that correct implantation technique is pivotal to reduce complication rates with the ABSORB BVS. Adequate lesion preparation is needed because the weaker BVS skeleton can be damaged by recalcitrant fibrocalcific lesions or be underexpanded due to the opposing forces from the vessel wall. Post dilatation is needed because the struts are thick and thus need to be firmly embedded so as not disturb blood flow and create a pro-thrombotic environment. Early registries had suboptimal deployment techniques with higher complication rates[24,25]. The later registries such as the ABSORB UK reflected the lessons learnt from those registries[26]. Technical aspects of implantation were refined with the recognition of the importance of adequate lesion preparation, post dilatation and use of intravascular imaging. This has led to the development of a BVS specific implantation protocol dubbed PSP[27]. The three critical components of implantation are identified by the 3 letters: **P** stands for **P**redilatation with a NC balloon with a 1:1 balloon: vessel ratio, **S** implies careful

Sizing of the vessel preferably with intravascular imaging and the final **P** stands for **P**ostdilatation with a NC balloon to high pressure (>18atm) while staying within the expansion limits of the scaffold. Whether the same principle can be extended to bifurcation lesions is unknown.

1.3 Bifurcation disease

1.3.1 Overview

A coronary bifurcation lesion is defined as one occurring at or next to a significant branch of an epicardial artery. The pattern of disease is commonly described using the Medina classification[28]. In brief, the Medina classification comprises of a set of 3 numbers, each containing either a 0 or 1 (0: no disease, 1: disease present). The first number refers to the proximal segment of the main vessel, the second number to the distal segment of the main vessel and the third number to the side branch. For example, a patient with Medina type 1,1,0 has disease in the proximal and distal segment of the main vessel but not in the side branch. Bifurcation lesions of Medina type x,x,0 (where x can be 0 or 1) are also known as 'false' bifurcations since the side branch is not diseased.

Coronary bifurcations are involved in approximately 15% of percutaneous coronary interventions[29]. A large variety of bifurcation stenting techniques have been described in the literature and include single stent strategy (provisional T stenting[30],) or two stent strategies (e.g Culotte stenting[31], DK-Crush technique[32] amongst others). The provisional T stenting strategy involves placing a stent in the main vessel across the side branch and treating the side branch only if flow is compromised or there is severe stenosis. Stent deployment in the mother vessel is followed by the proximal optimisation technique (POT). This involves inflating a shorter and bigger balloon proximal to the carina. POT restores the original anatomical configuration of the bifurcation[33] and addresses the issue of underdeployment of the proximal part of the stent. The provisional approach is the technique of choice when treating main vessel disease in the absence of significant disease in the side branch also known as 'false' bifurcations. With regards to two-stent techniques, the MADS classification proposed by the EBC

provides a systematic way of organising the myriad techniques described in the literature[34].

Despite the relatively high frequency of bifurcation lesions, bifurcation stenting is associated with lower procedural success rates and worse clinical outcome compared to non-bifurcation PCI[35]. The optimal treatment of bifurcations remains controversial. Several trials have investigated the different percutaneous treatment options but variation in endpoints and the plethora of stenting techniques available, including dedicated bifurcation stents, makes comparison quite difficult. Part of the problem also resides in the diversity of bifurcation anatomy which precludes a unique therapeutic solution. Nonetheless, the results of several published meta-analysis show that a single stent strategy is generally preferable over dual-stenting[36,37]. However it is important to note that several of theses trials have included 'false' bifurcations and side branches <2.50mm both of which may favour a single stent strategy.

1.3.2 Use of the ABSORB BVS in bifurcations

There are theoretical advantages to using a resorbable scaffold over a metallic one in treating bifurcations. Permanent jailing of the side branch, i.e leaving a meshwork of metal struts across the orifice of the side branch, could potentially be avoided. Restoration of the vessel structure after strut resorption could lead to a physiologically favourable haemodynamic environment thereby reducing the risk of restenosis. However, there are challenges unique to the design of the ABSORB BVS when applied to the treatment of coronary bifurcations. Firstly, the lactic acid polymer is not as robust as stainless steel or Cobalt Chromium stents. Aggressive balloon dilatations, which are typically well tolerated in metallic platforms, can potentially lead to device fracture. Secondly, the scaffold is bulkier than contemporary drug eluting stent (DES) with a strut thickness of 157 micrometres. While the thickness provides sufficient radial support to prevent recoil, this could be problematic if more than 1 scaffold is utilised in an overlapping manner for complex bifurcation treatment strategies. Notwithstanding the technical challenges of a two scaffold strategy with thicker struts, there is a possibility of obstructive coronary flow disruption and haemodynamic impairment. So far, trials involving bioresorbable vascular scaffolds (BVS) have

excluded patients with significant bifurcation disease. Our current knowledge in this subgroup of coronary lesions rests on bench studies, case reports and registries.

Bench studies

The ABSORB scaffold consists of sinusoidal hoops each individually linked by three longitudinal connectors. The calculated circular diameter of a cell is 3.0mm in the 2.5/3mm BVS and 3.6mm in the 3.5mm scaffold. Ormiston et al. investigated the effect of different bifurcation techniques on the degree of stent distortion[38]. SB dilatation was performed using balloons of increasing size (2.0, 2.5,3mm) in both 3.0 and 3.5mm BVS. Rupture of hoop and connector were observed in 14% of cases with the 2.5mm and 3mm balloons inflated to 14atm while none was observed with the 2mm balloon. The fractures were confined to single cells and did not cause malapposition of the scaffold. In contrast, a lower pressure of 10 atm in the larger 3.0mm NC balloon did not cause strut fracture. When mini-Final Kissing Balloon Dilatation (mini-FKBD) was performed using two 3.0mm NC balloons in a 3.0mm scaffold, fractures occurred beyond an inflation pressure of 5atm. The degree of stent distortion was similar to those induced in metallic stents and was worse with shallower bifurcation angles as well as larger balloons.

Dzavik et al. analysed the effects of different bifurcation treatment strategies in phantom models[39]. Scanning electron microscopy and Micro CT was used to visualize the stents following the application of provisional stenting with final kissing balloon inflation (FKBI), modified T stent with FKBI, crush and culotte techniques in a total of 8 models. The main branch was 3.0mm in diameter while the side branch was 2.5mm. In the provisional stenting strategy, FKBI to 8 atmospheres did not cause significant stent distortion. On the other hand, FKBI in the modified T stenting technique to 10 atmospheres resulted in disruption of the BVS ring at the level the side branch. The more complex two-stent strategies were associated with some degree of malapposition. The study suggests that single stent procedures coupled with SB balloon dilatation optimally opens the SB without compromising the stent architecture. In a two-stent strategy, the T stent with small

protrusion technique appears to be the technique of choice offering the least distortion of struts while ensuring good coverage of the ostium of the SB.

The bench tests essentially demonstrate that current BVS do not tolerate post dilatation beyond a fairly conservative limit. This is in stark contrast with our experience with metal stents. The combination of balloon size and pressure is important but it seems that expansion with low big balloons at low pressure is relatively safer than small balloons at higher pressure. Bifurcation angle is also an important factor with shallower angles faring worse with aggressive balloon dilatation. It is important for the interventionalist to fully understand the expansion limits of BVS before making the decision to use them in bifurcation treatment

Registry data

Several units have reported either their single centre experience or published their data pooled with a few other centres (Table 1). The provisional strategy (PS) is the most commonly used technique in all studies. MACE rates vary from 2.8% to 16.1% at 1 year. This is similar to published data on the use of metal stents in bifurcation disease[40]. Scaffold thrombosis (ST) rates range between 1.1% and 2.5% at 1 year which are again comparable to metal stents in bifurcation treatment. It is worth highlighting some of the limitations when comparing data from such a heterogeneous group. There exists a wide variation in the diameters of side branches in these studies. Follow up periods are not standardized and most studies report only early to mid-term follow up. This is particularly pertinent with regards to ST given the reports of very late scaffold thrombosis (VLST) published in the literature[41] and thus, careful follow-up long term is crucial. Randomised trial data on the use of the ABSORB BVS in bifurcations is currently lacking.

Study	n	PS (%)	Fup	Major adverse events (%)	TLR (%)	ST (%)
Kawamoto et al.[42]	122	81.1	1 yr	All death, MI, TVR: 10.5	10	1.1
De Paolis et al.[43]	107	93.4	1 yr	Cardiac death, MI, TVR: 5.5	3.3	2.2

DeLezo et al.[44]	194	96	14 mths	All death, MI, TLR: 8.7	5.6	1.3
Wiebe et al.[45]	28	81.5	1 yr	Cardiac death, MI, TLR: 16.1	12.1	8.1
Naganuma et al.[46]	302	86	1 yr	Cardiac death, TV-MI, TLR : 9.0	5.7	2.5
Tanaka et al.[47]	42	0	2 yr	All death, MI, TVR: 20.9	14	0
Poznan registry[48]	121	92	1 yr	Cardiac death, TV-MI, TVR 2.8	0.9	1.9
GHOST Ferrarotto registry[49]	71	76.1	776 days (median)	All death, any MI, any revasc: 13.5	8.6	1.4

n- Number of patients; Fup- follow up; PS- Provisional strategy; MI- Myocardial infarction; TVR- Target vessel revascularisation; TLR – Target lesion revascularisation; TV-MI- Target vessel myocardial infarction; ST- Scaffold thrombosis; revasc- revascularisation

Table 1: Outcome of studies of BVS in coronary bifurcations

1.3.3 Sizing issue in bifurcation PCI

The diameter of a coronary artery does not gradually taper as it courses down the heart[50]. Instead it has a relatively constant diameter in between bifurcations. At each branch, there is a discrete reduction in size depending on the size of the side branch. A number of models that describe the mathematical relationship between the size of the proximal main vessel (MV) and its daughter vessels have been described. Murray's law is one commonly used model and is stated below[51].

$$(\text{Proximal MV diameter})^3 = (\text{Distal MV diameter})^3 + (\text{SB diameter})^3$$

This law was proposed nearly 90 years ago and is based on the principle of minimum energy. It assumes laminar flow and a constant wall shear stress within the bifurcation.

Another model which is based on fractal geometry is Finet's formula, shown below[52]:

$$\text{Proximal MV diameter} = 0.678 \times (\text{Distal MV diameter} + \text{SB diameter})$$

As is apparent from the above equations, there can be a marked discrepancy between the proximal and distal main vessel diameters if the side branch is large.

This poses the problem of selecting an appropriate stent size that can effectively treat two segments of differing diameters. Choosing a stent diameter commensurate with the proximal diameter can cause overexpansion of the distal vessel. This can result in carina shift leading to compromise of flow in the SB as well as dissection of the smaller distal segment[53]. Conversely, if a smaller stent is chosen based on the distal diameter, there is a risk of the stent being malapposed in the proximal segment. This risk is higher when the difference between the proximal and distal diameters is large i.e. when the side branch is large. In essence, when deciding on the choice of scaffold size, the risk of malappostion with underdeployment needs to be carefully balanced against the risk of scaffold fracture/ vessel dissection with overdeployment

With metal stents, the European Bifurcation Club (EBC) recommends that the size of the stent is based on the distal reference diameter[54]. The Proximal Optimisation Technique (POT) or Final Kissing Balloon Inflation (FKBI) can be used to ensure good apposition proximally. This strategy has its limitations when applied to the ABSORB BVS. The expansion characteristics of the scaffold restrict the extent to which the proximal end can be safely postdilated. The manufacturers of the ABSORB BVS generally advise using a balloon size no greater than 0.5mm of the scaffold diameter for post dilatation. Overexpansion beyond this limit can adversely affect the mechanical properties of the scaffold even in the absence of overt fractures. Another strategy that can be considered is deploying a larger BVS based on the proximal reference diameter at low pressure[38] (Figure 3). In theory, this would ensure good apposition proximally but the larger scaffold runs the risk of damaging the vessel distally. Which of the two strategies is more favourable with BVS is currently unknown.

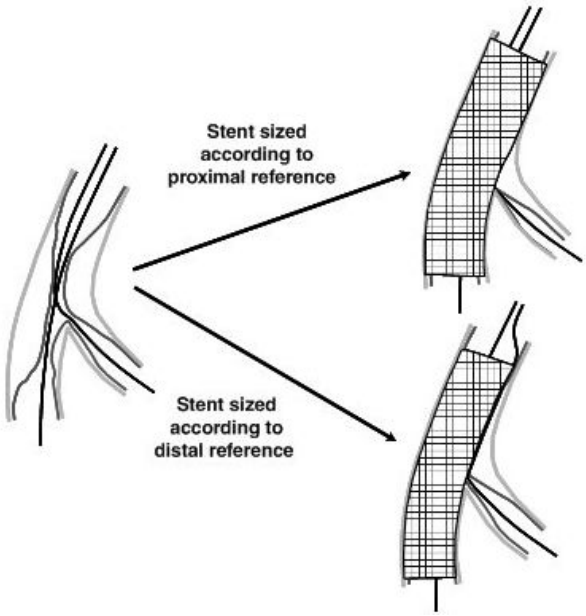

Figure 3: Schematic representation of two sizing strategies in coronary bifurcation PCI. When a stent size is chosen according to the proximal reference, the stent is well apposed at the proximal bifurcation segment but can lead to overexpansion of the distal segment. Conversely, choosing a stent based on the distal reference vessel limits distal vessel damage but can lead to proximal malapposition. (Reproduced from Bifurcation stenting)[55]

1.4 Inflammation and neointimal response after PCI

1.4.1 Healing process after PCI

In order to assess the role of inflammation in neointimal growth, it is important to have an understanding of the vascular response to arterial wall injury. The introduction of a foreign device within an artery initiates a complex cascade of physiological processes aimed at eliminating damaged cells and repairing the vessel. Vessel healing following percutaneous intervention can be divided into three steps[56-58] (Figure 4):

- Early phase of thrombus formation and inflammation.
- Intermediate phase of granulation tissue formation with smooth muscle cell migration.
- Late phase of vascular remodelling

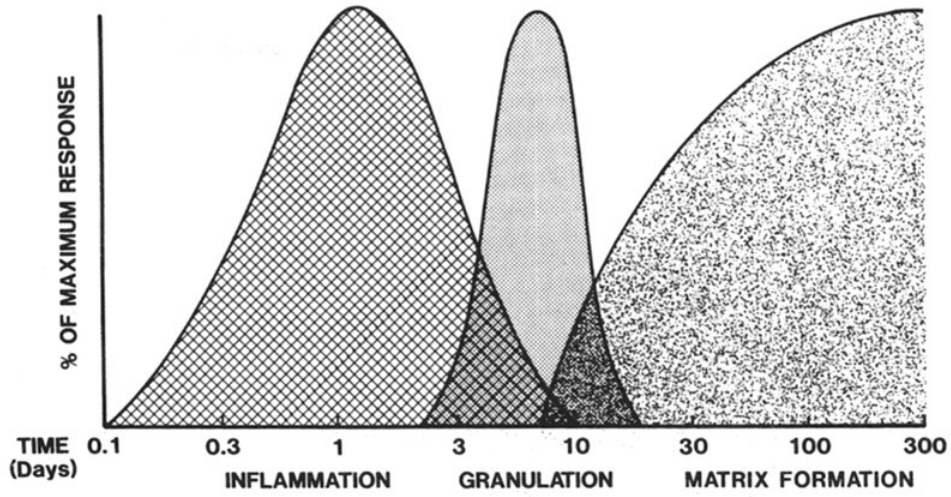

Figure 4: The three phases of wound healing after arterial injury: 1) Inflammatory phase begins at instant of injury and predominant features include platelet aggregation, deposit of fibronectin extracellular matrix and infiltration of inflammatory cells 2) Granulation phase typically lasts for 1 to 2 weeks and consists of migration and proliferation of mesenchymal cells to the wound site 3) Matrix remodelling phase persists for months consisting of proteoglycan deposition, followed by conversion of extracellular matrix to collagen and elastin. (Reproduced from Forrester et al.)[56]

Early phase: Balloon inflation and stent deployment injures the inner luminal wall thereby exposing the subendothelial matrix to blood constituents. This initiates an immediate thrombotic response mediated by platelets and coagulation factors. Platelets adhere to the damaged surface and are activated by the exposed collagen from the underlying matrix. Concomitant activation of the coagulation cascade generates fibrin strands which bind to aggregated platelets to form a dense meshwork. The result is a thin layer of thrombus that prevents further exposure of blood to the damaged wall. This thrombotic effect is tempered by antiplatelet therapy. The generation of thrombus is followed by an inflammatory reaction. Activated platelets release a wide variety of cytokines and express adhesive glycoproteins such as CD40 ligand, all of which initiate and sustain inflammation. Leucocytes are recruited to the site of injury through chemokine signalling. Monocyte chemoattractant protein-1 (MCP-1) is an example of a chemotactic factor secreted during this stage. The initial tethering and rolling of the leucocytes onto the thrombotic layer occurs through ligand-receptor interaction between glycoproteins on white blood cells (WBC) and p-selectin on the cell membrane of activated platelets and undamaged endothelial cells.

Leucocyte 'arrest' is mediated in a similar manner involving cell surface integrins. Transmigration across the platelet-fibrin layer and diapedesis into the tissue wall is driven by chemical gradients of cytokines. Activated monocytes and macrophages sustain the inflammatory process through the release of more cytokines and chemokines such as Interleukin-6 (IL-6). This is aimed at repairing the injured vessel. Within the first 24hrs, there is also systemic response to coronary inflammation. Local release of inflammatory cytokines such as IL-6 and TNF-α trigger an acute-phase response causing liver cells to release reactants such as C Reactive Protein (CRP). These substances amplify the local inflammatory process.

Intermediate phase: In this stage, endothelial cells proliferate over the wounded area while the initial thrombotic layer is gradually replaced by granulation tissue by vascular smooth muscle cells (VSMC) and macrophages.. The processes involved in this stage include phenotypic transformation and migration of VSMC followed by deposition of extracellular matrix (ECM). Activation of VSMC by growth factors/cytokines causes them to switch from their usual resting contractile phenotype to a proliferative synthetic one. Unlike the elongated shapes usually attributed to muscle cells, the latter cells are more rounded and have the ability to synthesise collagen and elastin. The release of potent mitogens such as platelet derived growth factor (PDGF) by activated platelets and macrophages stimulates both the migration and proliferation of VSMC from the media and adventia into the intimal layer. This process is also influenced by mechanical factors such as wall stress generated by the compressive forces exerted by the stent on the wall and wall shear stress (WSS) resulting from blood flow within the stented artery. An extracellular matrix composed of large molecules such as fibrin, fibrinogen and fibronectin is initially deposited by VSMC. These provide structural support to surrounding cells to begin the repair process. VSMC then secrete hyaluronan and proteoglycans to stabilise the provisional matrix. Damaged cells are cleared by macrophages.

Late phase: In this phase, remodelling of the granulation tissue by matrix metalloproteinases (MMP) occurs. Inflammatory cells, mobilised within the region, secrete an array of matrix metalloproteineases that break down hyaluronan and allow the deposit of type I and III collagen fibres. Collagen inhibits further

smooth muscle proliferation completing the healing process. In the balloon angioplasty era, this phase was responsible for constrictive remodelling and vessel shrinkage.

Re-endothelialisation occurs in parallel with the reparative process. Reparative stem cells from the bone marrow (CD34+) are mobilised. These travel to the site of vessel injury and can differentiate into either endothelial progenitor cells or smooth muscle progenitor cells. This is mediated by the release of inflammatory and hematopoietic cytokines such as granulocyte colony stimulating factor. Data from necropsy studies show that coverage of the neointima with endothelial cells is complete several weeks after implantation of BMS. The addition of antiproliferative drugs within drug eluting devices alters the vascular response. Histopathological analysis of restenotic tissue in DES demonstrates that there is a greater amount of old thrombus and fibrin with reduced endothelialisation compared to BMS. The cellular composition varies from a predominant T lymphocyte rich infiltrate to the more characteristic BMS composition of ECM and VSMC-rich tissue[59].

1.4.2 Healing process after ABSORB BVS implantation

The histological characteristics of the vessel wall following ABSORB BVS implantation have been studied in preclinical models[60]. During the resorption process, the polymer progressively breaks down and is replaced by a complex of proteoglycans. This is followed by integration of the device into the vessel structure – a process during which organised tissue replaces the polymeric and proteoglycan material. The polymer coating and backbone are absorbed by 9 months and 2-3 years respectively. While the vast majority of struts are still identifiable on optical coherence tomography (OCT) at 2 years, most of the polymer has been replaced with a proteoglycan complex by that time. Four years after BVS implantation, infiltration of the strut areas with connective tissue is complete and the scaffold is fully integrated into the vessel wall. Transmission electron microscopy comparing histological specimens at 1 month and 36 months after BVS implantation shows maturation of the endothelium between these two time points[61]. At 1 month, the newly generated endothelial cells have weak junctions but by 36 months, these have evolved into dense, continuous junctions.

Smooth muscle cells within the neointima also switch from a secretive phenotype to their typical contractile state during that time. Invivo studies have also shown comparable long term safety and efficacy of the ABSORB BVS compared to the Xience DES[62].

While the histological evolution of the healing process after BVS insertion has not been characterised in humans, intracoronary imaging studies have provided us with significant insight in this setting. The neointimal proliferative response persists up to 2 years and is accompanied by an increase in vessel area[63]. This positive remodelling of the coronary artery partly accommodates the neointimal tissue. Intramural lipid cores and calcification also appear to decrease within that time interval[64]. Even though the struts are still discernable at 2 years, the scaffold has lost its structural integrity by that point. This is evident by an increase in scaffold area due to scaffold dismantling and return of vasomotion in some patients[63]. The black cores of struts are still visible at 3 years but it is not possible to distinguish between polymer and proteoglycan infiltrate on OCT[18]. The healing process is also dependent on the clinical context in which the device is implanted. Strut coverage appears to be lower in ACS patients compared to those with stable angina[65]. The TROFI-II trial in which patients with acute STEMI were randomised to receive either an ABSORB BVS or an everolimus-eluting stent showed a similar vessel 'healing scores' at 6 months[66].

1.4.3 Scaffold thrombosis and restenosis

1.4.3.1 Scaffold thrombosis

The 'Achilles' heel of drug eluting stents is the occurrence of late stent thrombosis (ST). While the mechanisms leading to late DES thrombosis are varied, the final common pathway is a delay in arterial healing[59]. Bioresorbable technology was originally proposed as a possible solution for this potentially deadly phenomenon. The rationale was that after complete resorption of the scaffold, there would be no substrate left to induce either inflammation or thrombosis. Preliminary studies also hinted at a functional endothelium after 2 years[67]. However these observations have not translated in a lower rate of scaffold thrombosis. The GHOST-EU registry was one of the first studies to raise the alarm for scaffold thrombosis[24]. Subsequent registries confirmed the higher incidence of ST with

cumulative incidence of 3% reported at 1 year[27,68]. In the largest meta-analysis of trial data, the incidence of very late ST (VLST) at 2 years has been reported at 1.43% with BVS compared to 0.56% with DES[41]. Almost all events within the metal group occur within the first year with the incidence decreasing to almost zero (0.003%) after. In comparison, the incidence of thrombosis between year 1 and 2 with BVS is 0.24%.

The exact mechanism of scaffold thrombosis is not clear at the present moment[69]. Factors commonly responsible for thrombosis in metal stents probably have a similar causative role in scaffolds. Most cases of scaffold thrombosis occur within the first 30 days of implantation and those are likely to be related to procedural issues. Malapposition is the most common imaging finding in cases of early ST and may be the result of inadequate lesion preparation, undersized scaffold or inadequate post dilatation. Other mechanical factors such as geographical miss and scaffold underdeployment have also been identified in early ST. The inflammatory milieu also plays a role with more cases of thrombosis occurring in the context of an acute coronary syndrome than in stable patients.

While the above factors are common to both platforms, there are pathological mechanisms specific to BVS that may well explain the relatively higher thrombosis rates. The thicker BVS struts can disturb blood flow increasing thrombotic risk especially in small vessels. The larger width or 'footprint' of BVS also means that a larger surface area needs to be endothelialised[70]. Consequently, a larger percentage of uncovered surface can be present if healing is delayed. In addition, the thrombogenicity of the scaffold degradation products in humans is unknown. The provisional matrix left in the wake of resorption may potentially constitute a nidus for thrombus formation if uncovered. Finally, disintegration of the scaffold may be another source of ST[71]. Scaffold discontinuity is an anticipated consequence of the natural bioresorption process but can potentially be dangerous if it causes struts to protrude into the lumen. Disruption to blood flow as well as a delayed coverage can both precipitate thrombus formation in this scenario. These device specific issues are likely to be relevant in late and very late scaffold thrombosis.

It is worth noting that many of the registries and trials from which our current knowledge on BVS thrombotic rates is derived, were conducted at a time when

the method of optimal BVS implantation was still under development. It is now known that adequate predilatation, optimal scaffold sizing and high pressure postdilatation are absolute prerequisites to reduce adverse outcomes. Adherence to these rules reduces adverse event rates even in complex lesions. For example, a recent study on the use of BVS in chronic total occlusions (CTO) using contemporary implantation techniques did not identify any cases of thrombosis at a median follow up of 15months[72]. Interestingly, while stent thrombosis has a mortality of up to 40%[10], trials showing an excess of scaffold thrombosis have not demonstrated a proportional increase in mortality[73]. This discordance in outcome raises the interesting question as to whether scaffold thrombosis is a less malignant phenomenon and should be considered a distinct entity from stent thrombosis[74].

1.4.3.2 Scaffold Restenosis

The ABSORB BVS is associated with a significantly greater late luminal loss and instent restenosis (ISR) rate than DES[75]. The ABSORB II trial reported a three year insegment restenosis rate of 8.4% with ABSORB BVS compared to 3.3% with Xience DES[76]. It is likely that ISR with BVS share the same causes as ISR with metal stents. A subset analysis of the GHOST registry investigating scaffold failure found that geographical miss and scaffold underexpansion were the most common culprits in cases of ISR[77]. Scaffold fracture has also been found to be a potential cause of late BVS failure[78]. In contrast to restenosis in BMS, a heterogeneous tissue composition is observed in most cases of BVS restenosis[79]. Early lesions (<6months after implantation) are typically homogeneous suggesting a preponderance of smooth muscle cells and fibrotic tissue. Late restenosis (>6months after implantation) is associated with features suggestive of neoatherosclerosis. These include the presence of lipid-laden lesions within the neointimal layer with macrophage infiltration and the formation of microvessels within the lesions.

1.4.4 Inflammatory markers and neointimal response

The inflammatory response after PCI depends on both the patient's pre-existing inflammatory condition and that induced by the PCI procedure (Figure 5). In the

clinical setting, the extent of inflammatory activation can be assessed by measuring levels of various inflammatory mediators in blood.

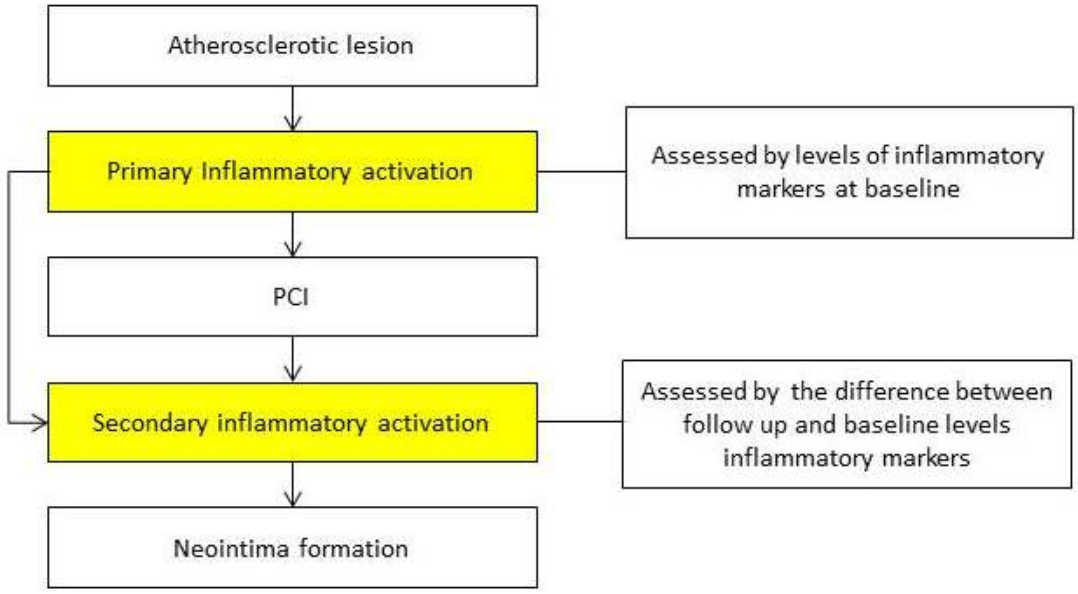

Figure 5: Relationship of baseline inflammation and secondary inflammatory activation on neointimal growth (Modified from Toutouzas et al.)[80]

Several studies have attempted to find inflammatory biomarkers that exert an influence on the neointimal tissue growth. Both local and systemic factors have been investigated in this context. IL6, CRP, MCP-1 and sCD40L are the most widely investigated systemic makers in studies on neointimal proliferation after percutaneous coronary intervention. We also chose these markers in an endeavour to investigate specific aspects of inflammation following PCI though considerable overlap exists in their functions due to the interconnectedness of inflammatory pathways. In brief, the CPR/IL6 axis examines macrophage induced local and systemic inflammation. MCP-1 assesses monocyte chemotaxis and is linked to neointimal growth. Finally sCD40L investigates platelet activation and aggregation both which are key to thrombus formation. More detailed accounts of the roles and functions of each of these markers are given below.

1.4.4.1 Interleukin-6

Interleukin-6 (IL6) is a polypeptide containing 185 amino acids, folded in 4 helices. It is produced primarily by adipose tissue, macrophages and T cells though it can be secreted by other cells within the cardiovascular system including endothelial cells, smooth muscle cells and ischaemic cardiomyocytes. Its receptor

exists in both a cellular (IL6R) and soluble form (sIL6R). The former is primarily located within hepatocytes where activation results in CRP production. Cells lacking IL6R can still respond to IL6 if the IL6-sIL6R complex binds to membrane bound gp130 in a process known as 'trans-signalling'. Its effect on endothelial, smooth muscles cells amongst others is effected via this mechanism[81]. IL6 is a pleiotropic cytokine performing a variety of biological activities. It plays an integral part in the normal function of both the innate and adaptive immune system. It is also involved in most chronic inflammatory states including atherosclerosis[82]. Its proinflammatory actions are protective in the short term and are aimed at restoring tissue integrity. Problems arise when IL6 is chronically elevated at which point it becomes pathogenic to the host. Several studies have confirmed the relationship between elevated serum IL6 levels and unfavourable clinical outcomes in patients with coronary disease[83,84].

The effect of IL-6 on neointimal infiltration and restenosis has been investigated in several studies. Hojo and colleagues showed a significant correlation between the rise in IL-6 concentration in the coronary sinus after POBA and the risk of late restenosis[85]. Kazmierczak et al found that an elevated level of IL-6 measured 1 month after PCI was associated with a higher risk of restenosis and denovo lesions[86]. A cut-off value of 3.0pg/ml had a positive predictive value of 90%. Similarly, Zurakowski et al. observed a positive correlation between IL-6 levels measured 6 months after BMS implantation and late luminal loss on angiography[87].

1.4.4.2 CRP

CRP is the most widely studied inflammatory marker in coronary heart disease. It is a circular protein consisting of five identical non-covalently bound polypeptide subunits, each containing 206 amino acid residues. It is primarily produced by hepatocytes but has also been found in smooth muscle cells within atherosclerotic plaques. Its production is regulated at a transcriptional level by IL-6 which signals the activation of the CRP gene on chromosome 1. CRP is an acute phase protein which increases in the sera of patients during inflammation. It shares many of the traits of antibodies including the ability to activate the complement cascade, promote agglutination and phagocytosis. Inflammatory stimuli that trigger its release range from exogenous bacterial infections to endogenous atherosclerotic

plaques. Its role in the initiation and progression of atherosclerosis has been extensively studied over the past two decades[88]. Several studies have confirmed its role as a both a biomarker and contributor to coronary heart disease[89,90]. The pathophysiological contribution of CRP to the development of atherosclerosis includes[91]:

- Complement activation leading to vascular wall damage
- Facilitation of LDL uptake into macrophages to form foam cells
- Inhibition of nitric oxide production by EC and of fibrinolysis through its potentiating effect on plasminogen activator inhibitor-1 (PAI-1)
- Upregulation of endothelial adhesion molecules mobilising leucocytes to the site of injury
- Fibrinolysis inhibition and activation of macrophages to secrete the procoagulant tissue factor.

An elevated CRP level is associated with adverse outcomes in the context of both acute MI and stable angina[88,92].

CRP has been found to predict adverse events after coronary stenting. In a meta-analysis of over 30,000 patients who underwent PCI, every 1mg/l increment in baseline CRP levels was associated with a 12% increase in future adverse cardiac events[93]. A high level at follow up also appears to be associated with ISR and poor clinical outcome possibly reflecting the deleterious effect of chronic inflammation[94]. A few studies have explored the effect of CRP on neointimal growth using intracoronary imaging. A larger amount of neointimal volume has been observed in patients with high baseline CRP levels[95]. High levels also seem to influence the morphology of the restenotic tissue causing more asymmetry, neoatherosclerosis and less strut coverage.[96-98]

1.4.4.3 MCP-1

Monocyte Chemoattractant Protein-1 (MCP-1) is a polypeptide chemokine belonging to the CC chemokine subfamily. It is a relatively small molecule consisting of 76 amino acid residues in its mature form. MCP-1 is produced by a variety of cells including endothelial and smooth muscle cells within the arterial system. Its main function as its name suggests is to attract monocytes to foci of

inflammation. MCP-1 plays a critical role in the development of cardiovascular diseases[99]. Vascular insults trigger the release and migration of MCP-1 onto the endothelial cell membrane. Once on the surface, its proximal end is exposed to the luminal contents while the distal part is anchored to the plasma membrane by proteoglycans. Rolling monocytes containing the surface CCR2 receptor recognise the molecule through ligand-receptor interaction and come to a halt. The monocytes migrate through the vessel wall where they transform into foam cells causing the formation of fatty streaks. MCP-1 also alters gene expression within monocytes leading to the production of proinflammatory cytokines and matrix metalloproteinases. In addition to its role in atherosclerosis, MCP-1 has also been implicated in other cardiovascular disorders including ischaemic cardiomyopathy, myocarditis and transplant vasculopathy.

The earliest evidence of the role of MCP-1 after percutaneous intervention emerged in the early 90s where balloon injury to the aorta in animal models was found to induce MCP-1 production[100]. Administration of MCP-1 antibodies has been shown to inhibit neotintimal growth in animal models[101]. Alteration of the gene producing MCP-1 or its receptor effectively suppresses neointimal hyperplasia[102]. Human studies on ISR have shown an association between plasma level of MCP-1 and likelihood of developing restenosis. Cipollone et al. evaluated the role of MCP-1 in patients treated with PTCA electively[103]. MCP-1 levels remained elevated up to 3 months in patients who developed ISR while in non-restenotic patients, MCP-1 normalised after 2 weeks. The adverse effect on neointimal growth appeared to partly be effected through the generation of reactive oxygen species by monocytes. In a histological comparison of restenotic and denovo lesions obtained during direct atherectomy in patients undergoing POBA, Hokimoto and collegues found a higher expression of MCP-1 in restenotic specimens[104]. An increase in MCP-1 level at 6mths compared to baseline has been found to positively correlate with in-stent late luminal loss[105]. The association between MCP-1 and restenotic rates has spawned interest as in its use as a potential target to combat restenosis. Arefeiva et al. developed an inhibitor constructed from the known active amino acid residues within the MCP-1 molecule and tested its effect on inflammation post PCI[106]. They found that the use of this antagonist reduces levels of CRP, fibrinogen and MCP-1. More

recently, a selective inhibitor of MCP-1 named Bindarit was tested in a double blind randomised trial of 148 patients undergoing elective PCI[107]. Patients were randomised to receive 600mg, 1200mg Bindarit or placebo. All patients had a follow up angiogram at 6mths. The primary endpoint of insegment luminal loss was not met but there was a significant reduction in instent luminal loss in the treated group suggesting a potential use in patients at high risk of restenosis.

1.4.4.4 sCD40L

CD40L is a protein belonging to the TNF family of cytokines. Soluble CD40 Ligand (sCD40L) is derived from the cleavage of surface CD40 ligand. While the CD40 ligand is expressed on the surface of different types of cells, almost all its soluble form is derived from activated platelets. CD40L-CD40 interaction has been implicated in the development of atherosclerosis[108]. Activation of endothelial cells by oxidised LDL and cytokines from leucocytes induces the expression of the CD40 receptor. Binding of cellular CD40L or its soluble form to receptors activates endothelial cells and macrophages. sCD40L also induces platelet activation and aggregation causing thrombus formation. Patients with stable coronary disease typically have a higher plasma level of sCD40L compared to healthy subjects. Levels are even higher in the context of acute coronary syndromes where levels exhibit a gradual progression with the severity of ACS[109].

The effect of the CD40- CD40L system on restenosis has been demonstrated in animal models. Following carotid denudation injury in atherogenic ApoE-/- mice, inhibition of CD40L with a monoclonal antibody was found to reduce neointimal formation[110]. In another study using wire injury, CD40-/- mice demonstrated lower neointimal proliferation and better healing than wild type mice[111]. The association of CD40L and its soluble form with restenosis has also been investigated in clinical studies. Cipollone et al. found that patients who developed ISR 6mths after balloon angioplasty (POBA) had more than twice the baseline level of sCD40L than those without[112]. The difference in plasma concentrations between the ISR and non-ISR group was sustained up to 6 months. In vitro analysis using patient sera showed that elevated levels of sCD40L inhibited endothelial cell migration, stimulated ECs to release MCP-1 and enhanced the expression of adhesion molecules on the endothelial surface. Sustained elevated levels of CD40L at 1 month after POBA have also been linked to the development

of restenosis[113]. Following elective PCI with metal stents, Turker et al. found that a high preprocedural sCD40Llevel was linked to ISR at 6 months[114]. In another study, patients who developed restenosis after elective PCI were found to have higher CD40L levels at 6 months[115].

1.5 Coronary Physiology

1.5.1 Basic mechanics of blood flow

The coronary circulation consists of the epicardial coronary arteries originating from the aortic annulus, arterioles, capillary network, venules and the epicardial veins draining into the right atrium. The flow of blood along this network is broadly governed by two factors: the pressure difference between the arterial and venous side and the resistance to flow offered by the vessels within that. This relationship is expressed below:

$$Q = \frac{(Pa - Pv)}{R}$$

where Q is flow of blood along the coronary circulation (volume/time), Pa is the arterial pressure (mm/Hg), Pv is the venous pressure (mm/Hg) and R is the resistance offered by blood vessel (mmHg x time/volume).

Resistance is primarily determined by the dimensions (diameter and length) of the vessels involved and by their arrangement (series v parallel). Blood viscosity and extravascular mechanical forces also play a role though their effect is usually fairly constant. Blood flow within a straight vessel can be modelled as flow along a circular pipe. Such a model in conjunction with some simplifying assumptions gives the following relationship between flow and vessel size.

$$Q \propto \Delta P.\frac{r4}{\mu L}$$

where Q is the flow rate, ΔP is the pressure drop across the vessel, μ is the viscosity of blood, L is the length of the vessel and r is its radius.

Similarly,

$$Resistance \propto \frac{\mu L}{r^4}$$

Changes in resistance in a blood vessel are primarily effected through changes in vessel size. Given the relationship to the fourth power, it is evident that a small change in radius will cause a large change in the overall resistance offered by that vessel. The total resistance of blood vessels connected in series is the sum of the individual resistance of each component forming the circuit. Thus, the total resistance of the coronary circulation is the sum of the resistances offered by the epicardial artery, arterioles, capillaries, venules and finally epicardial veins.

$$R_{total} = R_{artery} + R_{arteriole} + R_{capillary} + R_{venule} + R_{vein}$$

Generally, the pre-arteriolar and arteriolar resistances are the only significant contributors to the overall resistance in the coronary network.

1.5.2 Coronary Pressure-Flow relationship

The purpose of the coronary circulation is to distribute blood to meet the metabolic requirements of the cardiac myocytes. Matching coronary blood flow to the oxygen demand of cardiac tissue is crucial for the heart to function normally. As outlined in the previous section, coronary blood flow is dependent on perfusion pressure. This relationship has been extensively studied in animal models. Figure 6 shows the relation between coronary blood flow versus pressure in a healthy heart[116].

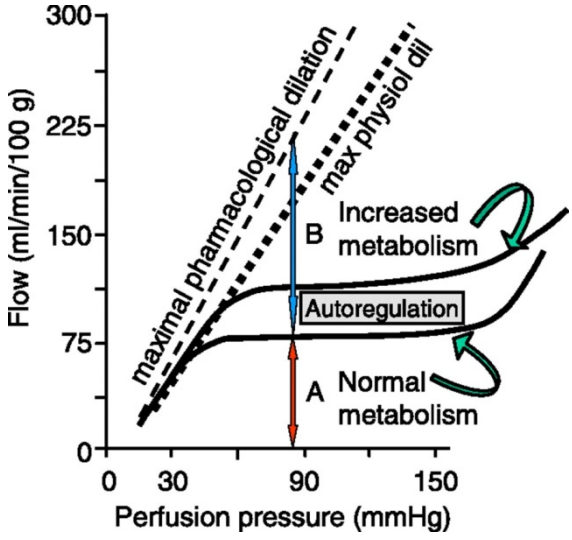

Figure 6: Graph of flow against perfusion pressure in the healthy heart. The autoregulatory plateau ensures constant flow over a range of perfusion pressures. The dashed line indicates maximal pharmacological vasodilatation while the dotted line shows maximal physiological dilatation. (Reproduced from Westerhof et al.)[116]

In the presence of vasoactive control, flow down the coronary arteries is fairly independent over a wide range of coronary pressures. The mechanism responsible for this is known as auto-regulation. It refers to the ability of the heart to maintain stable blood flow despite changes in perfusion pressure. The heart is able to achieve this by altering the coronary microvascular resistance through a variety of mechanisms (detailed in the section below). An increase in oxygen demand shifts the autoregulatory plateau upwards. This ensures that coronary blood flow increases during exercise. Note that this effect occurs independently of the increase in perfusion pressure. The autoregulatory mechanism can be abolished by inducing maximal vasodilatation. Typically, adenosine is used to induce hyperaemia. In this condition, a linear relationship exists between pressure and flow. The maximal hyperaemic dilatation achieved pharmacologically (dashed line) is typically greater than achievable physiologically e.g. during exercise (dotted line).

1.5.3 Microcirculation

1.5.3.1 Physiology

The coronary arterial microcirculation consists of pre-arterioles (100-500 microns in diameter) and arterioles (<100microns). It is the site where auto-regulatory mechanisms operate and blood flow is matched to the requirements of myocardial tissue. Control of blood flow is accomplished through changes in vascular resistance within that region mediated mainly by alteration in vessel diameter. This is done by three main mechanisms which roughly relate to the size of the vessels[117] (Figure 7)

- *Endothelium mediated response*: In a healthy vessel, the vascular endothelium regulates the behaviour of underlying vascular smooth muscle cells. The endothelium is particularly sensitive to blood velocity and in particular to the frictional force exerted by the flow of blood along its surface known as wall shear stress. Depending on the stimulus, the endothelium can secrete factors that elicit VSMC contraction or relaxation. Nitric oxide and prostacyclins are potent vasodilators while endothelin-1 acts as a vasoconstrictor. Increase in coronary flow velocity and hence wall shear stress induces vessel dilatation.

This leads to reduction in velocity and shear stress. Maintenance of a physiological shear stress is important in order to protect the endothelium against injury caused by viscous friction between flowing blood and the endothelial layer. This effect mostly occurs in the proximal pre-arteriolar vessels.

- *Myogenic response*: This response is primarily aimed at keeping the pressure delivered to the capillaries within a narrow range. Changes in blood pressure alter the perpendicular stress on vessel wall. For example, an increase in luminal pressure increases wall stress and stretches the arterial wall. Vascular smooth muscle cells within the vessel respond by contracting thereby reducing the size of that vessel. The net effect is a reduction in distal pressure. Transmission of high systemic pressures that could otherwise damage the fragile capillaries is prevented. Fluid exchange between intravascular and interstitial space within the capillary network is also very sensitive to pressure changes. The preservation of capillary pressure within a physiological range thus constitutes an important haemostatic mechanism. This response is strongest in the pre-arteriolar vessels with a diameter of about 100 microns.
- *Metabolic*: Blood flow is closely coupled to the oxygen demand and metabolic activity of myocardial cells. This effect is seen in the smallest arterioles. In regions of tissue hypoxia, the low partial pressure of oxygen induces vasodilatation to improve flow to that region. Ischaemic metabolites also stimulate the local release of vasodilators such as adenosine and nitric oxide.

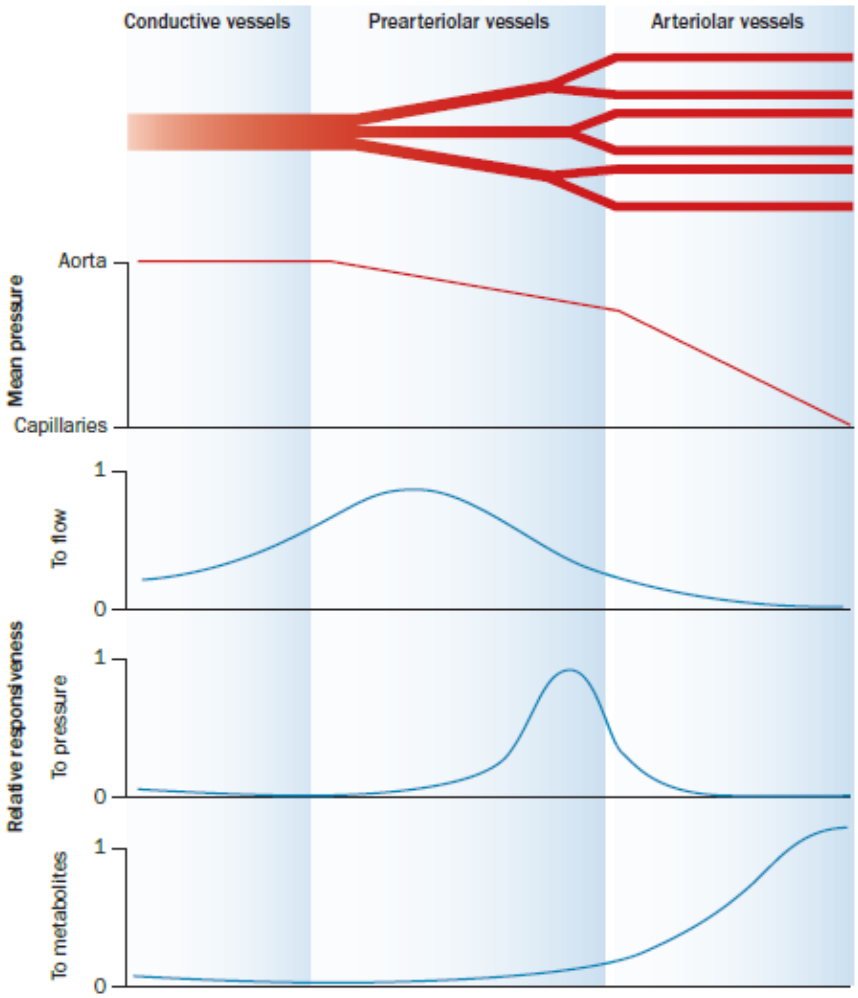

Figure 7: Pressure distribution along coronary arterial circulation and relative responsiveness of different compartments to flow, pressure and metabolites. Pressure drop across the epicardial artery is negligible in contrast to the pre-arterioles and arterioles which collectively form the microcirculation (Reproduced from Camici et al.)[117]

In physiological states, these mechanisms are responsible for protecting the coronary vessel and coupling blood flow to the metabolic demand of the heart. In the presence of atherosclerotic disease, they are critical to prevent myocardial ischaemia. Seminal studies conducted in open-chested, anaesthetised dogs in whom external vascular constrictors were used to mimic varying degrees of coronary stenosis showed that the coronary circulation is able to maintain a steady blood flow over a fairly extensive range of luminal narrowing[118]. As the lumen gets smaller, the distal pressure decreases. Autoregulatory mechanisms decrease resistance downstream in order to preserve the resting coronary blood flow. Only after the luminal reduction exceeds 50% does maximal blood flow start to

decrease. The threshold for baseline blood flow reduction is even higher with coronary flow being preserved even up to 85% diameter reduction. Once this limit has been exceeded, the mechanisms can no longer compensate for the reduction of flow upstream and coronary flow drops. The development of ischaemia in progressive coronary plaque formation is heavily dependent on the underlying coronary reserve. This reserve varies not only from person to person, but considerable heterogeneity can exist within different regions of the same heart[119].

1.5.3.2 Obstructive coronary disease

There is significant evidence that the presence of an epicardial stenosis upstream has a deleterious effect on the distal coronary microcirculatory network[120]. Arterioles embedded within an ischaemic region undergo inward remodelling leading to increased passive stiffness[121]. Post stenotic arterioles also exhibit a weaker myogenic response. Deranged responses to vasoactive agents have been reported including an increased sensitivity to the vasoconstricting agent, endothelin-1 and paradoxical vasoconstriction with agents such as serotonin and acetylcholine[122,123]. These structural and functional changes can increase the baseline microcirculatory resistance thereby reducing the ischaemic threshold of a stenosis. Activated platelets in atherosclerosis also affect coronary microvascular resistance (MR). The platelet releasate contains a wide range of vasocontrictive and pro-inflammatory substances that can have a pathological effect on the microvasculature[124]. Finally, the pressure drop induced by the epicardial stenosis can adversely affect how the coronary microcirculation responds to an increase in oxygen demand such as during exercise. Usually, an increase in heart rate is accompanied by a decrease in MR in order to increase blood flow to the myocytes. However, in the presence of an epicardial stenosis, an increase in coronary resistance can occur in response to tachycardia[123].

1.5.3.3 Post PCI

The aim of PCI is to restore perfusion to the cardiac tissue. However, restoration of epicardial flow does not necessarily equate with a normalisation of myocardial perfusion. Adequate myocardial perfusion is dependent not only on an unobstructed conduit artery but also on the resistance in the vascular bed downstream. Even if PCI improves flow along an epicardial artery, it may not necessarily restore normal perfusion if the downstream microcirculatory

resistance is high. This phenomenon is evident in a subgroup of patients who retain a persistently low coronary flow reserve (CFR) despite successful percutaneous treatment of their stenosis[125]. This phenomenon can happen through a number of mechanisms[120]. Firstly, structural remodelling of the microcirculatory network distal to a stenotic artery can occur causing a rise in microcirculatory resistance[121]. In this case, PCI relieves coronary obstruction but has no effect on the underlying microcirculation. Secondly, the PCI procedure itself may damage the microvessels due to distal embolization of atherosclerotic debris during the procedure[126]. This is often manifested as a post-procedural rise in cardiac enzymes in the absence of overt complications. The status of the microcirculation within the treated territory determines the coronary flow reserve available and influences the extent of myocardial necrosis. A high baseline resistance has been linked to a higher incidence of peri-procedural MI[127]. Thirdly, microvascular dysfunction may co-exist independently with epicardial disease and simply be unmasked once the epicardial narrowing has been dealt with.

1.5.4 Physiological Parameters

1.5.4.1 Fractional Flow Reserve (FFR)

Conceptually, fractional flow reserve is the ratio of hyperaemic blood flow in the presence of an epicardial stenosis to hyperaemic flow in the theoretical absence of the stenosis. Given the flow-pressure relationship at hyperaemia illustrated in Figure 6, this ratio can be re-expressed as a ratio of distal to aortic pressures (with certain assumptions)[128]. This ratio is known as FFR and provides a surrogate measure of myocardial blood flow based on the pressure drop across the stenosis at hyperaemia. This parameter has been extensively validated in clinical studies. It is recommended in clinical practice guidelines as the method of identifying physiologically relevant coronary stenosis[129,130]. A FFR cut off of 0.8 is currently taken as the threshold above which revascularisation of the stenosis can be deferred in patients with stable angina[131].

1.5.4.2 Coronary Flow Reserve (CFR)

Coronary Flow Reserve is defined as the ratio between blood flow at hyperaemia and blood flow at rest at the same perfusion pressure in a given coronary artery. It reflects the ability of a vessel to increase blood supply in response to an increase

in metabolic demand within the myocardial territory that it supplies. In the presence of an intact autoregulatory mechanism and absent epicardial disease, coronary flow can increase up to four times during exercise. Several variables such as heart rate, left ventricular pressure and left ventricular function affect CFR[132]. The variability of basal blood flow not only between patients but also within the same patient depending on the physiological conditions at the time of measurement makes it difficult to obtain a standard reference range for the general population. Nevertheless, clinical studies generally use a CFR level of 2 as the threshold below which a stenosis should be treated[133]. The difference between FFR and CFR in a stenotic artery is illustrated in Figure 8[128].

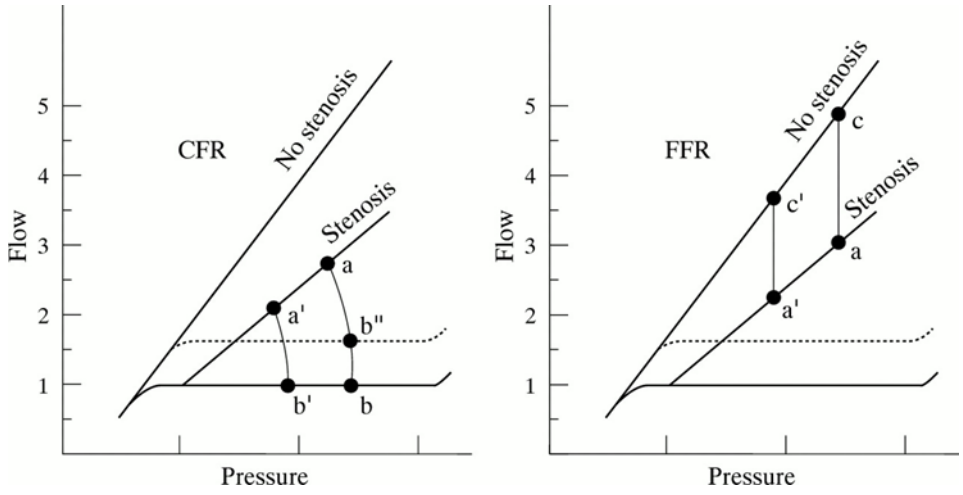

Figure 8: Graph of flow against pressure illustrating the difference between CFR and FFR. Coronary pressure-flow relation at maximal hyperaemia is indicated for both a normal artery and one with a stenosis. Resting pressure-flow relation is shown by the horizontal line. (Left) CFR is defined as ratio of hyperaemic to resting blood flow (a/b). A change in blood pressure will change the value (a′/b′). Similarly, a change in resting flow conditions will affect CFR (a/b′′). Therefore no uniform value of CFR can be defined. (Right) FFR is defined at the ratio of maximal flow in the presence of a stenosis to that of normal hyperaemic flow (a/c). This ratio is unaffected by changes in blood pressure (a/c = a′/c′) or by variations in resting flow. (Reproduced from Pijls et al.)[128]

1.5.4.3 Index of Microvascular Resistance (IMR)

IMR is a surrogate measure of the microcirculatory resistance distal to the artery being studied. It is derived using the principles of thermodilution. In the presence of an epicardial stenosis, the accurate determination of IMR requires knowledge of the coronary wedge pressure (Pw) which reflects the contribution of collateral flow. How accurately coronary wedge pressure reflects collateral flow is a matter

of debate. Animal and experimental data suggest that the relationship between Pw and collateral flow is not linear due to the dependence of Pw on other factors such as venous pressure, heart rate and end-diastolic left ventricular pressure[134]. Aarnoudse et al. showed that for mild to moderate epicardial stenosis, wedge pressure correction was not generally required[135]. However the contribution of collateral flow cannot be ignored with more severe stenosis. In this setting, IMR is given by:

$$IMR = Pa\ x\ Tmn\ x\ (Pd - Pw)/\ (Pa - Pw)$$

where Pa is the aortic pressure, Pd is the distal coronary pressure, Pw is the coronary wedge pressure and Tmn is the thermodilution-derived mean transit time.

In the absence of significant epicardial disease, IMR is simply defined as the product of distal pressure and transit time at hyperaemia.

$$IMR = Pd\ x\ Tmn$$

This parameter has been validated both in animal and human studies[136,137]. While no standardised reference level is used, it is generally considered that values under 25 are normal[138].

1.5.4.4 Integration of physiological indices:

Impairment of myocardial blood flow occurs as a result of both obstructive and non-obstructive coronary disease. The physiological parameters described in the earlier sections assess different parts of the vasculature and their integration provides a more comprehensive assessment of the coronary circulation. FFR and IMR interrogate the epicardial and microcirculation respectively while CFR provides an overall assessment of the entire circulation of that artery. Figure 9 summarises the relationship between FFR, CFR and IMR[139]. It is important to note that CFR is affected not only by epicardial stenosis and microcirculatory dysfunction but also by the presence of diffuse atherosclerotic disease.

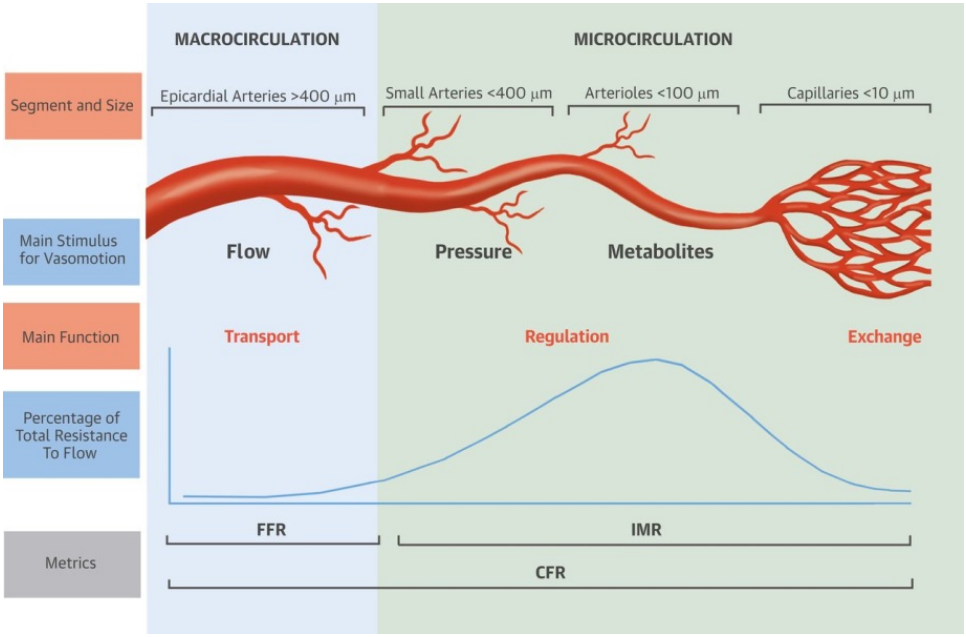

Figure 9: Relationship among FFR, IMR and CFR (Reproduced from De Bruyne et al.)[139]

1.6 Wall shear stress and Biomechanical modelling

Blood is a viscous fluid and exerts a force along the inner surface of the vessel as it flows. This frictional force known as wall shear stress (WSS) is sensed by endothelial cells. WSS plays an important role in pathological states such as atherosclerosis and in stent restenosis particularly in bifurcations. WSS cannot be experimentally measured. Instead it is derived using the principles of computational fluid dynamics (CFD). Historically the application of CFD to coronary haemodynamics has been used to study stent-vessel interaction in order to improve stent design. More recently, this technique has been used to investigate the effect of bifurcation treatment strategies on WSS distribution. The haemodynamic characteristics after stent deployment have a significant effect on the long term success of this procedure. While this relationship has been explored in arteries treated with the ABSORB BVS, analysis has been confined to relatively straight arteries. Extension of this technique to bifurcation stenting with the ABSORB BVS can help compare the haemodynamic impact of different techniques in the percutaneous treatment of coronary bifurcations.

1.7 Aims of thesis

This aims of the present work are the following:

- To investigate the procedural and clinical outcomes in patients treated with BVS for coronary bifurcation lesions based on distal versus proximal sizing of the scaffold.
- To investigate the effect of BVS on coronary microvascular resistance immediately after PCI and at 9 month follow up.
- To investigate the effects of BVS on inflammatory mediators and to assess whether levels of biomarkers correlate with neointimal coverage at 9 month follow up.
- To review the use of WSS and biomechanical modelling in bifurcations and assess the feasibility of using a CFD model in bifurcations treated with the ABSORB BVS.

2 Methods

2.1 Study overview

2.1.1 Study design

The Absorb in Bifurcation Coronary (ABC-1) trial was a single centre, randomized comparison of two sizing strategies when using bioresorbable scaffolds for the treatment of bifurcation disease. The trial included patients who had stable angina secondary to coronary bifurcation disease and required elective percutaneous coronary intervention. The pattern of bifurcation disease involved the main vessel but not the side branch. We used the Medina classification of bifurcation disease in selecting our patients[28]. For our study, we recruited patients with Medina type 1,1,0, or 0,1,0 or 1,0,0.

Patients who fulfilled the inclusion and exclusion criteria and consented to the study were randomised in randomly permutated blocks of randomly varying lengths (2, 4, and 6). This ensured roughly equal number of patients in each arm at any point in time. The randomisation sequence was generated electronically. The randomised allocation for each case was stored in sealed envelopes by an independent party not involved with the trial. The outside of the envelope was labelled with the allocated number of the case. On the day of the procedure, I opened the envelope and informed the operator of the randomisation strategy after OCT imaging of the prepared lesion. This ensured that the person doing the procedure was blinded to the sizing strategy until the moment of scaffold selection.

2.1.2 Recruitment

Patients were recruited from two sources. The first group consisted of patients referred from cardiology clinic for elective angiography and found to have denovo bifurcation disease. The second group comprised patients who initially presented with an acute STEMI at our institution and were found to have significant bifurcation disease in a non-culprit artery. To qualify for the study, the lesions needed to be stable enough to be dealt with in an elective setting.

All elective angiograms performed at the Royal Sussex County Hospital were screened by me to assess eligibility. I contacted patients who fulfilled the inclusion criteria via telephone and offered them the option of discussing the study in person. A copy of the patient information sheet was posted or emailed to the patient depending on their preference. If the patient was willing to participate but did not wish to undertake an additional visit, then consent was taken on the day of the procedure.

2.1.3 Inclusion and exclusion criteria

Patients were prospectively enrolled if they met all of the following inclusion criteria:

- Bifurcation disease with >70% stenosis in the main vessel on angiographic assessment and
  - Ischaemic symptoms, or
  - Positive non-invasive imaging for ischaemia, or
  - Positive FFR
- Bifurcation lesion Medina type 1,1,0 or 1,0,0 or 0,1,0
- Side branch diameter >2.0mm
- Patient ≥18 years old

Exclusion criteria were:

- ACS or STEMI patients
- Chronic total occlusion of either main or side branch
- 3 vessel coronary disease
- Bifurcation disease involving the LMS
- Platelet count ≤50 x 109/mm3
- Left ventricular ejection fraction ≤20%
- Patient life expectancy less than 24 months
- Participation in another investigational drug or device study
- Female of child-bearing potential unless negative pregnancy test or surgical contraception
- Patient unable to undergo required follow-up visits
- Patient unable to give informed consent

2.1.4 Ethics

The clinical investigational plan, consent form and all amendments to the study documents were reviewed and approved by the South East Coast (Brighton and Sussex) Research Ethics Committee.

2.1.5 Trial endpoints and definitions

2.1.5.1 Primary endpoint

The primary endpoint was a composite of death, myocardial infarction, scaffold thrombosis and target vessel revascularisation at a median of 9 months after randomisation.

2.1.5.2 Secondary endpoints

The secondary endpoints of our study included

- Imaging characteristics of the scaffolded segment after BVS insertion including degree of malappostion and dissection
- Imaging characteristics of the scaffolded segment at 9 months including degree of neointimal proliferation
- Death, MI, ST and TVR rates at 9 months
- Change in IMR post BVS insertion and at 9 months compared to baseline
- Change in the levels of CRP, IL-6, MCP-1 and sCD40L at 9 months compared to baseline and correlation with neointimal burden on OCT

2.1.5.3 Definition of clinical outcomes

Procedure success: The procedure was deemed successful if all the criteria below were met:

- Successful placement of BVS
- TIMI 3 flow and <50% stenosis in the stented segment
- TIMI 3 flow in any unstented vessel.

Device success: This was defined as a final diameter stenosis of <50% in the stented segment at the end of the procedure.

Death: In cases of death, information on the cause of death would be obtained from the patient's GP and recorded.

Myocardial Infarction: The expert consensus definition of PCI-related MI was used in this study[140]. For a diagnosis of PCI-related MI, the troponin measured post-PCI needed to rise by 5x local laboratory upper limit of normal or >20% if baseline values were elevated.

Target Vessel Revascularisation: Target Vessel Revascularisation was deemed to have occurred at follow-up if either the previously treated main vessel or the side vessel underwent attempted repeat revascularisation with balloon angioplasty, stenting, or coronary artery bypass grafting.

Scaffold thrombosis: Any case of scaffold thrombosis (ST) was to be assessed according to the Academic Research Consortium (ARC) criteria, both by virtue of timing and probability[141]:

- Timing - Acute ST: 0 to 24 hours after scaffold implantation; subacute ST: > 24 hours to 30 days after scaffold implantation; late ST: >30 days to 1 year after scaffold implantation; Very late ST: >1 year after scaffold implantation.
- Probability - Definite ST, Probable ST, Possible ST, as per the ARC definition.

Side branch compromise: This was defined as:

- <TIMI 3 flow in the side-vessel
- Severe ostial pinching of the SB (>90%)
- Threatened SB vessel closure defined as narrowing >50% with evidence of acute ischaemia (chest pain or ECG changes)
- Dissection of the SB (>type A)

2.1.6 Follow up visit

All patients were required to have repeat coronary imaging and pressure study at 9 months +/- 30 days after BVS implantation. Clinical endpoints were assessed and documented at that stage. Patients admitted to hospital during the follow-up period with either a troponin positive ACS or an ST elevation myocardial infarction were expected to undergo angiographic assessment during that admission, both for clinical purposes, and to establish involvement or otherwise of

the treated bifurcation vessel in the acute presentation. During follow-up, the ESC/ACC definition of myocardial infarction was used[140].

2.1.7 Adverse event reporting

All major adverse cardiac events and all endpoint related events were recorded in the case report form (CRF). All patients who had these events were followed up until the event was resolved. For all these events, the causal relationship with the procedure was established by the principal investigator, Dr James Cockburn. These were classified as:

- Unrelated: the event is definitely not associated with the procedure.
- Possible: the temporal sequence between the procedure and the event is such that the relationship is likely or patient's condition or concomitant therapy could have caused the adverse event.
- Probable: the temporal sequence between the procedure and the event is relevant or the event abates upon procedure completion or the event cannot be reasonably explained by the patient's condition
- Definite: the temporal sequence is relevant and the event abates upon completion of the procedure.

The information for any event included the date of onset and resolution, the action taken, the corrective treatment and whether the subject recovered with or without sequelae. Serious Adverse Events (SAE) were reported to the sponsor and Health Research Authority (HRA).

2.2 Protocol for PCI with BVS

Figure 10 shows a schematic outline of the PCI protocol

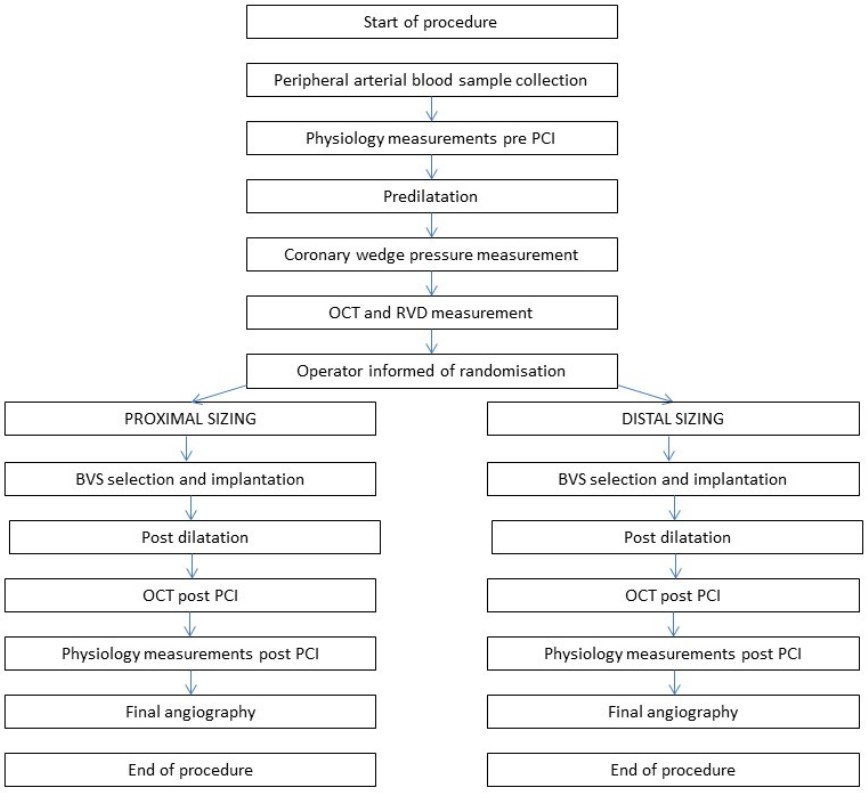

Figure 10: Outline of PCI protocol

2.2.1.1 Preparation

All patients had dual antiplatelet treatment prior to the procedure. If a patient was already established on 75mg aspirin i.e. been taking it for more than 3 days, the medication was continued at the same dose. If not, aspirin 300mg was given >3 hours prior to PCI. Similarly in patients established on 75mg Clopidogrel, the medication was continued and if not, Clopidogrel 600mg was given >3 hours prior to PCI. Prasugrel, Ticagrelor or other preferred antiplatelet agents were used in appropriate cases if preferred.

Peripheral intravenous access was secured preferably via the antecubital fossa or femoral vein. An infusion of adenosine was prepared at a dose of 140 micrograms/kg/min.

2.2.1.2 Blood sample collection pre PCI

PCI was undertaken via the access site of choice of the operator. 10 mls of blood was collected from the arterial sheath into EDTA-tubes at the start of the procedure. Intravenous unfractionated heparin (70 IU/kg) was administered

aiming for a target ACT ≥250 seconds. The operator's workhorse wire of choice was then inserted into the target vessel.

2.2.1.3 IMR measurement before BVS insertion

A 0.014-inch pressure guidewire (St Jude Medical Inc., Minnesota, USA) was calibrated outside the body and advanced into the guidecatheter until the pressure sensor was positioned at the ostium of the coronary artery. Aortic and guidewire pressures were equalised at that point following which the pressure wire was advanced so that the distal sensor was 2-3cm beyond the lesion and at least 6cm from the coronary ostium. The position of the pressure wire was stored on fluoroscopy. A bolus of 500 micrograms of intracoronary nitrate was administered into the vessel to obviate potential coronary spasm. Simultaneous distal pressure (Pd) and aortic pressures (Pa) were recorded. 5mls boluses of normal saline at room temperature were briskly injected into the coronary artery to obtain thermodilution curves. On average, 3 measurements were done and the mean baseline transit time (Tmn) recorded. Measurements that deviated by more than 30% were repeated. Intravenous adenosine (140 μg/kg/min) was then infused peripherally via a volume controlled infusion pump. Hyperaemia was usually heralded by either the development of symptoms or by a dip in blood pressure. Thermodilution derived measurements were repeated once stable hyperaemia was achieved.

2.2.1.4 Lesion preparation

The decision to insert a wire in the side branch was left at the discretion of the operator. Lesion preparation was undertaken using the predilatation guidelines for BVS including the use of adjuncts such as cutting balloons. A 1:1 balloon to artery ratio was used whenever possible preferably with a non-compliant balloon. The aim was to achieve a residual stenosis between 20-40% after predilatation.

2.2.1.5 Coronary wedge pressure measurement

The coronary wedge pressure was recorded during predilatation of the culprit lesion by keeping the balloon inflated for 30 seconds. This ensured total occlusion of antegrade flow. Before removing the pressure wire, the pressure at the tip of the guidecatheter was noted to ensure that there was no significant drift.

2.2.1.6 OCT measurement before BVS implantation

OCT was then performed to obtain the diameter of the proximal and distal main vessel. Autocalibration or Z-offset was first performed with the OCT catheter in the holder tube. The OCT catheter was then carefully advanced over a guidewire beyond the target lesion. While contrast was continuously injected at a rate of 4ml/s, OCT images of the main vessel were acquired at a rate of 160 frames/second with a pullback speed of 20mm/s. The diameters of the vessel were measured in the least diseased segment before and after to the bifurcation.

2.2.1.7 BVS implantation

The sealed envelope containing the randomisation strategy was opened. The operator was informed of the randomisation strategy and the appropriate size of BVS was chosen. The scaffold was deployed progressively at a balloon inflation rate of 2 atmospheres every 5 seconds until nominal pressure was achieved. The target deployment pressure was maintained for 30 seconds unless this caused chest pain or haemodynamic compromise. The Proximal Optimisation Technique (POT) was then performed with a non-compliant (NC) balloon. Post dilatation of the distal portion of the scaffold was performed with a NC balloon of the same diameter as the distal vessel. If the side branch was not compromised, this marked the end of the stenting procedure. In case of SB compromise after POT, the first line strategy was to open the cell at the ostium of the side branch using an undersized NC balloon (<2.5mm). POT was then repeated with a larger balloon in the proximal main vessel. Routine Final Kissing Balloon Inflation (FKBI) was not recommended but mini-FKBI ('snuggle balloon dilatation') with minimal overlap was performed if deemed necessary. In the latter case, the proximal marker of the SB balloon was positioned in the main vessel immediately proximal to the SB ostium and the balloon inflated to low pressure (5atm typically). Stenting of the side branch or conversion to complex 2 scaffold strategies were to be utilised only as bail-out.

2.2.1.8 OCT post BVS implantation

An OCT pullback was performed in the main vessel to confirm adequate strut apposition and exclude major dissections. In case of significant malapposition, further inflation with either larger balloons and/or higher pressures was performed. Significant edge dissections were sealed with stents/scaffolds. Any

correction was followed by another OCT run to confirm satisfactory resolution of complications.

2.2.1.9 IMR measurement post BVS insertion

The St Jude Certus wire was reinserted into the guidecatheter and pressure equalised at the ostium of the coronary artery. The distal sensor was advanced to the same location recorded on fluoroscopy before insertion of the BVS. Thermodilution curves and transit times were recorded in triplicate at baseline and hyperaemia as previously described.

2.2.1.10 Final angiography

The stented artery was imaged in at least two orthogonal angiographic views.

2.2.1.11 Post PCI

Haemostatic technique and use of vascular closure devices was at the discretion of the operator. Aspirin 75mg daily was continued long-term. Clopidogrel 75mg daily was continued for a minimum of 24 months (or appropriate dose of Prasugrel or Ticagrelor). Discontinuation of antiplatelet agents for soft indications was strongly discouraged.

2.3 Protocol at follow up

2.3.1.1 Patient preparation

IV access was secured via antecubital fossa or femoral vein. An infusion of adenosine at a dose of 140microg/kg/min was prepared.

2.3.1.2 Blood sampling

At the start of the procedure, 10 mls of blood was collected into EDTA-tubes from the peripheral arterial sheath.

2.3.1.3 IMR measurement

The dual pressure/temperature wire was calibrated and pressures equalised as previously described. The wire was advanced so that the sensor was positioned at the same location as in the baseline procedure. Thermodilution curves and transit times were recorded at rest and during hyperaemia.

2.3.1.4 OCT imaging

The OCT catheter was inserted over the pressure wire and positioned distal to the scaffold. Image acquisition was performed in a similar manner to baseline.

2.3.1.5 Final angiography

Fluoroscopic images were acquired in at least two views where the bifurcation segment was adequately visualised.

2.4 Invasive coronary physiological assessment

2.4.1 Guidewire

The commercially available Certus wire (St Jude Medical Inc., Minnesota, USA) contains a dual pressure/thermistor sensor located 3 cm from the tip. This allows simultaneous recording of pressure and temperature with an accuracy of 0.02ºC. The proximal shaft of the wire acts as a second thermistor sensing the injection of saline at the coronary ostium. Signals are displayed on the RADI analyzer interface. Pressure and temperature are sampled at a frequency of 500 Hz.

2.4.2 Protocol

Haemodynamic measurements were obtained before and after BVS implantation as well as at 9 month follow up as described in the PCI and follow up protocols.

2.4.3 Analysis

Off-line analysis was performed using a dedicated software and interface provided by St Jude (RADI analyzer). An example of a recording performed after PCI is shown in Figure 11.

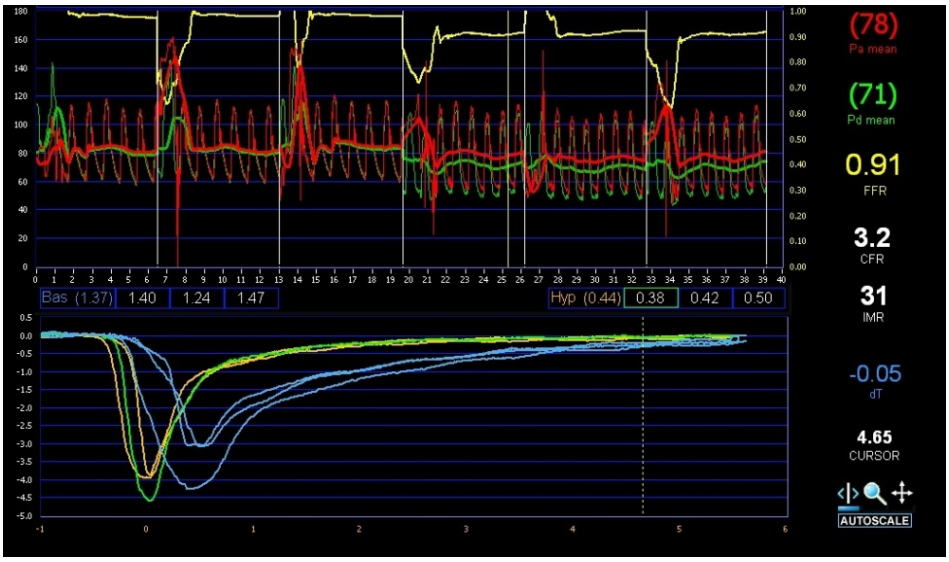

Figure 11: Thermodilution curves at baseline and hyperaemia with simultaneous aortic and distal pressure waveforms.

2.4.3.1 Index of Microcirculatory Resistance (IMR)

Two different equations were used to calculate IMR depending on the presence or absence of epicardial stenosis. Since all our cases had angiographically severe stenosis, we corrected for coronary wedge pressure when calculating IMR before PCI[142] (below)

$$(Pre\ PCI) \qquad IMR = Pa\ x\ Tmn\ x\ (Pd - Pw)/\ (Pa - Pw)$$

where Pa is the aortic pressure, Pd is the distal coronary pressure, Pw is the coronary wedge pressure and Tmn is the thermodilution-derived mean transit time, all measured at hyperaemia.

We used the equation below to calculate IMR after BVS insertion and at follow up.

$$(Post\ PCI\ or\ Fup) \qquad IMR = Pd\ x\ Tmn$$

2.4.3.2 Coronary Flow Reserve (CFR)

CFR was calculated as the ratio of the mean transit time at rest to the one at hyperaemia as shown below.

$$CFR = Tmn\ (rest)\ /\ Tmn\ (hyperaemia)$$

2.4.3.3 Fractional Flow Reserve (FFR)

FFR was calculated as the ratio of distal coronary pressure (Pd) recorded by the pressure wire to the aortic pressure (Pa) measured by the guiding catheter at maximal hyperaemia induced by peripheral adenosine infusion.

$$FFR = Pd / Pa$$

2.5 Quantitative angiographic analysis

QCA analysis was performed offline using software integrated within the cardiac catheterisation workflow in Centricity Cardiology CA 1000 (version 1.0). Calibration was done using the 6Fr guide catheter size as reference. Measurements were done in end-diastolic frames. Manual correction of the contour line was performed if the automated result was incorrect.

The scaffolded segment was analysed in matched angiographic views at baseline, post procedure and at 9 month follow up. The following parameters were computed:

1. Proximal and distal main reference vessel diameter (RVD) on either side of the bifurcation segment.
2. Lesion length
3. Minimum luminal diameter (MLD)
4. Diameter stenosis - defined as the ratio of MLD to the RVD of the segment where the lesion was located.
5. Ostial diameter, RVD and diameter stenosis of the side branch (SB)

Binary angiographic restenosis was defined as >50% luminal loss on follow up. Late luminal loss was defined as the difference between MLD immediately after stenting and at angiographic follow-up.

Three dimensional reconstruction of the bifurcation was performed using the Cardiovascular Angiography Analysis System (CASS; Pie Medical Imaging, Maastricht, Netherlands) in order to assess bifurcation angle. The three segments of a bifurcation generate three angles (Figure 12) – A: between the proximal

segment and SB, B- between the SB and distal segment and C – between the proximal and distal main vessel. We reported angle B in our findings.

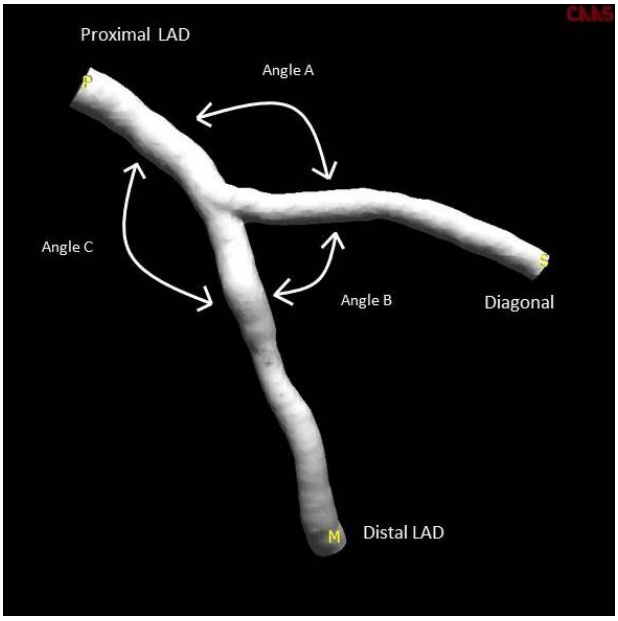

Figure 12: Illustration of bifurcation angles in a stented LAD/Diagonal system.

2.6 Optical Coherence Tomography analysis

2.6.1 Characteristics of the ABSORB BVS on OCT

OCT generates an image using the reflection of near-infrared light (wavelength of approximately 1300 nm) off the internal microstructures within biological tissue[143]. Red blood cells interfere with the light source causing scattering and signal attenuation. During image acquisition, blood is cleared from the system through the continuous injection of contrast material. The interaction of light of the OCT machine differs significantly with polymeric struts compared to metal ones. Metal structures do not allow light to penetrate beyond. On the other hand, light is transmitted through the polymeric struts of the ABSORB BVS with a degree of reflection occurring at the strut borders. The end result is that a strut is seen as a black box on OCT surrounded by a bright reflective frame. The shape of a strut in a cross-sectional OCT image varies according to its position along the scaffold (Figure 13). The vessel wall distal to the strut is also easily visualised.

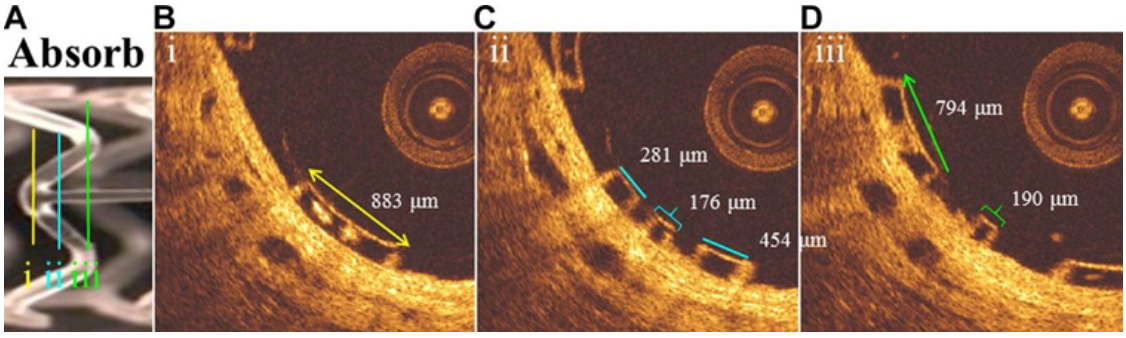

Figure 13: Appearance of the ABSORB BVS on OCT. The appearance of struts is determined by the position along the scaffold at which the image is taken (Modified from Serruys et al.)[70]

2.6.2 OCT acquisition

OCT imaging was performed using the FastView catheter R and the Lunawave coronary imaging console (Terumo Corporation, Tokyo, Japan). The OCT catheter was carefully advanced over a guidewire beyond the target area. While contrast was continuously injected at a rate of 4ml/s, OCT images of the main vessel were acquired at a rate of 160 frames/second with a pullback speed of 20mm/s.

2.6.3 OCT analysis

OCT analysis was performed offline using software provided by Terumo (Terumo Corporation, Toyko, Japan). At the set pullback speed for the trial, frames were acquired at 0.125mm intervals (8 frames per mm). The scaffold and edge segments (5mm on either side of the scaffold) were analysed at 1mm intervals. All struts visible in the slices containing the side branch were evaluated. Frame-by-frame analysis was carried within this area.

2.6.3.1 Definitions

Scaffold edge: The edge of the scaffold was defined as the first cross-section in which struts were present in at least three quadrants. Regions of overlap with another scaffold or stent were disregarded for edge analysis.

Proximal segment: This was defined as the portion of the artery before the origin of the side branch.

Side branch segment: This was identified as the interval between the most proximal and distal frames where the side branch was visible.

Distal segment: This was defined as the part of artery after the most distal slice containing the side branch.

Lumen: The lumen was defined as the continuous boundary between blood and the vessel wall. We excluded intraluminal masses that were not adherent to the vessel wall. The lumen contour was traced around the endoluminal side of struts apposed to the vessel wall (Figure 14).

Scaffold: The scaffold contour was delineated at the abluminal contour of the struts (Figure 14).

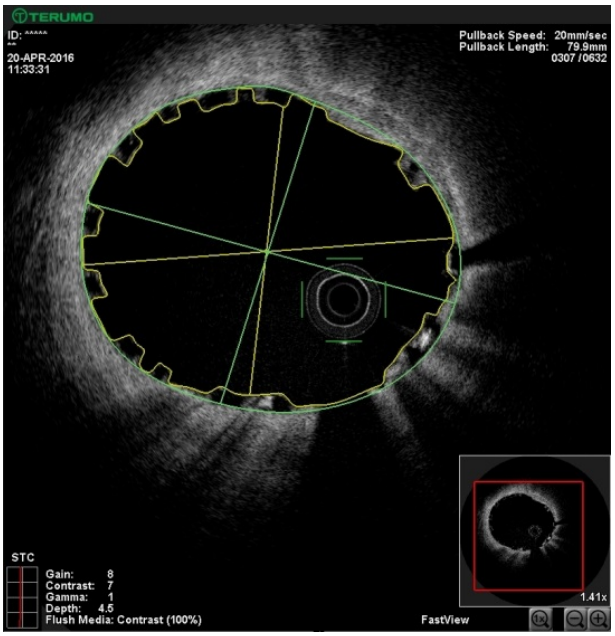

Figure 14: Implanted scaffold at baseline. The lumen is enclosed by the yellow line while the scaffold is bounded in green.

Scaffold Eccentricity Index (EI): EI was defined as the ratio of the minimal and maximal diameter of the scaffold. Both measurements were derived from the same cross-section[144].

Strut: Using a linear interpolation algorithm, the strut area was traced around the bright reflective frame after PCI and around the black box in the follow up OCT images.

Plaque morphology: The characteristics of the tissue in atherosclerotic plaque affect its brightness (intensity) and the ability to visualise structures behind it (attenuation). Three main types of plaque have been characterised in stable coronary disease depending on the dominant tissue composition[145] (Figure 15).

- Fibroatheroma composed of a lipid pool ± necrotic core – This causes low intensity, high attenuation signal.
- Fibrocalcific composed of predominantly calcified plaque – this is characterised by a low intensity and low attenuation signal giving it an appearance of a well delineated dark region with sharp borders.
- Fibrotic composed of smooth muscle cells and extracellular matrix - this is characterised as a high intensity homogenous low attenuation area. The higher the amount of proteoglycan within the lesion, the lower is the intensity of the signal. Conversely, a higher smooth muscle cell or collagen content increases signal intensity.

We categorised plaque composition according to the recommendations above.

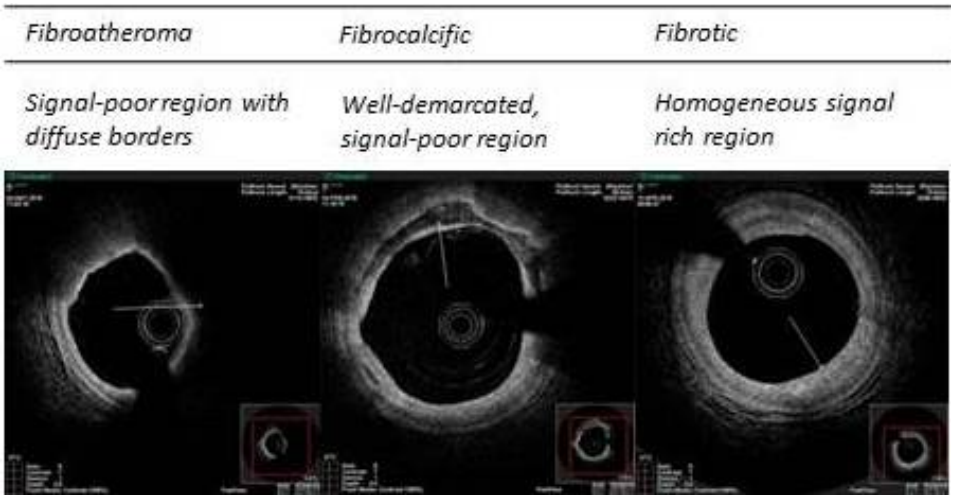

Figure 15: Plaque composition on OCT. Arrows show the location of each type of plaque.

Strut embedment: A curvi-linear interpolated contour was drawn in the lumen using the two edges of strut as reference points. The embedment depth was measured as the distance between the midpoint of the abluminal strut surface and the interpolated lumen contour[146] (Figure 16). Struts across a side branch were excluded from this analysis.

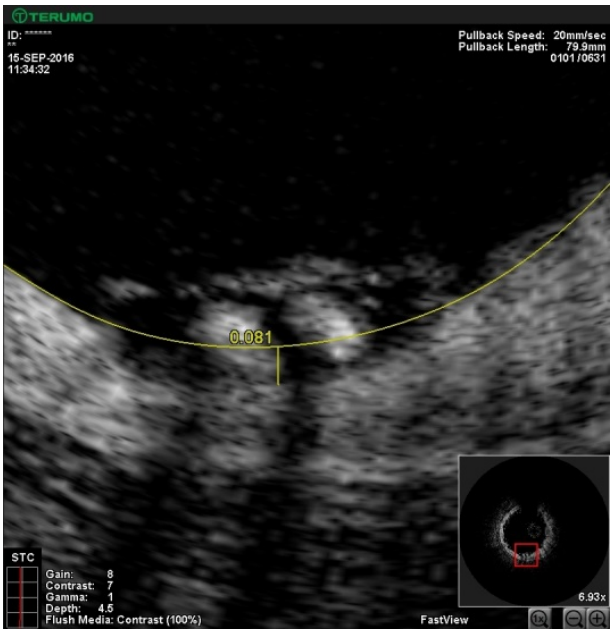

Figure 16: Assessment of strut embedment. The interpolated lumen contour is drawn using the edges of the strut as reference points. The embedment depth is 81 µm in this example.

Prolapse area: Protrusion of plaque between and on top of the struts after PCI was calculated as Scaffold area – (Lumen area + Strut area)

Neointimal tissue: Neointima was defined as tissue present between the abluminal scaffold contour and the vessel lumen excluding the space occupied by the struts on follow up OCT image. In line with expert recommendations, we used the abluminal scaffold contour as a surrogate for the internal elastic membrane after PCI[146]. Quantitative measurements were performed at 1mm intervals starting from the first image where at the scaffold was visible in at least 3 quadrants. In each slice, the lumen contour, abluminal scaffold contour and each strut core were traced (Figure 17). The abluminal scaffold area, total strut area and luminal area were recorded.

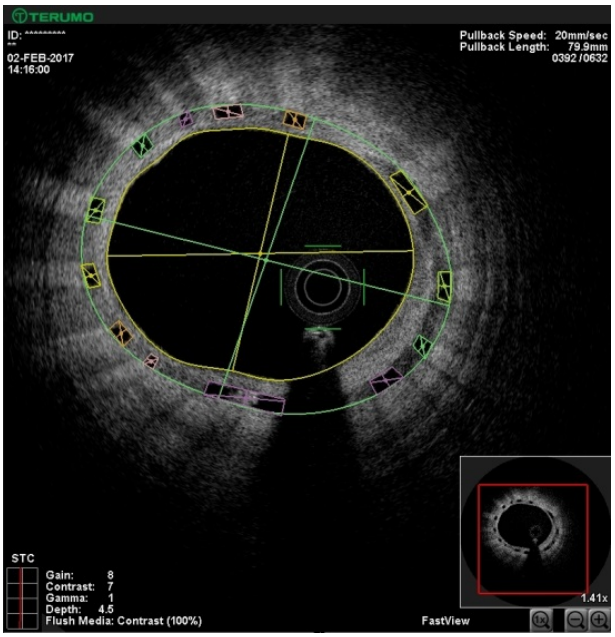

Figure 17: Follow up OCT image of scaffolded segment. Each strut is traced using a linear interpolation algorithm. Neointimal area is obtained by subtracting the luminal area (in yellow) and the total strut area from the scaffolded area (in green).

Neointimal area was calculated using the formula:

$$Neointimal\ area\ =$$

$$Abluminal\ scaffold\ area - (lumen\ area\ +\ total\ strut\ area)$$

Using this methodology, the neointimal tissue both above and in between the struts was quantified while the area occupied by the scaffold was excluded. From the equation above, it is apparent that the length of the scaffold affects the neointimal area with longer scaffolds generally having more tissue regardless of the degree of neointimal response. In order to circumvent this problem, we computed the neointimal burden using the equation below:

$$Neointimal\ burden\ =\ (Neointimal\ area/\ Scaffold\ area\ )x100\ \%$$

This parameter allowed direct comparison of the neointimal response between different patients.

Strut coverage: The region of interest was the scaffolded segment containing the side branch and the adjacent 5mm of vessel on either side. Measurements were done at 1 mm intervals on either side of the side branch and on every single frame where the side branch was visible. Neointimal coverage on top of the struts was assessed by the neointimal thickness (NIT). This was measured along the

centreline of the strut and defined as the distance between the endoluminal border of the black box and the lumen contour (Figure 18). From previous studies, the thickness of the frame has been found to be approximately 30 μm. Since it is not possible to distinguish between the frame and neointimal on follow up images, a strut was classed as uncovered if the NIT was <30microns[147].

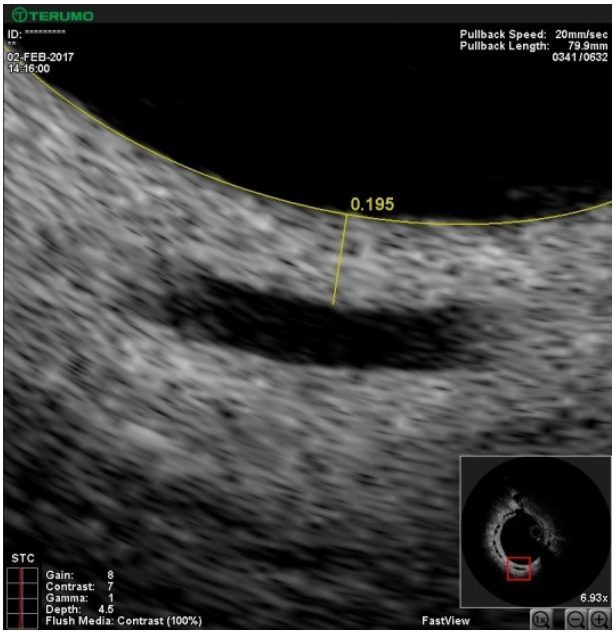

Figure 18: Measurement of NIT - A line perpendicular to the addluminal strut surface is joined from the midpoint of the strut to the lumen contour. In this example, the neointimal thickness is 195 μm.

Complications: Both the post implantation and follow up OCT recordings were scanned in their entirety to look for complications such as strut malapposition and edge dissection.

Malapposition: A strut was considered to be malapposed if the abluminal edge was not in contact with the vessel wall. Every single frame of the scaffold was analysed for evidence of malapposition. Malapposition distance was defined as the distance between the abluminal strut edge and vessel wall. We defined a malapposition distance of >300 μm as being significant. Struts opposite a side branch were analysed separately as non apposed side branch struts (NASB) [148].

Edge Dissection: Edge dissections were defined as a breach of luminal surface present within 5mm of the scaffold edge. The maximal depth into plaque, circumferential extent (in degrees using a protractor centred on the lumen) and

length were calculated in each case. A dissection was considered severe if it extended to the medial layer, had a circumferential luminal involvement of >60° and was at least 2mm in length[149].

Thrombus: Thrombus was identified as an intraluminal mass either floating within the lumen or adherent to the vessel wall.

Coronary evagination: This was identified as a bulge of the lumen in between well apposed struts.

2.7 Processing of blood samples

2.7.1 Sample collection and processing

Two sets of 10 ml blood samples were taken from the arterial sheath from each patient – first before scaffold implantation and again at 9 months after implantation. Blood was collected in EDTA-tubes (BD Vacutainers, purple cap) and centrifuged at 1500 rpm for 10 min. The resulting plasma was collected and aliquoted into 5 samples of 500 µl each. All samples were processed and frozen within 3 hours of collection. Samples were stored at -80˚C at the Royal Sussex County Hospital.

2.7.2 Analysis

Samples were transferred on dry ice to Brighton and Sussex Medical School for analysis. The ELISA kits used for each marker are outlined in Table 2

Substance analysed	Test	Minimum detectable level	Intra-assay CV (%)	Inter-assay CV (%)
CRP	HsCRP ELISA, DRG instruments GmbH	0.02 ug/ml	4.2	4.1
IL-6	Hs-huIL6 Quantikine, R&D systems	0.039 pg/ml	6.9	9.6
MCP-1	HuMCP1 Quantikine, R&D systems	1.7 pg/ml	4.2	5.9
sCD40L	HuCD40L Quantikine, R&D systems	4.2 pg/ml	5.1	6.4

Table 2: Description of kits used to test inflammatory mediators. Both the intra-assay and inter-assay precisions are reported using the Coefficient of Variability (CV) relevant to the range of results found in our study.

The principle of ELISA testing to detect a particular antigen is described below. Each assay consists of an array of wells coated with a monoclonal anti-antigen antibody. Patient samples are diluted in accordance with manufacturer's instructions and incubated in wells for a specified period of time. During this process, the antigen from the patient's plasma specifically binds to the immobilized antibody. Unbound plasma proteins are then washed away to leave antigen-antibody complexes in each well. Specific enzyme-linked polyclonal antibodies are then added to detect the complex for another specified incubation period. The washing procedure is repeated to remove any unbound antibody-enzyme reagent. Finally a chromogen/substrate solution is added to each well. This substrate turns to a particular colour in contact with the enzyme complex and the intensity of the colour is proportional to the amount of antigen present. After a prescribed amount of time, a stopping solution is added to halt the enzymatic reaction. The plate is then inserted in a plate reader which measures the absorbance of light at a wavelength of 450nm in each well. A standard curve is obtained by plotting absorbance values against the standard antigen concentrations supplied by the manufacturer. The concentration of the antigen in each well is obtained by interpolation from this curve. The standard curves for each of the markers utilised are shown in Figure 21.

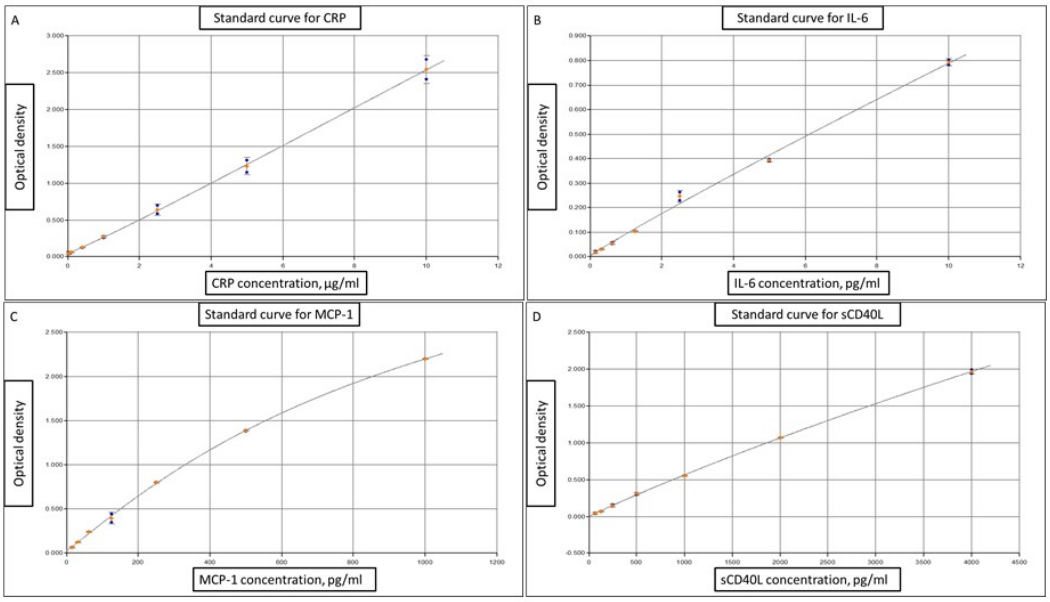

Figure 19: Standard curves were obtained by plotting absorbance values against standard antigen concentrations supplied by the manufacturer - A: CRP, B: IL-6, C: MCP-1 and D: sCD40L

2.8 Computational Flow modelling

2.8.1 CFD methodology

In collaboration with biomedical engineers in Politecnico di Milano (Italy), we developed a method of simulating blood flow across the scaffold. The lumen contour and scaffold structure were first separately extracted from the OCT imaging data. A shape recognition algorithm was created in MATLAB to detect the luminal contour using the edge based technique. This technique is based on the fact that at an edge, there is a rapid change in intensity in neighbouring pixels. Pixels are classified as either edge where there is a rapid change in value or non-edge where pixels have similar intensities within the vicinity. Using the algorithm, pixels representing the luminal contour and scaffold struts were identified and selected. This yielded a series of concentric points for the luminal contour and discrete points at the location of the struts at each cross-sectional image of the OCT known as point clouds as shown in Figure 21.

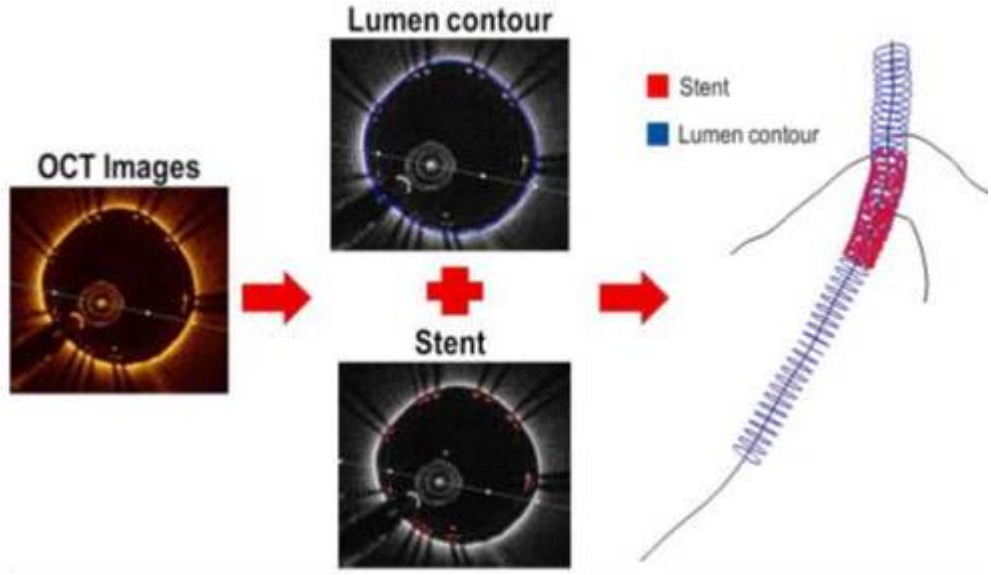

Figure 20: 3D reconstruction algorithm

The vessel curvature was obtained from the angiographic data. A dedicated software (Pie Imaging) was used to obtain the 3-D centreline through the lumen using two different radiographic projections. The luminal point clouds were stacked onto the centreline creating a 3D skeleton of the artery. The vessel wall was added to the frame using Rhinoceros software. The scaffold data was processed in a similar manner. First the three dimensional structure of the scaffold was created by superimposing the extracted point clouds of the struts from the OCT data onto the known stent configuration using the Hypermesh software. Next, the reconstructed stent frame was aligned along the luminal centreline to complete the model of the scaffolded artery (Figure 21).

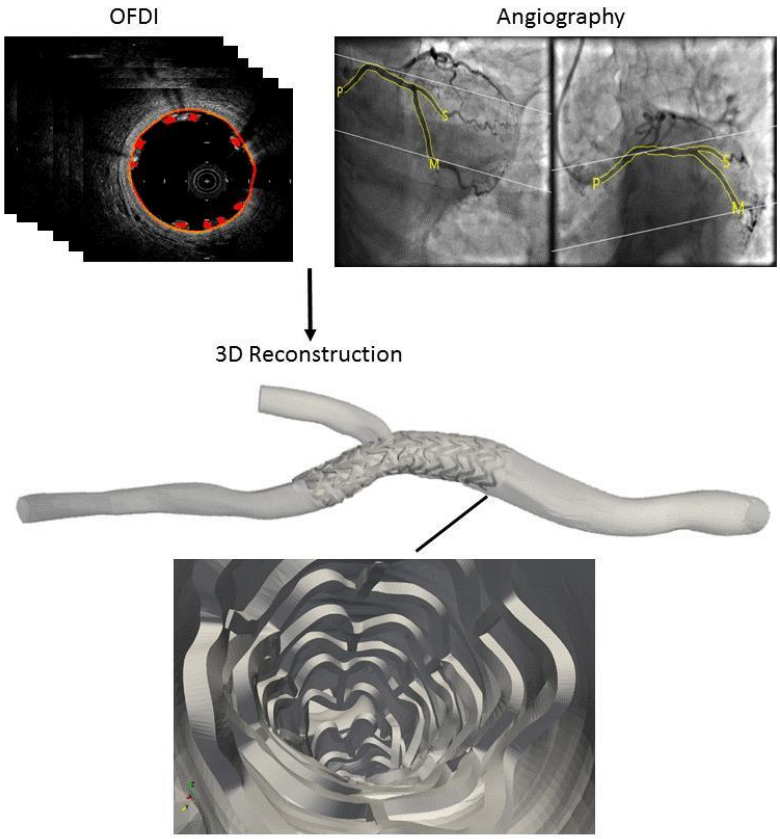

Figure 21: Fusion of OCT and angiographic data to reconstruct the scaffolded artery.

The computational fluid domain was then created by subtracting the strut geometry from the 3D model. Blood was modelled as a non-Newtonian fluid with shear thinning properties (Carreau Model)[150] and a density of 1060 kg/m^3. Blood flow was assumed to be laminar and incompressible. The walls were considered to be rigid with no-slip boundary condition applied at the surface. At the inlet of the artery, a pulsatile velocity waveform was imposed from previously published data[151]. At the outlet, blood flow was assumed to be split between the two daughter branches using the relationship described by VanderGissen[152]. Blood flow rate at the inlet was derived from the time taken for contrast agent to pass through two points in an arterial segment devoid of significant side branches using the known cine frame rate as reference and the volume of that segment on QCA[153]. The flow rate across the vessel was estimated with a relation from the work of Sakamoto et al.[154]A mesh composed of tetrahedral components was generated within the region. The mesh density was increased within the scaffolded

area to obtain a more detailed picture of the haemodynamic microenvironment at the boundaries. The maximal diameter of the cell in that region was equal to approximately ¼ of the BVS strut thickness (i.e. 40microns).

The CFD simulation was run on the Ansys Fluent to solve the Navier-Stokes equations using the finite volume method. The mean value over a cardiac cycle was calculated to give the time averaged wall shear stress (TAWSS) distribution.

2.9 Statistical analysis

The ABC-1 trial was a pilot study designed to provide preliminary information on the performance of the ABSORB BVS in bifurcations. As such, it was not powered to detect differences in outcomes. Instead, the aim of this feasibility study was to generate hypothesis and provide information to allow sample size calculation for future adequately powered randomised controlled trials. The sample size was chosen based on an estimate of the number of patients likely to fit the inclusion criteria with a recruitment course of 1 year. Categorical outcomes are presented in frequency and absolute numbers. Continuous data is presented either as mean with standard deviation or as median with interquartile range. 95% confidence intervals for continuous data were calculated using the t-distribution method. Analysis was performed with the SPSS software (version 24, SPSS Inc., Chicago, Illinois). The statistical tests for data analysis are outlined in the 'statistical analysis' section in each chapter. Since no formal hypothesis testing was planned in this feasibility study, the p values presented are exploratory and should be cautiously interpreted.

3 A randomised trial comparing two stent sizing strategies in the treatment of coronary bifurcation lesions with the ABSORB BVS: Immediate procedural and imaging outcomes

3.1 Introduction

Bifurcation lesions are present in 15-20% of patients undergoing PCI[54]. Despite their fairly common frequency, clinical outcomes remain unsatisfactory. Major adverse event rates range between 3-15%[155]. A wide array of classifications and therapeutic techniques largely fuelled by the creativity of interventionalists has been proposed over the last couple of decades but a definite treatment strategy remains elusive[156]. The emergence of bioresorbable technology has added a new treatment option to our armamentarium. The use of a resorbable scaffold as an alternative to metal stents is particularly attractive in this subset of disease. Potential benefits include late unjailing of the side branch and restoration of the bifurcation anatomy after complete resorption. Choosing the right size of BVS for a bifurcation is crucial to avoid complications. With metal stents, it is generally recommended to choose the stent size according to the distal vessel diameter and to perform the proximal optimisation technique to ensure good apposition at the proximal end[157]. The ABSORB BVS is a more delicate device. Aggressive dilatation beyond the recommended limits can easily fracture hoops and connectors. This is particularly relevant for bifurcations where there can be a sizeable discrepancy between the proximal and distal diameters. This limits the extent to which proximal optimisation (POT) can be performed in the proximal main vessel (MV). In suitable anatomies, another strategy is to select the scaffold according to proximal MV diameter and to deploy at low pressure in order to avoid damaging the distal vessel, followed by adequate postdilatation of the proximal segment. Which of these two strategies is better with the ABSORB BVS is currently unknown.

3.2 Aim

- To compare the procedural, imaging and acute clinical outcomes of two sizing strategies when using the ABSORB BVS to treat coronary bifurcations.

3.3 Methods

3.3.1 Study population

Patients were recruited at the Royal Sussex County Hospital between February 2016 and March 2017. A total of 1148 coronary angiograms were reviewed to assess eligibility based on lesion characteristics. The clinical details of potential cases were then examined against the exclusion criteria. Each prospective case was discussed with both the patient's cardiologist and the principal investigator of the trial to determine suitability for participation in the study. Figure 22 charts the progress of patients through the phases of the randomised trial.

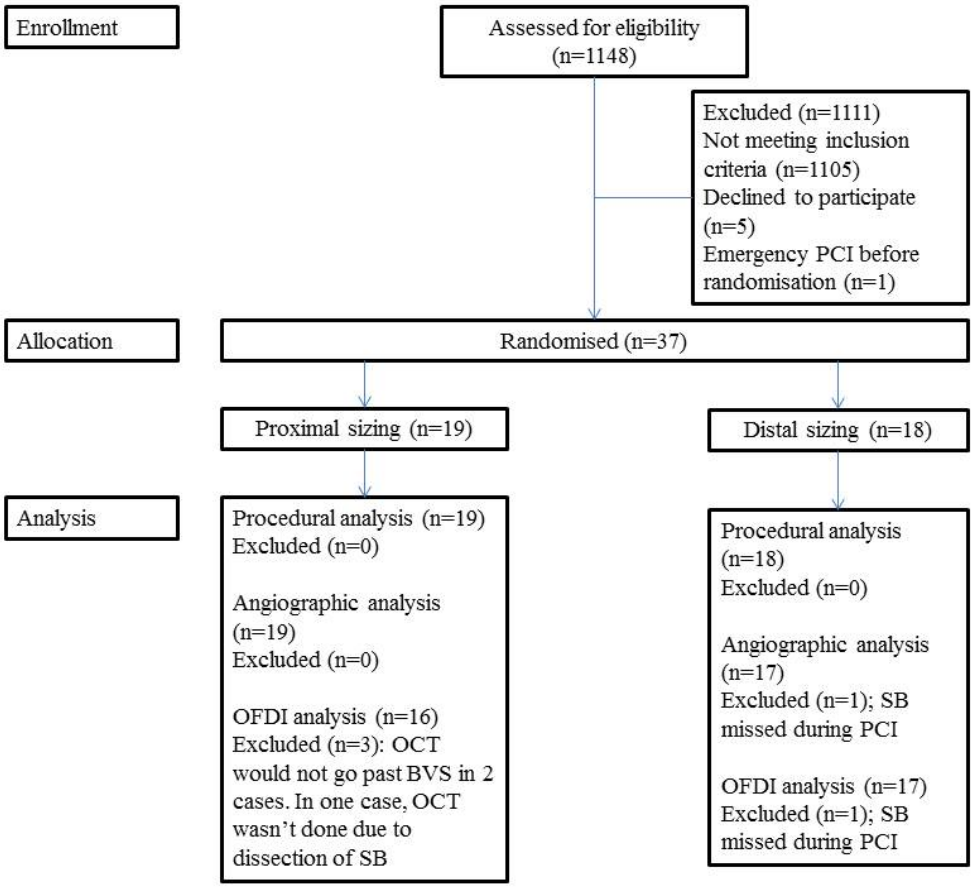

Figure 22: Patient flow diagram

3.3.2 BVS implantation procedure

As described in chapter 2.

3.3.3 Angiographic analysis

As described in chapter 2.

3.3.4 OCT imaging and analysis

As described in chapter 2.

3.3.5 Statistical analysis

Test for normality was performed using the Shapiro-Wilk test. Comparison between the two treatment arms was done using Mann-Whitney test for continuous data and Chi-squared test for categorical variables.

3.4 Results

3.4.1 Baseline characteristics of cohort

Thirty-seven patients were enrolled. The baseline characteristics of the cohort are presented in Table 3. The mean age of patients was 62.8 years and 76% were male. All patients had stable angina. Over 80% of treated lesions involved the LAD/D1 bifurcation. B2/C lesions were present in 65% of cases. Mean BMI, baseline creatinine and the proportion of patients with CCS angina class III/IV were higher in the proximal group.

	Prox (n=19)	Distal (n=18)	p value
Demographics			
Age [mean (sd)]	64.2 (± 4.4)	61.3 (± 5.2)	0.43
Gender (male) [%(n)]	73.7 (14)	77.8 (14)	0.77
BMI [mean (sd)]	31.6 (± 2.8)	25.7 (± 1.8)	0.001
Clinical characteristics			
Hypertension [%(n)]	42.1 (8)	55.6 (10)	0.41
Hyperlipidaemia [%(n)]	47.4 (9)	55.6 (10)	0.62
Current smoker [%(n)]	10.5 (2)	22.2 (4)	0.34
Diabetes Mellitus [%(n)]	10.5 (2)	27.8 (5)	0.18
Family History [%(n)]	26.3 (5)	44.4 (8)	0.25
Creatinine (μmol/l) [mean (sd)]	87.3 (± 6.7)	78.9 (± 7.8)	0.026
Previous MI [%(n)]	21.1 (4)	38.9 (7)	0.24
Previous PCI [%(n)]	26.3 (5)	38.9 (7)	0.41
Previous CABG [%(n)]	0	0	
Previous Stroke/TIA [%(n)]	5.3 (1)	0	0.32
Stable angina [%(n)]	100 (19)	100 (19)	
CCS 3/4 [%(n)]	36.8 (7)	5.6 (1)	0.021
LVEF >50% [%(n)]	73.7 (14)	83.3 (15)	0.48
Bifurcation Site			
LAD [%(n)]	84.2 (16)	83.3 (15)	0.94
LCx [%(n)]	15.8 (3)	5.6 (1)	0.32
RCA [%(n)]	0	11.1 (2)	0.14
Medina			
0,1,0 [%(n)]	47.4 (9)	44.4 (8)	0.86
1,0,0 [%(n)]	5.3 (1)	11.1 (2)	0.52
1,1,0 [%(n)]	47.3 (9)	44.4 (8)	0.86
AHA classification			
A [%(n)]	10.5 (2)	5.6 (1)	0.58
B1 [%(n)]	15.8 (3)	38.9 (7)	0.11
B2 [%(n)]	31.6 (6)	16.7 (3)	0.29
C [%(n)]	42.1 (8)	38.9 (7)	0.36
Mod/severe calcification [%(n)]	31.6 (6)	27.8 (5)	0.8

BMI-Body Mass Index; MI-Myocardial Infarction; PCI-Percutaneous Coronary Intervention; TIA-Transient Ischaemic Attack; CCS-Canadian Cardiovascular Society; LVEF-Left ventricular ejection fraction; LAD-Left Anterior Descending Artery; LCx-Left Circumflex Artery; RCA-Right Coronary Artery; AHA-American Heart Association

Table 3: Patient demographics and clinical features

3.4.2 Procedural characteristics

Table 4 shows the procedural characteristics of the trial. Predilatation was performed in all cases. The average vessel diameter measured on OCT was similar in both sizing groups. Postdilatation was performed in all proximal segments and in 59% of distal ones. The distal bifurcation segment was postdilated more often in the proximal sizing group than the distal group (p=0.031). Proximal Optimisation Technique using a 0.5mm or larger balloon than the BVS diameter was done in half the cases assigned to proximal sizing and three quarters of cases in the distal sizing group. Three patients had BVS expansion beyond the recommended 0.5mm above the BVS diameter with no adverse sequelae. The difference between the proximal and distal vessel diameters exceeded 0.5mm in those three cases. Significant proximal malapposition was present after performing POT with a balloon ≤0.5mm the BVS diameter thus necessitating more aggressive post dilatation. OCT imaging was done before BVS implantation in all cases and in 95% of cases at the end of the procedure. A single stent strategy was used in 100% of cases. SB dilatation was performed in 2 cases – the first due to angiographic pinching of the SB ostium and the second to improve flow after SB dissection.

Overall procedural success rate was 92%. There were two cases of periprocedural MI in the proximal arm. The first case was due to dissection of the side branch during manipulation of the pressure wire after BVS deployment. TIMI III flow in the SB was restored after dilatation of the BVS cell across the side branch. In the second case, the culprit was not identified. The patient had an uneventful procedure but complained of chest pain an hour after the procedure. There were no ischaemic changes on the ECG changes and the patient's symptoms settled with IV opiates. The following day, highly sensitive Troponin T was significantly elevated at 4500. The patient remained pain free and was discharged. An echocardiogram done 3 months later showed good left ventricular function. In the distal arm, there was one case of periprocedural MI due to side branch occlusion and distal main vessel dissection after scaffold deployment. TIMI III flow was achieved in the main vessel after the successful insertion of three metal stents distal to the BVS. Flow along the occluded side branch could not be restored.

	Proximal sizing	Distal sizing	p value
Lesion preparation			
Predilatation	100 (19)	100 (18)	
Max balloon diameter	2.6 (± 0.2)	2.6 (± 0.3)	0.94
Max balloon length	14.9 (± 2.8)	14.1 (± 3.7)	0.34
OFDI measurements			
Proximal RVD (mm)	3.50 (± 0.53)	3.30 (± 0.37)	0.36
Distal RVD (mm)	2.76 (± 0.44)	2.76 (± 0.55)	1
Proximal-distal RVD diameter (mm)	0.74 (± 0.59)	0.54 (± 0.49)	0.36
BVS			
Diameter (mm)	3.2 (± 0.3)	2.89 (± 0.39)	0.007
Length (mm)	23.3 (± 4.8)	21.8 (± 5.5)	0.48
Inflation Pressure (atm)	13.4 (± 3.0)	13.4 (± 2.6)	0.99
Post dilatation			
Proximal post dilatation	100 (19)	100 (18)	
POT	84.2 (16)	94.4 (17)	0.32
Balloon diameter for POT - BVS diameter	0.3 (± 0.2)	0.5 (± 0.2)	0.026
Maximal diameter (mm)	3.6 (± 0.3)	3.4 (± 0.4)	0.2
Maximal length (mm)	7.8 (± 2.4)	8.8 (± 3.1)	0.39
NC balloon	100 (19)	100 (18)	
Distal postdilatation	78.9 (15)	38.9 (7)	0.031
Maximal diameter (mm)	3.3 (± 0.9)	2.9 (± 1.2)	0.45
Maximal length (mm)	6.9 (± 1.5)	10.7 (± 3.9)	0.03
NC balloon	100 (19)	100 (18)	
Bifurcation technique			
MV stent only	100 (19)	100 (18)	
BVS SB fenestration	5.2 (1)	0	0.32
KBI	0	5.6 (1)	0.3
Conversion to Double Strategy	0	0	
Intravascular imaging			
Preimplant OCT	100 (19)	100 (18)	
Postimplant OCT	89.4 (17)	100 (18)	0.16
Procedural outcome			
Device success	100 (19)	100 (18)	
Procedural success	89.4 (17)	94.4 (17)	0.58
TIMI III flow in MV	100 (19)	100 (18)	
TIMI III flow in SB	100	88.9 (16)	0.14
SBO (end of procedure)	0	5.6 (1)	0.3

NC- Non Compliant; RVD-Reference Vessel Diameter; POT-Proximal Optimisation Technique; MV-Main Vessel; SB-Side Branch; KBI-Kissing Balloon Inflation; SBO-Side branch occlusion

Data is presented as mean (SD) or frequency (n)

Table 4: Procedural characteristics

3.4.3 Angiographic results

Table 5 shows the results of the QCA analysis. Mean side branch diameter in the cohort was 2.24 (±0.13) mm. The diameter of the ostium of the side branch was larger in the proximal group (1.85 v 1.54 p=0.02). Comparable acute luminal gains were achieved in the proximal arm (1mm) and distal arm (1.02mm). In general, luminal size was underestimated on QCA when compared to OCT measurements. The side branch ostium was narrower after the PCI procedure irrespective of the sizing strategy (average SB ostial stenosis of 44% post PCI versus 24% pre PCI. p=0.007).

	Prox (n=19)	**Distal (n=17)**	**p value**
PrePCI			
Proximal RVD (mm)	3.18 (± 0.49)	2.98 (± 0.51)	0.23
Distal RVD (mm)	2.58 (± 0.36)	2.43 (± 0.51)	0.29
MLD (mm)	1.24 (± 0.37)	1.14 (± 0.39)	0.51
DS (%)	57 (± 12)	56 (± 13)	0.62
Lesion length (mm)	18.90 (± 9.28)	15.87 (± 7.29)	0.36
SB ostial diameter (mm)	1.85 (± 0.45)	1.54 (± 0.31)	0.02
SB RVD (mm)	2.30 (± 0.46)	2.17 (± 0.25)	0.35
SB stenosis (%)	20 (± 15)	28 (± 16)	0.05
Bifurcation angle (◦)	67 (± 24)#	57 (± 23)$	0.25
Post PCI			
Proximal RVD (mm)	3.23 (± 0.38)	3.09 (± 0.35)	0.3
Distal RVD (mm)	2.77 (± 0.33)	2.54 (± 0.39)	0.05
In device MLD (mm)	2.24 (± 0.39)	2.16 (± 0.40)	0.62
In device DS(%)	20 (± 18)	16 (± 8)	0.27
SB ostial diameter (mm)	1.40 (± 0.53)	1.07 (± 0.43)	0.09
SB RVD (mm)	2.31 (±0.41)	1.81 (± 0.76)	0.14
SB stenosis (%)	38 (± 21)	51 (± 23)	0.09
*Bifurcation angle (◦)	61 (± 24)#	58 (± 25)$	0.66

*n=26, #n=13, $n=13; RVD-Reference Vessel Diameter; SB- Side Branch; DS-Diameter Stenosis; MLD-Minimum Luminal Diameter
Data is presented as mean (SD) or frequency (n)

Table 5: Angiographic characteristics before and after PCI

We were able to reconstruct the 3-dimensional geometry of the bifurcation in 72% of angiographic images. We were unable to do so in the remaining cases due to poor angiographic delineation of the bifurcation segment. Figure 23 illustrates one

of the cases. There was no significant change in bifurcation angle after PCI with a BVS compared to baseline.

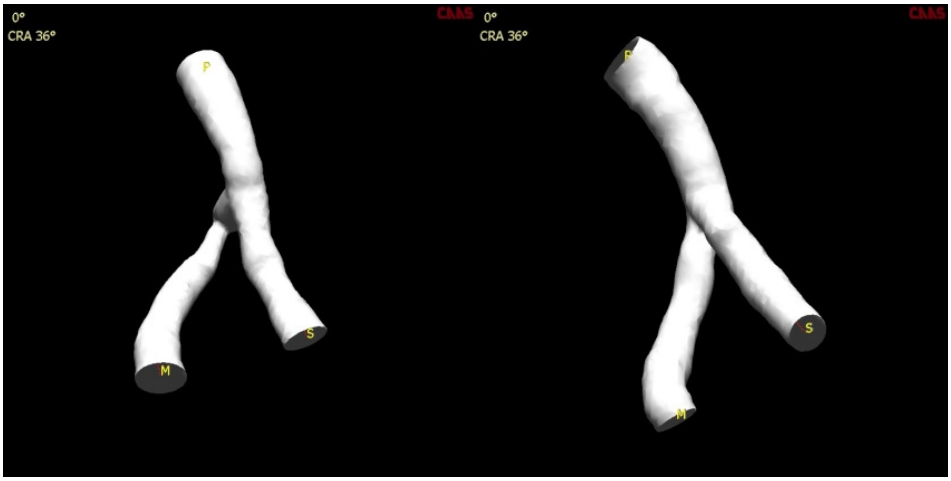

Figure 23: Example of 3D reconstruction of bifurcation anatomy in a patient randomised to proximal sizing. The letters P, M and S correspond to the proximal main vessel, distal main vessel and side branch respectively. The artery is visualised in the AP cranial radiographic projection (36 degrees angulation cranially). The prePCI image (left) demonstrates a tight stenosis within the distal segment of the main vessel. The post PCI image (right) shows an improvement in luminal size following PCI with the ABSORB BVS. Bifurcation angle (angle between the distal main vessel and the side branch) was 42º before and 36º after BVS insertion.

3.4.4 OCT analysis post implantation

Figure 24 illustrates a typical example of the OCT findings after bifurcation stenting with the ABSORB BVS.

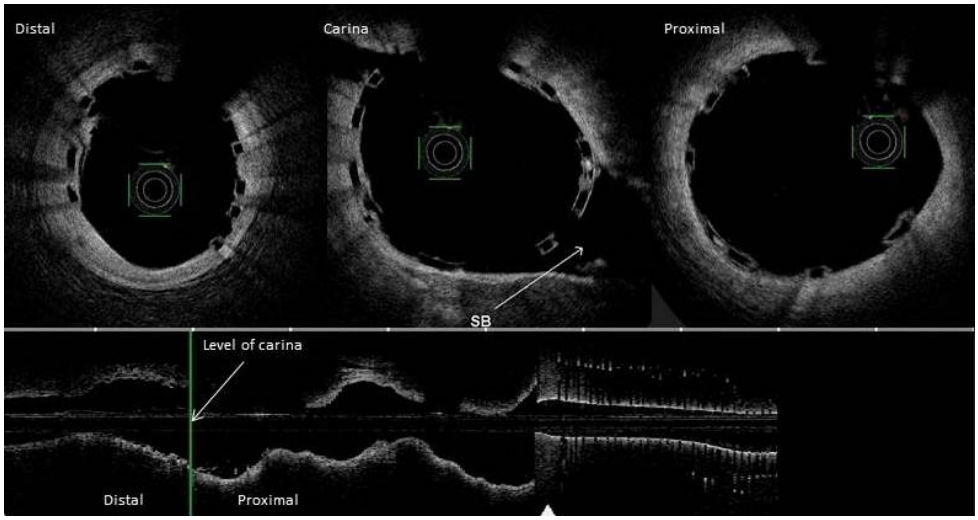

Figure 24: OCT image of bifurcation stenting of the LAD/D1 system with the ABSORB BVS. The top panel shows the cross-sectional image at each of the three bifurcation segments (distal, carina and proximal). The bottom panel shows the longitudinal view of the artery

Table 6 outlines the intracoronary characteristics in each group. Mean flow and scaffold areas were comparable in both arms.

	Proximal sizing (n=16)	**Distal sizing (n=17)**	**p value**
Scaffold level analysis			
Plaque composition			
Fibrous (%)	6.3 (1)	0	0.3
Fibroatheroma (%)	31.3 (5)	47.1 (8)	0.35
Fibrocalcific (%)	62.5 (10)	52.9 (9)	0.58
Segment analysis			
Overall			
mean flow area (mm^2)	7.09 (± 1.71)	6.70 (± 1.54)	0.56
min flow area (mm^2)	4.32 (± 1.33)	4.41 (± 1.50)	0.86
mean scaffold area (mm^2)	7.97 (± 1.80)	7.43 (± 1.65)	0.56
min scaffold area (mm^2)	6.04 (± 1.38)	5.68 (± 1.31)	0.47
mean luminal diameter (mm)	2.96 (± 0.35)	2.88 (± 0.34)	0.56
min luminal diameter (mm)	2.32 (± 0.37)	2.30 (± 0.43)	0.48
mean overall EI	0.88 (± 0.04)	0.87 (± 0.05)	0.48
mean embedment depth (μm)	43 (± 24)	32 (± 14)	0.11
Proximal segment			
mean flow area (mm^2)	8.19 (± 2.39)	7.85 (± 1.62)	0.9
min flow area (mm^2)	7.20 (± 2.22)	6.92 (± 1.60)	0.96

mean scaffold area (mm^2)	8.71 (± 2.36)	8.32 (± 1.65)	0.96
min scaffold area (mm^2)	7.73 (± 2.11)	7.33 (± 1.67)	0.9
mean luminal diameter (mm)	3.20 (± 0.46)	3.15 (± 0.32)	0.90
min luminal diameter (mm)	3.00 (± 0.45)	2.95 (± 0.34)	0.93
mean prox EI	0.88 (± 0.05)	0.89 (± 0.05)	0.81
prox embedment depth (μm)	31 (± 33)	24 (± 17)	0.3
Distal segment			
mean flow area (mm^2)	6.58 (± 1.58)	6.16 (± 1.72)	0.42
min flow area (mm^2)	5.50 (± 1.60)	5.01 (± 1.25)	0.33
mean scaffold area (mm^2)	7.40 (± 1.65)	6.87 (± 1.79)	0.35
min scaffold area (mm^2)	6.24 (± 1.76)	5.68 (± 1.31)	0.4
mean luminal diameter (mm)	2.87 (± 0.34)	2.77 (± 0.38)	0.44
min luminal diameter (mm)	2.62 (± 0.38)	2.51 (± 0.31)	0.3
mean distal EI	0.87 (± 0.04)	0.87 (± 0.05)	0.69
distal embedment depth (μm)	52 (± 32)	40 (± 18)	0.15
Scaffold disruption	0	6 (1%)	0.33
Edge Dissection			
Proximal	6.3 (1)	11.8 (2)	0.58
Distal	31.3 (5)	11.8 (2)	0.17
Post implant OFDI changing management	29 (5/17)	24 (4/17)	0.62
Malapposition needed dilatation	24 (4/17)	18 (3/7)	0.61
Dissection needed stent	6 (1/7)	6 (1/7)	0.97
Strut level analysis			
Total No. of struts analysed	17835	19367	
Total no of malapposed struts whole segment	4.8 (858)	6.4 (1231)	0.18
Proximal segment	3.1 (552)	4.5 (862)	0.23
Distal segment	1.7 (306)	1.9 (369)	0.29
Total no of significantly malapposed struts (>300 microns)			
whole segment	0.8 (142)	2.3 (451)	0.023
proximal segment	0.8 (142)	2.3 (451)	0.023
distal segment	0	0	

Data expressed as Frequency (number) or Mean (± sd)

Table 6: OCT measurements after BVS insertion

Performing an OCT after scaffold implantation changed management in a quarter of cases. In seven cases (20%), significant malapposition was evident after POT and further postdilatation with a bigger balloon was necessary. In two cases (6%), OCT identified significant distal dissections which were successfully treated with further stenting.

Sizing strategy did not have a significant impact on the overall scaffold geometry as assessed by the Eccentricity Index (p=0.48). Strut embedment was similar in both arms (p=0.11).

Figure 25 shows a typical example of proximal malapposition associated with a distal sizing strategy.

Figure 25: Image of malapposition on OCT: A 2.5x18mm ABSORB BVS was deployed in a bifurcation with a proximal RVD of 3.46mm and distal RVD of 2.26mm. POT was done using a 3.0x6mm NC balloon inflated to 20 atm. OCT imaging after POT showed significant proximal malapposition. Further proximal dilatation was done using a 3.25x6mm NC balloon inflated to 10 atm. Repeat OCT (shown above) revealed residual malapposition. We elected not to perform additional postdilatation so as not to incur the risk of scaffold fracture.

Analysis at a strut level showed that there were numerically more malapposed struts in the distal arm but this was not statistically significant (p=0.18). However, there was a higher incidence of significant proximal edge malapposition (defined as >300 microns) in the distal arm (2.3% v 0.8%, p=0.023). Even though there

was a trend towards more distal edge dissections in the proximal arm (31.3% vs 11.8%) with one patient requiring additional PCI to seal the dissection flap (Figure 26), this increased incidence did not reach statistical significance (p=0.17)..

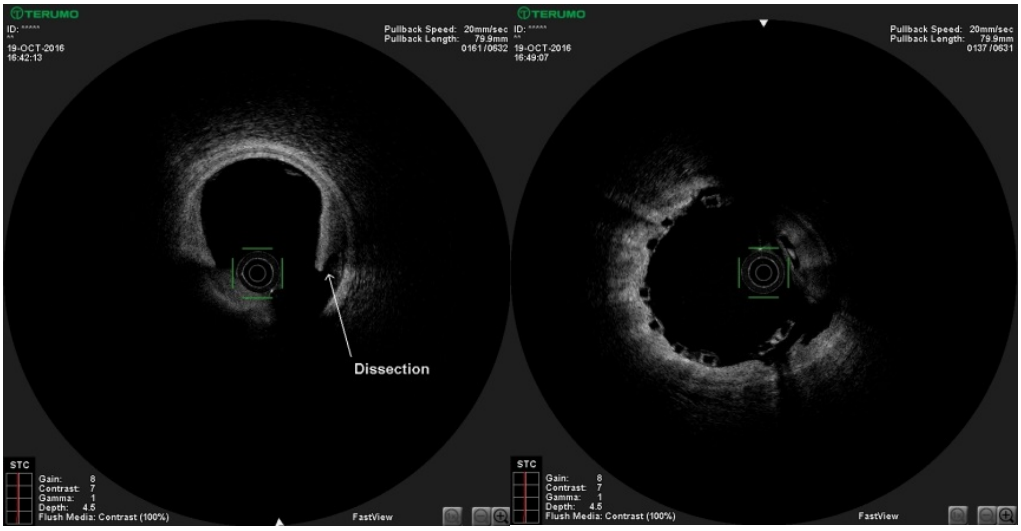

Figure 26: Image of dissection on OCT: A 3.5x18mm BVS was deployed at 16atm in a patient randomised to proximal sizing. RVD was 3.88mm proximally and 2.49mm distally. POT was done with a 4x6mm NC balloon inflated to 10atm. The image on the left shows a distal edge dissection after postdilatation. A 3.0x8mm BVS was inserted distally to seal the dissection as shown in the image on the right.

There was one case of strut fracture in the distal arm. A 2.5x23mm BVS was deployed in an artery with a proximal RVD of 2.92mm and distal RVD of 2.35mm at 16atms. POT was carried out with 3.0x6mm NC balloon inflated to 16atms. There was significant angiographic pinching of the SB ostium after POT. A 2.0x12mm balloon was inflated through the cells of the scaffold into the SB followed by KBI with the same 2.0x12mm balloon in the SB and a 3.0x6mm balloon in the main vessel. Final OCT showed a single strut fracture at the ostium of the side branch presumably due to the balloon inflation through the cell of the BVS (Figure 27).

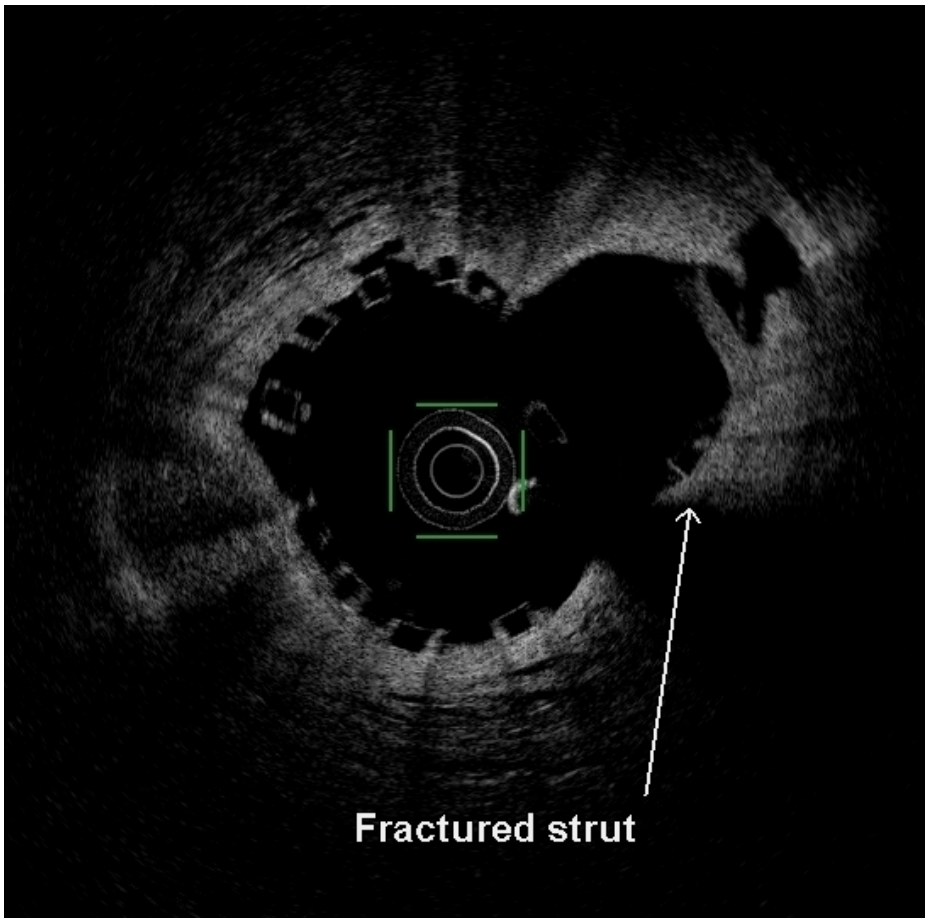

Figure 27: Image of acute scaffold fracture on OCT. The arrows shows a single strut protruding into the lumen of the side branch which is likely due to a break in the scaffold.

3.5 Discussion

The main findings of our study are: 1) Treating bifurcations with the ABSORB BVS using a provisional strategy is feasible and associated with good procedural outcomes. 2) A distal sizing strategy is associated with more significant proximal malapposition on intravascular imaging but both approaches have similar clinical complication rates. To our knowledge, this is the first prospective trial of two sizing strategies using the ABSORB BVS in coronary bifurcation.

Procedural issues

Our high rate of intracoronary imaging, predilatation and postdilatation may explain our low rates of clinical complications. We adjusted the PSP implantation protocol for use in a bifurcation anatomy. Predilatation was performed in all cases using a similar sized balloon as the distal reference vessel in order to avoid

excessive wall injury prior to scaffold deployment. Post dilatation was performed in all proximal segments. However this was not necessary in all distal segments due to the tapering nature of the bifurcation anatomy. Since the implanted scaffold was imaged at the end of the procedure, we determined the need for distal post dilatation based on the final OCT image. We demonstrated that the adoption of a PSP protocol tailored to bifurcation disease is feasible and associated with low complication rates. The comparable rates of peri-procedural complications between treatment arms is perhaps unsurprising since the methods of implantation except for BVS size were broadly similar. We originally intended to perform POT only in the distal arm as in theory, choosing a larger BVS similar based on the proximal vessel diameter would obviate the need for postdilatation. However, we found that even with proximal sizing, strut malapposition in the proximal segment was sometimes present on OCT and needed correction with POT. Part of the issue arose due to the limited sizes of scaffold commercially available. This was particularly problematic when the proximal RVD was above 3.5mm since the largest available ABSORB device was 3.5mm. Adherence to our original aim would probably have allowed us to observe a larger difference in treatment effect between the two groups but we felt that it was ethically unacceptable to leave a suboptimally deployed BVS untreated.

Abnormalities detected on OCT after scaffold deployment led to a change in management in approximately one in four cases. Other studies have confirmed the importance of intracoronary imaging even after satisfactory angiographic appearance when using the ABSORB BVS[158,159].

Embedment

Ensuring that struts are well apposed and embedded following implantation is essential to avoid complications. Firstly, the more a strut protrudes above the luminal surface, the more it can disrupt blood flow causing areas of low shear stress and higher thrombogenicity. Secondly, strut coverage is easier if the strut surface is close to the intimal layer[160]. The BVS strut has a larger surface area or 'footprint' than current metallic stents[70]. Thus the same force from balloon dilatation generates less pressure on the vessel wall with a BVS strut as opposed to a metal one resulting in less embedment. In our study, strut embedment into the arterial wall was unaffected by sizing strategy. In a subgroup analysis of the

ABSORB Japan study, plaque morphology was found to be a greater determinant of strut embedment than implantation technique[160] which may explain our result.

Geometry

The final geometry of a metal stent or scaffold exerts an influence on clinical outcomes. In a subset analysis of the ABSORB II trial, post procedural scaffold eccentricity was related to higher event rates[161]. In our study, we did not find a difference in scaffold eccentricity index between the two sizing strategies. This is perhaps not surprising. While bigger BVS were chosen in the proximal arm, the eccentricity index is a ratio of diameters and therefore less dependent on absolute scaffold dimensions. Plaque composition (in particular calcific content) affects the final geometry of a scaffold and these were similar in both arms. Finally, the method of lesion preparation with respect to balloon inflation size and pressures was comparable in both arms. One would thus expect equivalent plaque modification and consequently, the scaffold to be accommodated in a similar manner within a stenotic lesion.

Bifurcation PCI can change the 3-dimensional structure of the bifurcation segment[162]. Bifurcation with metal stents 'stiffens' the artery and typically decreases the angle between the distal main vessel and side branch. This phenomenon has been observed after both single and complex stenting[163]. The resulting artificial configuration may adversely affect local haemodynamics leading to restenosis long term. In contrast to studies with metal stents, we did not observe any significant change in bifurcation angle before and after PCI with BVS[164]. This may be due to the more conformable nature of BVS allowing the natural architecture of the bifurcation to be better preserved particularly in a provisional strategy[165].

Edge dissections

Contrary to our expectations, we did not observe a statistically significant increase in distal edge dissections when using a bigger scaffold in a proximal sizing strategy. In both groups, the balloon size and inflation pressures used for post dilatation of the distal bifurcation segment were similar. This may be more important than actual scaffold size in determining the risk of damage to the distal vessel. Interestingly, more post dilatation was performed within the distal segment

in the proximal sizing group. The fact that post dilatation was guided by OCT may explain that unusual occurrence. Our reported dissection rate of 30.3% is comparable to the 36.5% rate reported in the ABSORB B OCT substudy[166]. The image resolution of OCT imaging allows visualisation of the intracoronary environment to an unprecedented level of detail. One of the consequences is a greater ability to diagnose small dissection flaps, which hitherto would have gone unnoticed on angiography or even IVUS. Indeed reported edge dissection rates from IVUS are around 10%[167] but climb up to 25-40% with OCT in similar patient populations[168]. The clinical relevance of edge dissections detected on intracoronary imaging is still unclear. In study using IVUS, there was no difference in clinical outcomes in patients with edge dissection compared to those without[169]. Conversely, other studies have found a link between the presence of these dissections and development of subacute stent thrombosis[170]. Even though the ABSORB B OCT cohort had a high dissection rate, only 1 adverse event (periprocedural MI) was directly attributed to a dissection. As intravascular imaging especially OCT is increasingly utilised in the future, the exact clinical significance and optimal management of small edge dissections should become clearer.

Malapposition:

In a study with drug eluting stents in patients with stable angina, a malapposition distance of >300 μm showed the highest likelihood of delayed strut healing and persistence on follow up imaging[171]. Conversely, another study with metal stents found that struts with a malapposition distance of <270 μm are more likely to be apposed at 9 months[172]. Based on these observations, we chose a cut off of 300 μm to define a significantly malapposed strut. The greater malapposition burden observed with the smaller BVS in the distal arm is not unexpected. The same effect occurs in metal stents. However in the latter case, the discrepancy in main vessel size can be overcome by liberal post dilatation proximally. On the other hand, the safe expansion limit of the ABSORB BVS restricts the magnitude of postdilatation and by proxy the ability to correct proximal malappostion. The significance of ISA is still contentious. Acute ISA has been linked to delayed or absent strut coverage at follow-up[9], both of which are known risk factors for stent thrombosis. Other studies have failed to show a significant relationship between

either ISA after DES implantation or at follow up and adverse outcomes[173]. The small rate of adverse events with current generation of stents makes it difficult to precisely quantify the risk of ISA. The answer should become clearer with more widespread use of intravascular imaging.

Side branch stenosis:

Our side branch occlusion rate of 2.7% is similar to reported rates in studies using the ABSORB BVS in bifurcations[42-44]. Given their large strut width (190.5 μm for the 3.0mm and 215.9 μm for the 3.5mm BVS), there is concern that BVS use in bifurcations can lead to a higher rate of side branch occlusion than conventional metal stents. The largest analysis of small side branch occlusion was performed in a cohort from the ABSORB-Extend registry[174]. An analysis of 1209 side branches with a mean diameter of 1.18mm revealed an occlusion rate of 6%. Larger side branches (>2mm) seem to have a lower risk of impairment with reported rates of occlusion ranging from 0% to 3.7%[42,175,176]. Whether side branch occlusion (SBO) due to BVS is associated with significant myocardial injury is less clear. In our study, only 2 cases of periprocedural MI (5.4%) were directly attributable to side branch compromise. However we did not routinely measure cardiac enzymes after PCI and the degree of perprocedural MI may have been underestimated in our study. Two studies have investigated the prevalence of periprocedural MI (PMI) due to side branch occlusion in the context of BVS implantation. Tanaka et al. analysed 729 jailed side branches (of which 14.4% were >2mm) and found a PMI rate of 18.8% due to SBO[175]. Muramatsu et al. found that small side branches were more likely to occlude causing a periprocedural cardiac enzyme rise if jailed by the thicker ABSORB scaffold[174].

In our study, ostial side branch narrowing was worse after BVS deployment. With metal stents, plaque shift and carina shift following MV stenting have been implicated in side branch compromise[177]. Stent implantation redistributes plaque both axially and longitudinally within the vessel wall. There is a greater tendency for plaque to shift away from the lesion towards the distal segment than proximally[178]. This is particularly relevant to bifurcations as plaque will move into the side branch more easily if the side branch is located distal to the lesion. Plaque morphology also influences the degree of SB stenosis. Lipid rich plaques especially in the proximal main vessel have been associated with a higher rate of

SBO[179]. One plausible explanation is that softer lipid plaques are more easily displaced than hard calcific plaques during stent insertion. The same mechanisms outlined above are likely to be responsible for the deterioration in SB stenosis observed after BVS implantation. However, the clinical significance of this finding is unclear. An angiographically tight lesion is less likely to be physiologically significant if present at the ostium of the side branch compared to the main vessel. In cases where the narrowing is <75%, almost all SBs will have negative pressure wire studies[180]. Possible explanations include the reshaping of the circular ostium into a slit like configuration which when visualised in a particular angiographic angle shows it in the worst possible light, slow flow after PCI, generation of turbulent flow impeding contrast filling and border artefact[55].

Scaffold fracture:

Our single case of scaffold fracture was most likely caused by our attempt to dilate the scaffold across the side branch in order to improve flow. Reported incidences of acute scaffold disruption range from 3.9 to 5.8%[69]. They have been linked to the occurrence of scaffold thrombosis. The safe limit to which the cell of a BVS can be dilated has been investigated in bench studies[38]. Strut fracture did not occur when a 2.0mm balloon is inflated up to 14atm through the cells of a 3.0 and a 3.5mm BVS. When mini-Final Kissing Balloon Inflation (mini-FKBI) was performed using two 3.0mm NC balloons in scaffolds of the same size, fractures occurred beyond an inflation pressure of only 5atm. One study has specifically analysed the effect of side branch dilatation in BVS in vivo[181]. It involved a retrospective analysis of a cohort of 49 patients in whom SB dilatation was done after BVS implantation in the MV because of either compromise in SB flow or visually severe SB stenosis. Strut fractures were observed on OCT in 6% of the cases and occurred with the inflation of a 2.5mm balloon to 9-10atm. The diameter of the implanted BVS had no bearing on the likelihood of scaffold damage. At a mean follow up of 14 months, the overall TLR and ST rate in the group were 4% and 2% respectively but interestingly none of the cases with scaffold damage were involved.

Our case highlights the undesirable situation where the methods needed to optimise flow, overlap with those that can fracture the scaffold. The threshold for damage appears to be lower in vivo than predicted by bench studies. Caution must

be exercised when dilating through a BVS strut and we would recommend doing it only if there is significant compromise of blood flow in the daughter vessel.

3.6 Limitations

Since this was a pilot study, it was not powered to detect statistically significant differences. Cardiac enzymes were not routinely measured and thus periprocedural MI may have been underdiagnosed in our cohort. As previously mentioned, we did not adhere to our original plan of performing POT only in the distal sizing arm as we were guided by the intracoronary scaffold appearance during each case for optimal expansion and apposition. This may have mitigated treatment effects between the two arms. The limited availability of BVS sizes (2.5, 3.0 and 3.5) restricted their usefulness in our trial. In 4 cases randomised to distal sizing, the largest BVS available (3.5mm) was similar to the diameter of the distal vessel. In 8 cases, the difference between stent diameter and proximal and distal diameters were the same. Thus scaffold choice was independent of randomisation in the aforementioned cases.

3.7 Conclusion

We examined the effect of sizing strategy on immediate imaging and procedural outcomes in coronary bifurcations using the ABSORB BVS. The provisional approach with a modified 'PSP' strategy is safe and feasible when using the ABSORB BVS in bifurcations. While procedural complication rates from the two sizing strategies are comparable, the proximal sizing strategy results in less significant malapposition and may be more advantageous. The risk of underdeployment with scaffold malapposition in distal sizing needs be carefully weighed against the risk of overdeployment with scaffold damage in proximal sizing. Larger studies are needed to corroborate our findings.

4 9-month clinical and imaging outcomes of the Absorb in Bifurcation Coronary (ABC-1) study

4.1 Introduction

The long term performance of the ABSORB BVS in bifurcations has not been assessed in the context of a trial. Using a resorbable scaffold to treat bifurcation lesions has theoretical benefits in the long term. Firstly, the obstruction due to struts at the orifice of the side branch (SB) may only be a temporary issue and blood flow into the SB could improve over time. Secondly, the hypothetically higher thrombogenic risk posed by uncovered struts over a side branch orifice is potentially curtailed following resorption of the scaffold. However whether these putative advantages translate into better clinical outcomes is uncertain. The bulkier struts may impede blood flow across the side branch leading to SB restenosis. Similarly re-endothelialisation and neointimal coverage over the SB ostium may be impaired thereby increasing the risk of thrombus formation. In addition, the more aggressive implantation technique warranted in bifurcation lesions may have a negative effect on long term scaffold integrity and vascular healing. Appropriate scaffold size selection may mitigate some of these adverse effects.

4.2 Aim

- To compare the nine month clinical and imaging outcomes between two sizing strategies using the ABSORB BVS to treat coronary bifurcations.

4.3 Methods

4.3.1 Study population

The cohort consisted of seventeen patients recruited in the ABC-1 trial on whom nine month follow up data was available by June 2017. The clinical and imaging endpoints at follow up have been described in chapter 2.

4.3.2 Angiographic assessment

QCA analysis was performed on the treated segments post procedure and at follow up in matching angiographic frames. The details of the analysis are outlined in chapter 2.

4.3.3 Optical Coherence Tomography

All patients had intravascular OCT imaging at 9 month follow up. Analysis was performed offline using proprietary software (Terumo Corporation, Toyko, Japan). The main quantitative measurements have been described in chapter 2.

4.3.4 Statistical analysis

Test for normality, using the Shapiro-Wilk test, revealed that neither angiographic nor OCT parameters had a Gaussian distribution. Comparison between the two treatment arms was done using Mann-Whitney test for continuous data and Chi-squared test for categorical variables. Overall comparison of serial angiographic measurements and paired OCT parameters was made using the Wilcoxon signed-rank test.

4.4 Results

4.4.1 Clinical outcome

Table 7 shows the primary and secondary clinical endpoints at 9 months.

Endpoint	Total (n=17)	Proximal (n=9)	Distal (n=8)
Primary			
Composite (Death, MI, ST and TVR)	2 (11.8)	2 (22.2)	0
Secondary			
Death	0	0	0
MI	2 (11.8)	2 (22.2)	0
ST	0	0	0
TVR	0	0	0

MI-Myocardial Infarction, ST-Scaffold Thrombosis, TVR-Target Vessel Revascularisation
Data expressed in number of patients (%)

Table 7: Primary and secondary clinical endpoints at 9 months

All patients were on dual antiplatelet treatment at follow up. There were no cases of scaffold thrombosis. Our MACE rate was driven solely by two cases of periprocedural myocardial infarction (PMI) in the proximal arm. These two cases have been described in detail in chapter 3. In brief, PMI was caused by SB

dissection in one case while no obvious culprit was identified in the other. Figure 28 shows the post procedural and follow up angiographic image in the case of side branch dissection.

Figure 28: Comparison of post procedural (left) and follow up (right) angiographic images of a case with side branch dissection. The side branch is shown by the arrow. At follow up, the false lumen was sealed with minimal residual flow. Ostial side branch stenosis was 55% on QCA.

4.4.2 Quantitative Coronary Angiography

Table 8 shows the results of QCA analysis. There were no cases of instent restenosis. Average late luminal loss for the cohort was 0.16 (±0.16) mm. All side branches were patent with TIMI III flow at follow up. The percentage of side branches with binary stenosis decreased from 35% post BVS implantation to 24% at 9 months in the study population.

On follow up, the degree of ostial SB narrowing remained similar compared to postprocedural values in the both groups. Sizing strategy had no effect on the degree of residual stenosis within the main vessel.

	Prox (n=9)	Distal (n=8)	p value
Post PCI			
Proximal RVD (mm)	3.27 (± 0.41)	3.13 (± 0.30)	0.54
Distal RVD (mm)	2.73 (± 0.31)	2.65 (± 0.45)	0.96
In device MLD (mm)	2.26 (± 0.38)	2.21 (± 0.42)	0.42
In device DS(%)	19 (± 12)	17 (± 10)	0.09
SB ostial diameter (mm)	1.42 (± 0.59)	1.14 (± 0.27)	0.89
SB RVD (mm)	2.37 (± 0.45)	2.09 (± 0.25)	0.23
SB stenosis (%)	40 (± 19)	46 (± 14)	0.89
Follow up			
Proximal RVD (mm)	3.07 (± 0.42)	2.79 (± 0.31)	0.28
Distal RVD (mm)	2.66 (± 0.36)	2.37 (± 0.41)	0.24
In device MLD (mm)	2.28 (± 0.48)	1.85 (± 0.33)	0.37
In device DS(%)	19 (± 12)	23 (± 11)	0.14
SB ostial diameter (mm)	1.33 (± 0.32)	1.38 (± 0.45)	0.54
SB RVD (mm)	2.30 (± 0.44)	1.95 (± 0.39)	0.17
SB stenosis (%)	40 (± 22)	29 (± 18)	0.82
Δ (postPCI - fup)			
Proximal RVD (mm)	0.20 (± 0.32)	0.33 (± 0.31)	0.17
Distal RVD (mm)	0.07 (± 0.23)	0.28 (± 0.36)	0.05
In device MLD (mm)	-0.02 (± 0.20)	0.36 (± 0.28)	0.37
In device DS(%)	0 (± 6.46)	-6 (± 11)	0.82
SB ostial diameter (mm)	0.09 (± 0.64)	-0.24 (± 0.51)	1
SB RVD (mm)	0.07 (± 0.26)	-0.39 (± 1.17)	0.89
SB stenosis (%)	0 (± 21)	17 (± 19)	0.61

*n=8, #n=3, $n=5, RVD-Reference Vessel Diameter, MLD-Minimum Luminal Diameter, DS-Diameter Stenosis, SB-Side Branch#

Data expressed as Mean (± sd)

Table 8: QCA analysis post PCI and at follow up. The change between procedural and follow up values is shown as Δ

4.4.3 Optical Coherence Tomography

4.4.3.1 General

Paired post procedural and follow up OCT imaging was available in 14 patients. In the proximal arm, two patients did not have post procedural OCT. In the first case, the OCT catheter would not go past the BVS. The second case was complicated by SB dissection and OCT was not performed in order to minimise

injection of contrast. At follow up, one patient had suboptimal OCT image quality. These three cases were excluded from analysis.

Quantitative measurements of device and lumen dimensions in the overall group are presented in Table 9. In line with the angiographic findings, mean lumen size in the main vessel was generally smaller on follow up.

	Baseline	Fup	p value
In segment MLD (mm)	2.29 (± 0.32)	2.26 (± 0.37)	0.58
In segment MLA (mm2)	4.38 (± 1.19)	4.10 (± 1.42)	0.25
In segment MeLD (mm)	2.94 (± 0.32)	2.75 (± 0.34)	0.005
In segment MeLA (mm2)	6.99 (± 1.63)	6.11 (± 1.57)	0.004
Mean SA (mm2)	7.84 (± 2.02)	7.73 (± 1.90)	0.22
Minimum SA (mm2)	5.85 (± 1.42)	5.97 (± 1.96)	0.62
NIA per frame (mm2)		1.50 (± 0.52)	
Neointimal burden (%) *		19.5 (± 6.1)	

*MLD-Minimum Luminal Diameter, MLA-Minimum Luminal Area, MeLD-Mean Luminal Diameter, MeLA-Mean Luminal Area, SA-Scaffold Area, NIA-Neointimal Area

Data expressed as mean (± sd)

Table 9: Comparison of OCT characteristics at baseline and follow up.

4.4.3.2 Strut coverage

Strut coverage was assessed at 1mm interval over 5mm on either side of the side branch. At the bifurcation level, each frame where the side branch was visible was analysed. Table 10 shows the neointimal coverage along the three segments.

	Proximal sizing	Distal sizing	p value
Proximal segment			
No of struts analysed	250	275	
NIT (μm)	72 (± 25)	96 (± 63)	0.07
% uncovered struts (n)	3.2 (8)	0.7 (2)	0.001
SB segment			
No. of struts analysed	700	754	
Average NIT per strut (μm)	71 (± 14)	98 (± 42)	0.06
Average NIT per NASB strut (μm)	65 (± 16)	86 (± 56)	0.12
Average NIT per strut opp SB (μm)	73 (± 17)	102 (± 46)	0.05
% of NASB struts with bridge (n)	50 (350)	40 (302)	0.16
% of uncovered struts (n)	7.2 (50)	1.1 (8)	0.001
Distal segment			
No of struts analysed	327	315	
Distal segment NIT (μm)	96 (± 30)	100 (± 39)	0.67
% uncovered struts (n)	2.4 (8)	0.6 (2)	0.02

NIT-Neointimal Thickness, NASB-Non Apposed SB strut, opp- opposite
Data expressed as mean (± sd), % (n) or number

Table 10: Comparison of strut coverage according to sizing.

There were more uncovered struts with a proximal sizing strategy. This was observed in all three sections of the bifurcation segment. Struts in the bifurcation segment were separated into two groups for further analysis– those lying across the SB ostium termed non opposed SB struts (NASB) and those along the arterial wall. NASB struts had lesser intimal coverage independent of the sizing strategy (p=0.04) (Figure 29).

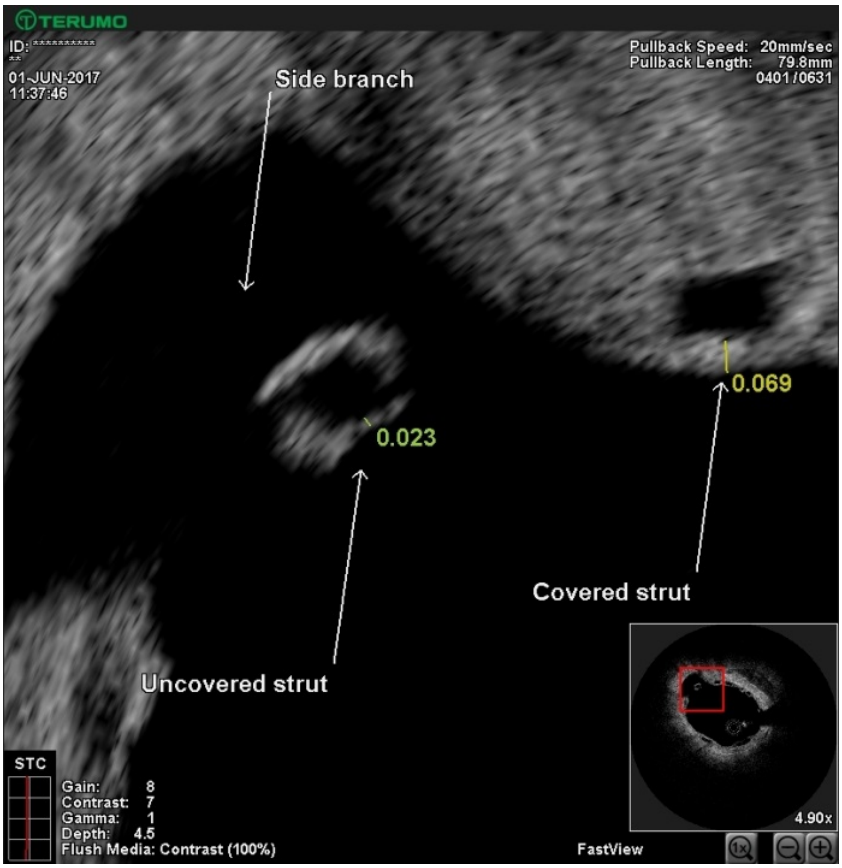

Figure 29: Neointimal coverage of struts in the segment containing the side branch. NIT is less for NASB strut (23 µm) compared to the strut opposite the SB (69 µm).

Approximately half of the NASB struts were connected to the main vessel with a tissue bridge as shown in Figure 30.

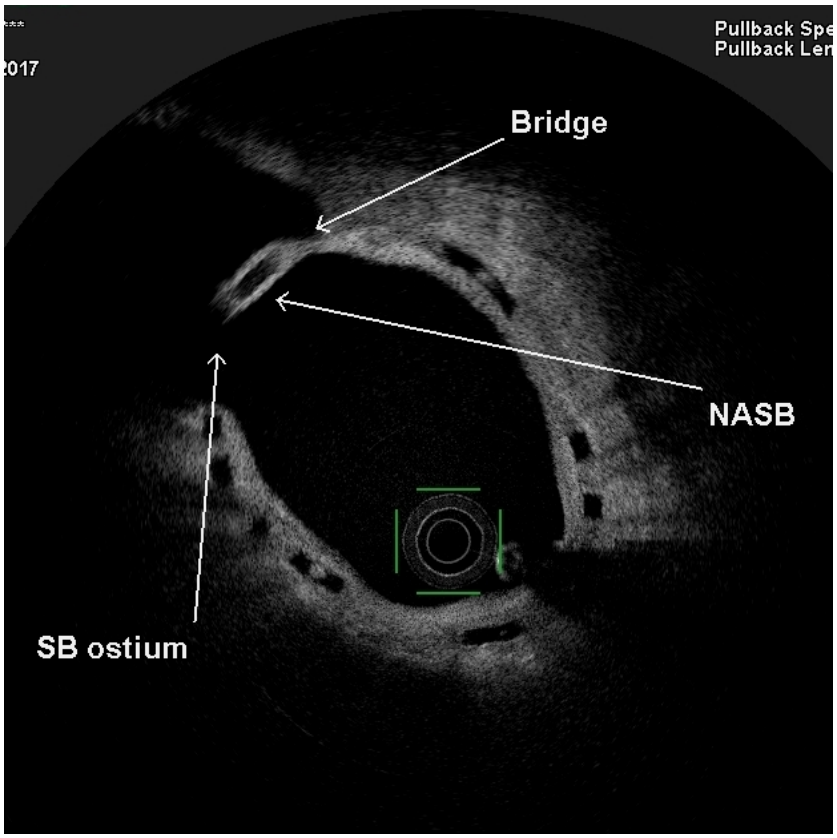

Figure 30: OCT image of a connecting bridge linking a NASB strut to the main vessel wall.

4.4.3.3 Malapposition

Strut apposition was assessed in 16 patients on follow up OCT. Malapposed struts were present in 50% of cases in the proximal group (4/8 cases) and in 37.5% (3/8 cases) in the distal arm at follow up. Analysis of paired post procedural and follow up OCT images was performed in 13 cases (Table 11).

	Proximal (n=5)	Distal (n=8)
Baseline		
Patient level analysis		
No of lesions with >1 malapposed strut	100%	100%
Strut level analysis		
Total no. of malapp struts	223	699
Average no. of malapp struts per case	45	87
No. of malapp struts that become apposed at fup	212 (95%)	664 (95%)
Fup		
Patient level analysis		
No of lesions with >1 malapposed strut	2 (40%)	3 (38%)
No of lesions with persistent ISA	1 (20%)	2 (25%)
No of lesions with late ISA	2 (40%)	2 (25%)
Strut level analysis		
Total no. of malapposed struts	55	208
No. of struts with late malapposition	44 (80%)	173 (83%)
No. of struts that were malapposed at baseline	11 (20%)	35 (17%)

ISA: Incomplete stent apposition
Data expressed as number (%)

Table 11: Comparison of malapposition between sizing strategies

95% of struts that were malapposed after the procedure were apposed by 9 months. At a patient level, the incidence of late acquired ISA (LAISA) and persistent ISA in the whole group was 31% and 23% respectively. The contribution of late ISA to overall malapposition burden was much higher at a strut level analysis due to a significant LAISA in one patient. Positive vessel remodelling with luminal enlargement caused late malapposition in 3 cases while 1 case of LAISA was due to late scaffold recoil. Given the small numbers in each sizing arm, we could not determine the influence of sizing strategy on malapposition. Figure 31 shows a typical case with late malapposition caused by adaptive vessel remodelling.

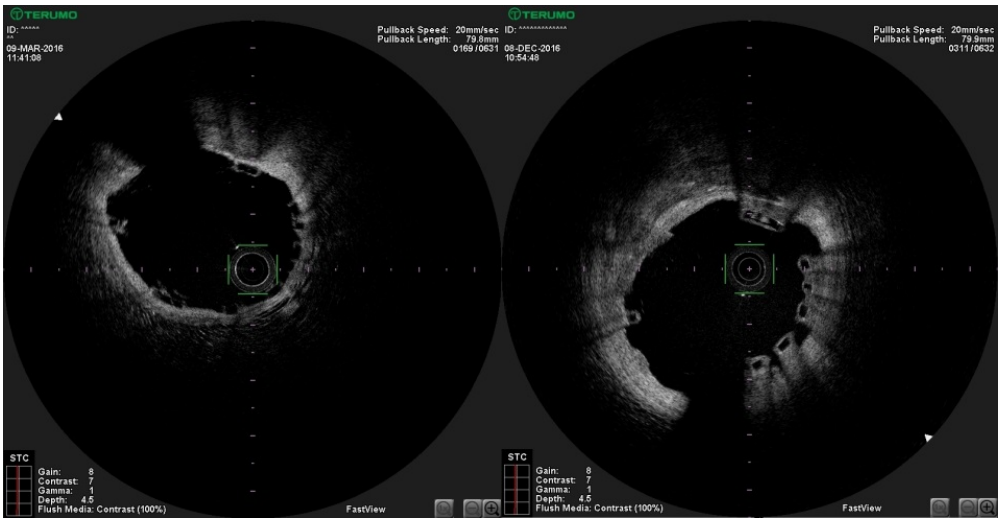

Figure 31: Post procedural (left) and fup (right) OCT images with LAISA- The postprocedural luminal and scaffold areas were 3.14 mm2 and 3.20mm2 respectively. On follow up imaging, strut malappostion was evident (12 to 6 o'clock). The follow up luminal and scaffold areas were 3.55mm2 and 3.25mm2 respectively i.e the scaffold area was comparable to the postprocedural value while the lumen area had increased. Thus in this case, LAISA was caused by positive vessel remodelling

4.4.3.4 Scaffold discontinuity

Overhanging or stacked struts were seen in 23.5% of cases (2 patients in each group) at 9 months. Most of the struts involved were covered with neointimal tissue (Table 12). Only 4 out of 47 discontinuous struts were both uncovered and malapposed. Comparison with post procedural images did not reveal any scaffold damage after implantation at the site of the subsequent discontinuity.

	Proximal	Distal
No. of cases	2 (22)	2 (25)
Strut level analysis		
Total number	17	39
Covered/apposed (%)	2 (11.8)	25 (64.1)
Covered/malapposed (%)	11 (64.7)	13 (33.3)
Uncovered/apposed (%)	1 (5.9)	0
Uncovered/malapposed (%)	3 (17.6)	1 (2.6)

Data expressed as n (%)

Table 12: Coverage of discontinuous struts

Figure 32 illustrates one of the cases with marked protrusion of the strut within the lumen along with the corresponding image immediately after BVS implantation.

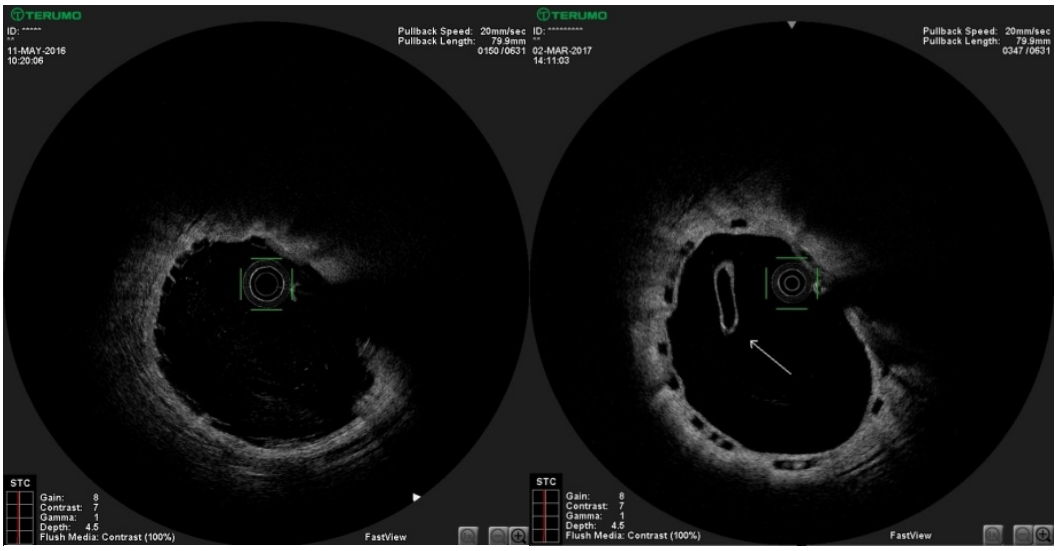

Figure 32: Paired postprocedural (left) and follow up (right) OCT images with late scaffold discontinuity. There is no apparent fracture or abnormality on the postprocedural image.

Scaffold discontinuity was sometimes accompanied by late scaffold recoil causing concomitant malapposition as shown in Figure 33.

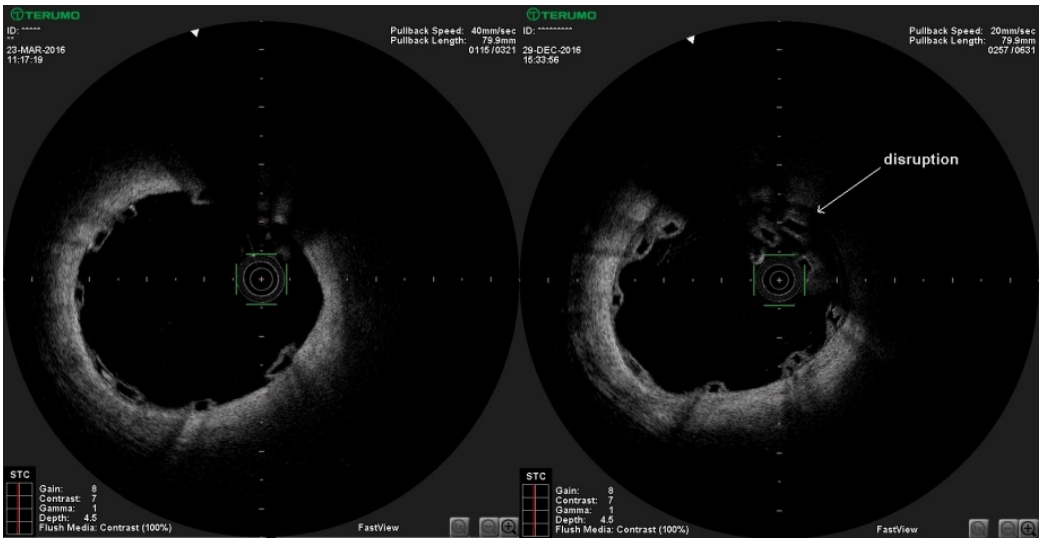

Figure 33: Paired OCT images illustrating the co-existence of LAISA and scaffold discontinuity. Post procedural scaffold area was 4.06mm2 compared to 3.67mm2 at follow up showing late scaffold recoil to be the mechanism of LAISA and possibly scaffold disruption.

4.4.3.5 Evaginations

Coronary evaginations were seen in about half the follow up cases (4 cases in each arm). Figure 34 illustrates one such example. There were no cases of coronary aneurysm.

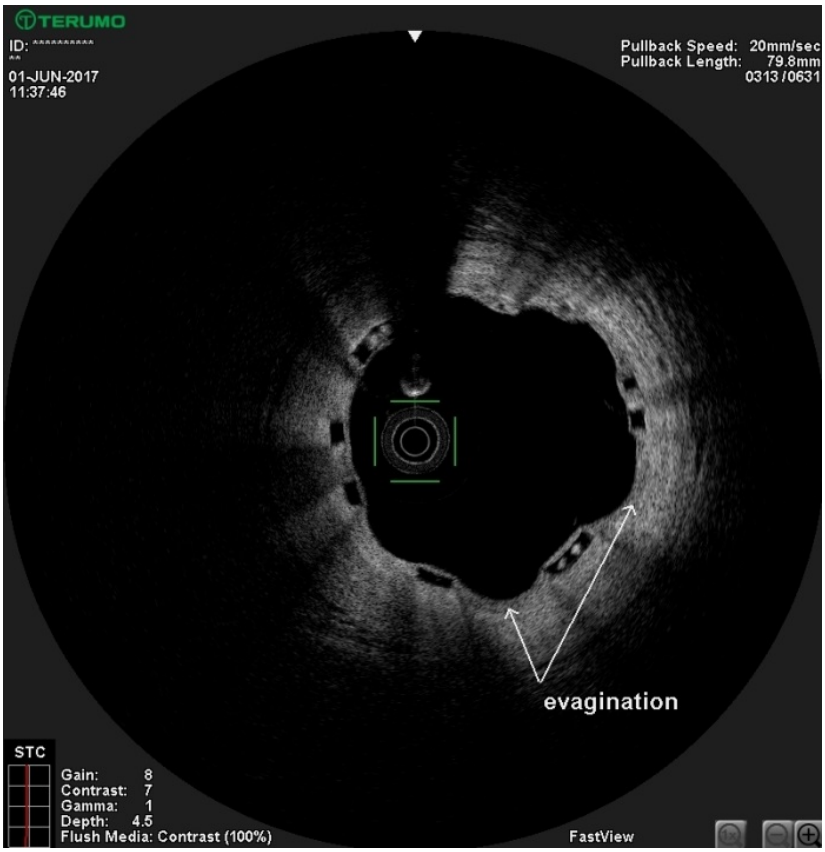

Figure 34: Multiple coronary evaginations at 9 months

Rarely, intraluminal masses were present within coronary evaginations as shown in Figure 35.

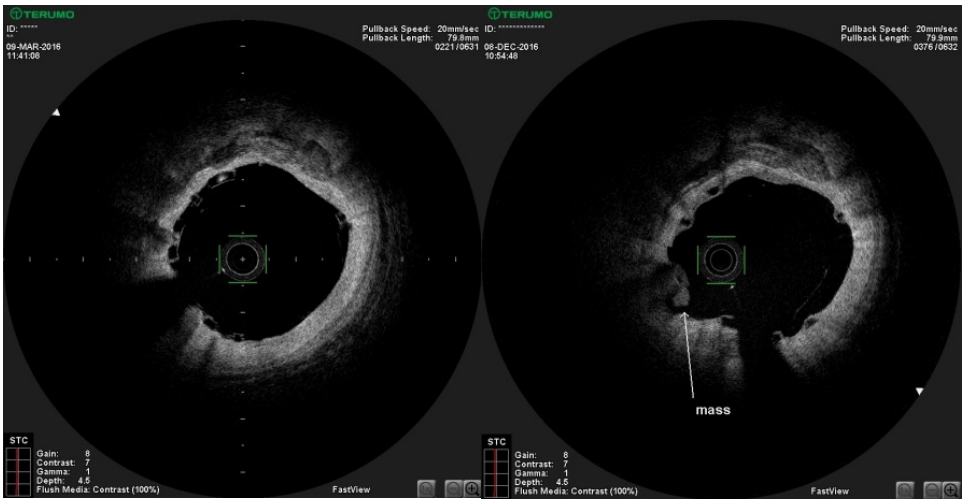

Figure 35: Paired OCT images with coronary evagination and thrombus. The image on the left was obtained immediately after the procedure while the one on the right was obtained at 9 months. There is an outward bulge at 7 o'clock at follow up with an intraluminal mass abutting a strut. The latter could represent an organised thrombus.

4.5 Discussion

4.5.1 Clinical outcomes

Our clinical event rates are comparable with previously published data. The ABSORB trials reported 1 year event rates between 3.4-7.8%[182-184]. MACE rates of up 16.1% at 1 year have been reported in registries where the ABSORB BVS has been used in bifurcations[45]. To date, the largest report on the use of BVS in bifurcations comes from a subset analysis of the European multi-centre GHOST EU registry[46]. 27% of patients from the registry (totalling 302 bifurcations) had treatment of a bifurcation lesion involving a side branch>2.25mm on visual assessment. The provisional approach of main vessel stenting was used in 86% of bifurcations with intravascular imaging use in under a quarter of cases. At 1 year, the MACE and TLR rates were 9.0% and 2.5% respectively.

We did not have any case of scaffold thrombosis despite using the scaffold in a higher risk group than other RCTs have traditionally addressed. Most trials have confined the use of BVS to relatively simple lesions and in particular have excluded bifurcations. Registry data show that scaffold thrombosis rates in bifurcations reside between 1.1% and 2.5% at 1 year which are comparable to metal stents in bifurcation treatment[42,43]. Firm adherence to dual antiplatelet

treatment (DAPT) appears to be critical in reducing the risk of ST as illustrated by the results of the Giessen registry, where an inordinately high rate of ST (8.1%) was due to premature discontinuation of DAPT in all cases[45]. Although MACE and TLR rates are higher compared to metallic DES, outcomes can be improved with a meticulous implantation protocol with appropriate pre-dilatation, sizing and post-dilatation[27]. Correct deployment strategy and liberal use of intracoronary imaging may be the key in curbing the ST rates[185]. Seth et al. recently presented the long term clinical follow up of patients with B2/C complex lesions treated with PSP implantation technique and reported a 0.6% incidence of scaffold thrombosis at 3 years[186]. The blinded, pooled interim outcomes of ABSORB IV were presented at ACC earlier this year[187]. When compared to ABSORB III, more post dilatation was done (83% versus 66%) while fewer BVS were implanted in small vessels of <2.25mm diameter on QCA (4% versus 19%). Pooled ST rates at 1 year reflect this more careful approach with a reduction to 0.5% from 1.1% in ABSORB IV. To our knowledge, we have the one of the highest rates of intravascular imaging use and adherence to PSP technique published in the literature which may explain our ST result.

4.5.2 Neointimal response

4.5.2.1 Side branch

Our observation of poorer neointimal coverage in NASB compared to those opposite the side branch is consistent with previously published data from the ABSORB B cohort[148]. In a post hoc analysis, the percentage of uncovered struts across jailed SB was 4.8% compared to 0.4% on the opposite wall 1 year after BVS implantation. This difference was even more pronounced when large side branches were considered (8.7% v 0.3%). Over half of the NASB struts in our study had a connecting tissue bridge to the main vessel. Imaging studies using OCT have shown that tissue can grow across the struts overlying side branches leading to the formation of a 'neocarina'[188]. As the struts resorb, this 'neo carina' assumes the configuration of a network of thin tissue bridges determined by the size of the SB orifice. In an OCT analysis of 24 jailed orifices from the ABSORB B trial, Onuma et al. found that the ostial area decreased between 1 and 2 years but increased therafter[189]. The 5 year followup data was recently presented at the European Bifurcation Club conference[190]. Small compartments delineated by the

struts across the SB were fully incorporated within the neointima. Interestingly, these areas were associated with a regression of neointimal tissue leading to an overall increase in the ostial area. However neointimal bridges across large compartments remained despite resorption of the struts. This effect could be exploited when dealing with large side branches by routinely performing low pressure side branch dilatation in order to create one large and a few small compartments. It will be worth investigating this strategy in future trials.

4.5.2.2 Main vessel

The influence of sizing strategy on strut coverage in the main vessel is an interesting finding. The use of a larger BVS in the proximal group may have resulted in under-deployment or over-expansion since the vessel diameters in both groups were comparable. The association between these mechanical factors and scaffold thrombosis has previously been discussed and may in part be related to a delay in neointimal coverage[69]. Another plausible hypothesis is the occurrence of higher flow disturbance and lower WSS with proximal sizing. The thicker rectangular struts of the ABSORB BVS typically generate more flow disturbance creating a lower wall shear stress area within the scaffold[191]. An underdeployed scaffold is likely to induce greater reduction in WSS. A low WSS micro-environment can inhibit endothelial cell proliferation thus delaying re-endothelialisation of the strut surface. Biomechanical modelling of a provisional strategy using the ABSORB BVS would be useful to confirm our hypothesis.

4.5.3 Complications

4.5.3.1 Malapposition

Our incidence of malapposition is larger than those in previous studies. The incidence at 6 months was 0.8% (strut level) in the ABSORB B OCT substudy[148] and 7.8% (patient level) at 2 years in the ABSORB Japan trial[192]. Our larger rate of malapposition is most likely due to the fact that BVS were used in bifurcations in our study. In line with published data[148], we observed that most of the malapposed struts at baseline became well apposed at follow up.

The contribution of late ISA to the overall malapposition load at follow up was relatively high in our study with late ISA accounting for 57% of total ISA at a patient level and ~80% at a strut level. In contrast, malapposition at follow up in

ABSORB B was more often due to persistent ISA (81%) [148]. The ABSORB Japan study had a relatively higher proportion of LAISA (40%) but persistent ISA was still the main cause of malapposition[192]. Various mechanisms have been implicated in the generation of late ISA including positive vascular remodelling with luminal enlargement, dissolution of thrombus behind the struts after implantation, cytotoxic drug-induced vessel wall retraction and chronic recoil of the stent[193]. While it is not clear why the incidence of late ISA is higher in our study, we can propose a few hypotheses. The difference in implantation technique in bifurcations compared to relatively straight coronary segments may be important. Bifurcation stenting imparts different levels of wall stress in the proximal and distal segments which influence adaptive remodelling[194]. The different mechanical pressures experienced by the scaffold in bifurcations may also increase their likelihood of late recoil hence late ISA. The fate of late acquired scaffold malappostion is not clear. IVUS imaging at 3 years in the ABSORB B substudy showed that cases of late ISA detected at 1 year had resolved[195]. However, three new cases (6%) developed in between 1 and 3 years. The clinical significance of LAISA is currently unknown and requires long term imaging and clinical follow up.

4.5.3.2 Scaffold discontinuity

During the second phase of hydrolytic degradation, structural discontinuities are expected as the amorphous tie chains binding the crystalline domains are broken[22]. The orientation of crystallites during polymer processing determines the degree of radial or axial strength. Circumferentially oriented crystallites give radial strength to the hoops while axially oriented ones convey strength to the connectors. As radial strength is a key design feature, priority is usually given to circumferential orientation so that the connectors are usually more susceptible to cracks. The location of structural discontinuities is also dependent on the external stresses imparted by the surrounding tissue at that point. Scaffold discontinuities may have an iatrogenic cause. As resorption lowers the mechanical integrity of the BVS, any instrumentation within the coronary artery such as that needed for intracoronary imaging may damage the scaffold[196].

The ABSORB Japan trial reported an incidence of scaffold discontinuity of 25% at 2 years[192] while the ABSORB B reported an incidence of 42% by 3 years[18].

Even though our cohort had more complex lesions and a more aggressive implantation procedure, our incidence of late discontinuity was below that reported in the ABSORB studies. This may partly be due to our shorter follow up. Even so, it is encouraging to see that the use of the ABSORB BVS in bifurcations is not associated with excessive scaffold disruption.

While well-apposed, covered discontinuous struts are likely to be benign, uncovered struts protruding into the lumen can potentially have a nefarious effect. Intraluminal dismantling has been linked to the occurrence of VLST[69]. More data is needed to assess the clinical implications of late discontinuities in the ABSORB BVS scaffold.

4.5.3.3 Evagination and aneurysm:

Coronary evaginations were frequently observed after implantation of first generation DES. Procedural factors such as aggressive post dilatation, chronic inflammation and hypersensitivity reactions to a component of the stent (drug, polymer, metal) have been implicated though no particular culprit has been identified[197,198]. Newer iterations of metallic DES resulted in a significant reduction in the incidence of aneurysmal dilatation[199]. However this finding appears to have resurfaced with BVS implantation. In an analysis of 90 patients, Gori et al. found that 56% of patients had at least one evagination 1 year after BVS implantation[200].The need for high pressure post dilatation causing larger dissections and deeper arterial wall injury has been postulated as a possible explanation[201]. In our study, the high rate of pre and post dilatation did not confer a greater risk for the development of evaginations or aneurysms.

Coronary aneurysms have been associated with an increased risk of stent thrombosis[202]. The altered geometry of the vessel adversely alters the blood flow profile especially in the presence of malapposed struts. Disruption of the laminar blood flow in addition with ongoing vascular inflammation can lead to thrombus deposit[203]. Our finding of an intraluminal mass which is possibly thrombotic in origin at the site of a luminal protruberance would support this observation. The long term effect of these findings after BVS implantation needs further investigation.

4.6 Limitations

The following limitations have to be taken into consideration when interpreting the results of our follow up data. Firstly, the number of patients on whom follow up data was available was relatively small compared to the baseline group. Secondly, all the analysis was performed by a single investigator and not in a core laboratory. Since the investigator was not blinded to randomisation, this introduces a potential source of bias. Thirdly, our patient group had relatively 'simpler' bifurcation disease in that the side branch was free of significant stenosis. Our findings may not apply to the whole spectrum of bifurcation disease.

4.7 Conclusion

The provisional strategy with the ABSORB BVS has an acceptable MACE rate at 9 months. A distal sizing strategy is associated with fewer uncovered struts at follow up. Despite using the ABSORB BVS in more complex lesions, we observed similar rates of scaffold discontinuity and evaginations as trials involving simpler lesions.

5 The effect of elective implantation of the ABSORB BVS on coronary microvasculature

5.1 Introduction

Coronary disease represents a spectrum of conditions including epicardial stenosis, diffuse atherosclerotic disease and microvascular dysfunction. Percutaneous coronary intervention (PCI) has revolutionised the treatment of epicardial disease. While PCI successfully restores blood flow within the conduit artery, it can also affect the distal microvasculature. The technique of implantation plays an important role on post procedural coronary microvascular resistance (CMVR). Several studies have investigated the effect of coronary stenting with metal stents on the microcirculation[127,204,205]. Implanting an ABSORB BVS may not have the same impact on CMVR. The degree of wall damage and distal embolization of atherosclerotic debris is likely to differ between a polymer and metal platform. This may occur not only because of the different structural properties between the two materials but also due to the differing techniques of implantation. Appropriate implantation of the ABSORB BVS requires aggressive pre dilatation, post dilatation and additional instrumentation with intravascular probes for appropriate sizing (so called PSP protocol[27]), all of which may affect the integrity of the microcirculation. The impact of a BVS specific implantation protocol on downstream vasculature is currently unknown.

The interim 1 year report of the randomised ABSORB II trial reported that patients receiving BVS reported less angina and lower use of nitrates than those receiving Xience DES[182]. Restoration of vasomotion, better vascular compliance and better conformability[165] of the scaffold were initially postulated as possible explanations. It is now known that BVS implantation does not result in superior coronary vasoreactivity compared to metal stents even up to 3 years after insertion[76]. Similarly, while compliance mismatch and a poorly conformable device can cause excessive neointimal growth, BVS implantation has been found to have elicit a larger neointimal response than metal stents[75]. The improvement in angina observed in the ABSORB II trial may be mediated through its effect on the microvascular network.

5.2 Aim

1. To assess the impact of a bifurcation-specific BVS implantation protocol on coronary microcirculation.
2. To assess the influence of elective implantation of the ABSORB BVS on long term microvascular physiology.

5.3 Methods

5.3.1 Study population

The study population included patients from the ABC-1 trial undergoing elective implantation of a BVS for the treatment of bifurcation disease as described in chapter 2. Patients who had PCI with both metal stent and BVS during their index procedure were excluded.

5.3.2 Cardiac catheterization and haemodynamic measurements

The bifurcation specific implantation technique has been described in detail in chapter 2. Epicardial stenoses were evaluated using Fractional Flow Reserve (FFR) while the microcirculation was assessed using the index of microvascular resistance (IMR). Pre procedural IMR was corrected for collateral flow using the coronary wedge pressure (Pw). Overall coronary flow was assessed using Coronary Flow Reserve (CFR). Physiological parameters were measured before and after BVS insertion. In a smaller subset of patients, 9 month follow up haemodynamic data was available.

5.3.3 Data analysis

As described in chapter 2.

5.3.4 Statistical analysis

Categorical data are expressed at percentage (number of patients) while continuous variables are expressed as either mean (±standard deviation). Test for normality was carried out using the Shapiro-Wilk test. The IMR and CFR data were not normally distributed and thus overall comparison of serial measurements

was made using the Wilcoxon signed-rank test with a significance level set at $p<0.05$

5.4 Results

5.4.1 Patient characteristics

From February 2016 to June 2017, 38 patients were enrolled in the ABC-1 study. The patient flow diagram is outlined in Figure 36. Paired pre and post implantation IMR were available in 31 patients. We compared pre and post implantation haemodynamic data in this cohort. Nine-month physiology data was available in 14 patients by the time data collection was halted for the purpose of this thesis. We compared pre-PCI, post-PCI and follow up data in the latter cohort.

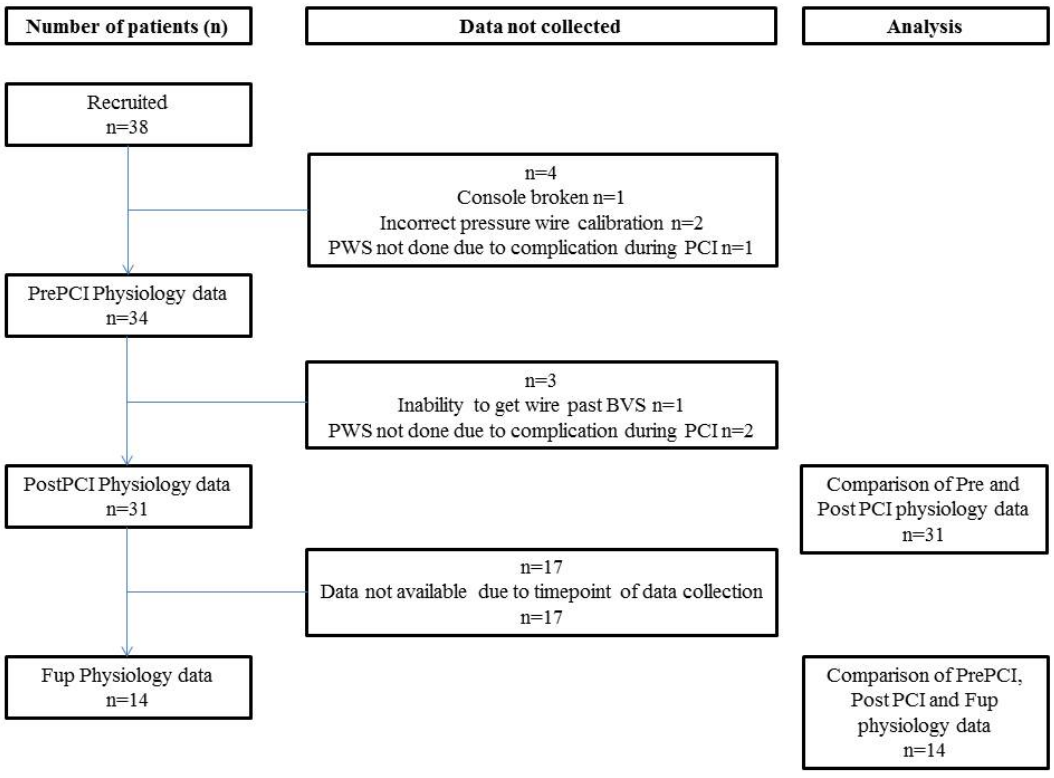

Figure 36: Patient flow diagram for haemodynamic assessment

The clinical and procedural characteristics of the 31 patients are presented in Table 13. The mean age was 62 years and 77% of patients were male. The culprit lesion was predominantly located in the LAD/diagonal system. Predilatation and

postdilatation rates were both 100%. All patients had intravascular imaging with OCT. There were no major complications during BVS implantation. One case did not meet the criteria for procedural success due to the presence of TIMI II flow in the side branch at the end of the procedure.

Patient characteristics	
Age	62.3 (± 10.3)
Gender (male)	77.4 (24)
BMI	28.9 (± 5.8)
Hypertension	48 (15)
Hyperlipidaemia	55 (17)
Current smoker	16 (5)
Diabetes Mellitus	19 (6)
Family History	32 (10)
Renal Impairment	6.5 (2)
eGFR	84 (± 18)
Previous MI	32 (10)
Previous PCI	32 (10)
Previous CABG	0
Previous Stroke/TIA	3.2 (1)
Stable angina	100 (31)
CCS 3/4	16 (5)
Lesion characteristics	
LAD	87 (27)
LCx	10 (3)
RCA	3 (1)
B2/C	65 (20)
mod/severe calcification	29 (9)
Procedural characteristics	
Predilatation	100 (31)
BVS Diameter (mm)	3.1 (± 0.36)
BVS Length (mm)	23 (± 5)
BVS Inflation Pressure (atm)	13 (± 2)
Post dilatation	100% (31)
Procedural success	97 (30)
TIMI III flow in MV	100 (31)
TIMI III flow in SB	97 (30)

Data expressed as Frequency (no of patients) or Mean (± sd)

Table 13: Patient and procedural characteristics of cohort undergoing haemodynamic assessment

5.4.2 Physiological parameters pre and post BVS insertion

Table 14 shows the physiological parameters measured before and after scaffold insertion. Our patient cohort had on average a higher IMR value at baseline compared to previously published reference levels[206]. PCI was accompanied by an average IMR reduction of 8.6 [95% CI: 1.6 - 15.6, p=0.02]. FFR improved after stenting by 0.16 (95% CI: 0.12-0.2, p<0.0001]. Mean CFR improved by 0.9 [95% CI: 0.2-1.6, p=0.02].

	Pre BVS (n=31)	Post BVS (n=31)	p value
Non hyperaemic Pa (mmHg)	89 (± 14)	90 (± 17)	0.69
Non hyperaemic Pd (mmHg)	79 (± 17)	85 (± 17)	0.02
Non hyperaemic Tmn (s)	1.05 (± 0.46)	0.89 (± 0.52)	0.15
Hyperaemic Pa (mmHg)	84 (± 19)	81 (± 19)	0.32
Hyperaemic Pd (mmHg)	64 (± 17)	75 (± 17)	<0.0001
FFR	0.77 (± 0.11)	0.92 (± 0.04)	<0.0001
Hyperaemic Tmn (s)	0.55 (± 0.36)	0.30 (± 0.16)	0.001
CFR	2.3 (± 1.1)	3.2 (± 1.8)	0.02
IMR	30.7 (± 18.4)	22.1 (± 12.2)	0.02

Pa- Aortic pressure; Pd- Distal pressure; Tmn- Transit time; FFR-Fractional Flow Reserve; CFR-Coronary Flow Reserve; IMR- Index of Microcirculatory Resistance

Data expressed as mean (± sd)

Table 14: Comparison of haemodynamic parameters before and after BVS insertion.

5.4.3 Physiological parameters prePCI and at follow up

The haemodynamic conditions at pre implantation and follow up in the 14 patients are presented in Table 15. The mean follow up period was 273 (±11) days. Inscaffold restenosis (ISR) did not occur in any of the cases. Similarly, there was no significant progression of native coronary disease in any of the cases.

	Pre BVS (n=14)	Fup (n=14)	p value
Non hyperaemic Pa (mmHg)	90 (± 11)	98 (± 13)	0.07
Non hyperaemic Pd (mmHg)	82 (± 11)	92 (± 13)	0.02
Non hyperaemic Tmn (s)	1.07 (± 0.58)	0.79 (± 0.39)	0.05
Hyperaemic Pa (mmHg)	84 (± 12)	87 (± 12)	0.48
Hyperamic Pd (mmHg)	66 (± 13)	80 (± 12)	0.01
FFR	0.78 (± 0.06)	0.92 (± 0.05)	0.001
Hyperaemic Tmn (s)	0.52 (± 0.36)	0.33 (± 0.17)	0.04
CFR	2.4 (± 1.0)	2.5 (± 1.0)	0.58
IMR	33.1 (± 22.2)	27.2 (± 16.8)	0.3

Pa- Aortic pressure; Pd- Distal pressure; Tmn- Transit time; FFR-Fractional Flow Reserve; CFR-Coronary Flow Reserve; IMR- Index of Microcirculatory Resistance

Data expressed as mean (± sd)

Table 15: Comparison of physiological parameters prePCI, postPCI and follow up.

FFR remained significant lower at follow up compared to pre-procedural values (p =0.001). In contrast, neither CFR nor IMR showed a significant difference between pre-procedural and follow-up levels (p=0.58 and p 0.30 respectively). Serial IMR changes of each 14 patients from pre-procedure, post-procedure and follow up are `illustrated in Figure 37.

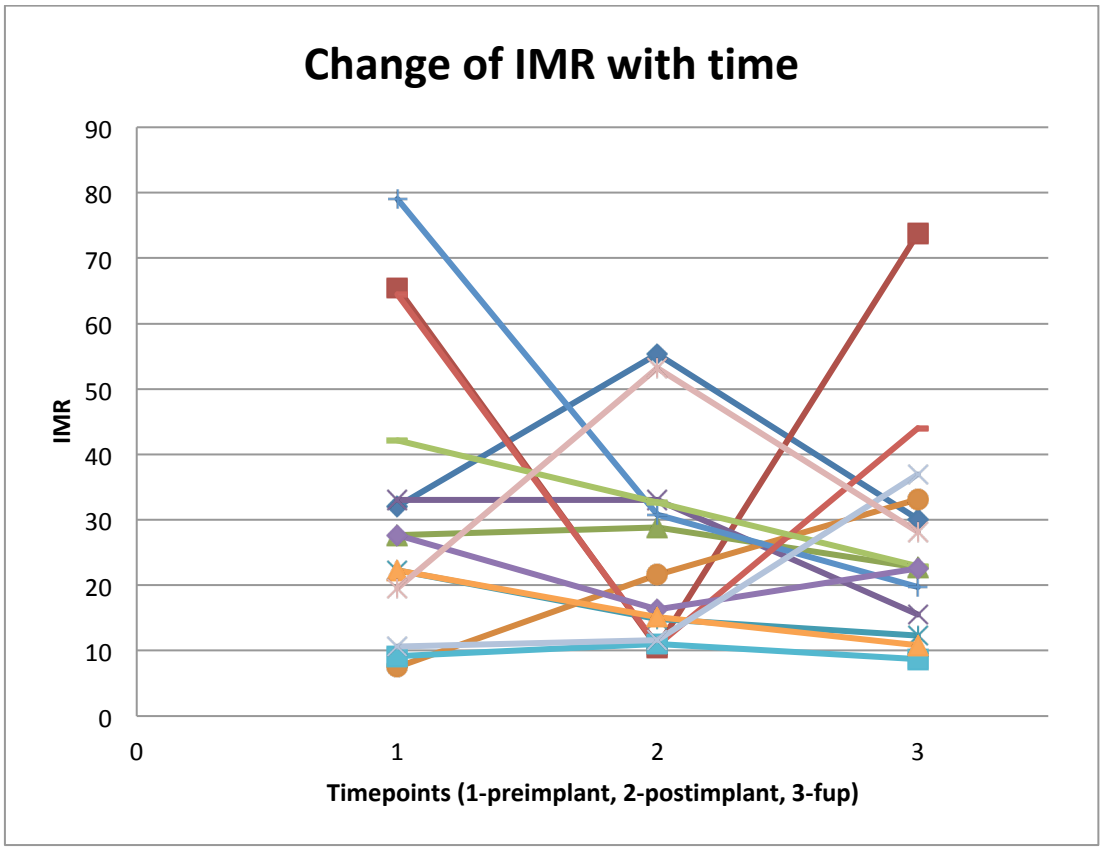

Figure 37: Serial IMR data for each of the 14 patients before PCI, after PCI and at follow up. Each specific colour traces the change in IMR for an individual patient at those three timepoints.

5.5 Discussion

Our findings can be summarised as follows 1) Both coronary microvascular resistance and coronary flow reserve improve immediately after PCI with the ABSORB BVS 2) The improvement in microcirculatory resistance is not sustained at follow up.

Our study is the first to compare invasive assessment of the coronary microvasculature before and after elective BVS implantation and at 9 month follow up. Data on the effect of BVS on coronary physiology is limited. In a study using positron emission tomography, patients treated electively with BVS had a lower coronary flow reserve at 1 month follow up than those treated with DES[207]. However in this study pre procedural CFR was not available and pre-exisiting differences in coronary resistance between the two groups may have been responsible for this finding. In a study of 15 patients undergoing elective PCI,

BVS implantation improved both IMR and CFR compared to baseline[208]. Comparison of physiological data with a propensity-matched metal stent cohort showed that IMR improved with BVS but deteriorated with metal stents.

Elective ABSORB BVS implantation causes an immediate reduction in microcirculatory resistance

In the setting of elective PCI, stent implantation technique affects microcirculatory resistance. Patients who have direct stenting have been found to have a lower IMR compared to those who had predilatation[209]. This is presumably due to a smaller amount of atherosclerotic plaque embolization with direct stenting compared to the combination of predilatation and stenting. Compared to metal stents, more extensive lesion preparation and post dilatation is required with BVS[27]. Our study shows that the more aggressive implantation technique does not adversely affect the distal microvasculature. Despite performing predilatation and postdilatation in all our cases, we did not observe a deterioration in microcirculatory resistance. In fact, IMR improved immediately after scaffold deployment. More extensive lesion preparation may paradoxically exert a protective effect on microcirculation by inducing a degree of ischaemic preconditioning. Another plausible explanation is that the larger width or 'footprint' of the BVS scaffold effectively shields atherosclerotic debris thereby reducing micro-embolization. Finally, the reduction in microvascular resistance may be due to the restoration of coronary perfusion pressure after successful treatment of epicardial stenosis. Myocardial perfusion downstream of a severe stenosis is markedly heterogeneous with blood being diverted to particular regions in place of others[210]. This is an adaptive mechanism aimed at preserving the transmicrocirculatory pressure gradient to allow normal metabolic exchange to occur in some regions despite ischaemia. Removal of a stenosis floods dormant vascular units with blood. If those units are set in a parallel configuration, the overall resistance in the network decreases[211]. This reduction in microvascular resistance coupled with the increase in blood flow within the conductance vessels would also improve coronary flow reserve.

The improvement in microvascular function is not preserved long term

The lack of a sustained improvement in microvascular resistance may be explained by a number of mechanisms. Firstly it is possible that the immediate improvement in resistance was only a transient effect mediated by passive distension of the microcirculation in response to a rise in perfusion pressure. In such a case, flow reserve would temporarily improve but once the circulation had acclimatised to this new 'normal', the vasodilatory capacity could come back down[212]. Secondly, it could be that microvascular function was restored after the procedure but microvascular disease progressed in the time interval between PCI and follow up. Although theoretically possible, this is less likely. The interval between the procedure and follow up was only 9 months. In addition, all patients were on secondary prevention therapy. These included treatment with statins and angiotensin enzyme inhibitors both of which exert a protective effect on the microvascular bed[213,214]. Therefore an aggressive progression of microvascular disease in patients in a short time interval is doubtful. Thirdly, restoration of blood flow may have exposed underlying microvascular disease which was concealed in the presence of epicardial disease.

Finally with regards to our original hypothesis, our results do not explain the improvement in angina reported in the ABSORB II trial. However this symptomatic improvement has not been replicated in subsequent larger trials suggesting that the improvement in angina in the BVS arm was a chance occurence[76].

5.6 Limitations

There are some important limitations which need to be mentioned. The relatively small number of patients in whom follow up data was available limits the interpretation of physiology data at that time point. Thermodilution curves were acquired after injections of 5mls of normal saline as opposed to 3mls which is conventionally used in most studies. We were unable to obtain an interpretable trace using boluses of 3mls in cases of very severe stenosis. This is possibly due to too small a volume of fluid being transmitted to the sensor distal to the narrowing. In animal studies, bolus injections of up to 5mls of saline have been shown not to affect coronary blood flow. Thus using a higher volume of injectate is unlikely to have adversely affected our measurements[215]. While we corrected

the pre-PCI IMR values for collateral supply by factoring the coronary wedge pressure in our calculation, we did not repeat wedge pressures after scaffold deployment. Periprocedural cardiac biomarker levels were not routinely collected in our study. Therefore we cannot overlook the influence of periprocedural MIs on our results. A comparator arm with a metal stent would have been useful. In its absence, direct comparison of our results with physiology studies using metallic stents has to be done with caution. Finally, it is possible that CFR was overestimated in our cohort due to the bifurcation anatomy especially when the side branch originated proximal to the stenosis. While this could have an effect on absolute values of haemodynamic parameters, it would not affect comparison in the same patient at different time points.

5.7 Conclusions

BVS implantation in an elective setting is accompanied by an immediate improvement in microvascular function but this effect is not sustained on long term follow up. The more aggressive lesion preparation mandated for optimal implantation does not have a deleterious effect on the microvasculature.

6 The effect of ABSORB BVS on inflammation following elective implantation

6.1 Introduction

Randomised controlled trials and registry data have shown that the ABSORB BVS is associated with a higher rate of thrombosis and late luminal loss[27,75]. Contributing factors such as malapposition, late scaffold dismantling and underdeployment[69] have been identified but the influence of inflammation on the restenotic/thrombotic response has not been investigated. Metal stents can induce a persistent inflammatory response causing a more potent neointimal response and a higher rate of in-stent restenosis (ISR)[216]. Histopathological analyses of restenotic tissue have shown a higher preponderance of inflammatory cells and fibrinoid tissue indicating an incomplete healing response[217]. Numerous mechanisms have been implicated in the development of a pathological inflammatory response after stenting. Biological factors include hypersensitivity reactions either to the metallic platform or to the polymer jacket and resistance to the anti-proliferative drug[9,218]. In contrast, healthy porcine coronary arteries treated with the ABSORB BVS have shown a relatively benign vessel response compared to first generation drug eluting stents[60]. Whether the lower levels of inflammation seen in these pre-clinical studies can be extrapolated to diseased human arteries is unknown.

The inflammatory response after PCI is influenced not only by the vascular injury induced by the procedure but also by the pre-existing inflammatory environment. In clinical settings, the baseline inflammatory status has been assessed with a wide variety of markers including CRP, IL-6, MCP-1 and sCD40L. In general, patients with high pre-interventional inflammatory activation seem to be at a greater risk of ISR. This observation has been consistently observed with bare metal stents (BMS) though the relationship in drug eluting stents (DES) is less clear cut[103,112,219-221]. So far, no study has investigated the effect of pre-procedural inflammatory state on subsequent neointimal growth after treatment with BVS.

6.2 Aim

- To assess whether routine implantation of the ABSORB BVS elicits a persistent systemic inflammatory response as assessed by circulating inflammatory markers.

- To assess whether the underlying inflammatory environment, as gauged by plasma levels of biomarkers, influences the neointimal hyperplastic response.

6.3 Methods

6.3.1 Study population

The study population consisted of patients from the ABC-1 trial who had follow up imaging data by June 2017. Patients with a history of PCI with metal stents were excluded. Patients had peripheral arterial blood sampling before PCI (baseline) and 9 months after the procedure (follow up). All patients underwent OCT imaging at follow up.

6.3.2 OCT measurements

Baseline and follow up measurements were performed according to the definitions and protocols outlined in chapter 2. Only scaffolds implanted within the bifurcation segment were considered. Neointimal burden was used as a measure of neointimal growth.

6.3.3 Inflammatory markers protocol

This has been described in chapter 2. In brief, we used four markers of inflammation – CRP, IL-6, MCP-1 and sCD40L. Baseline and follow up samples were examined using the same ELISA kit for each biomarker.

6.3.4 Data analysis

Neointimal burden was correlated with three parameters namely:

1. Levels of inflammatory mediators at baseline
2. Levels of inflammatory mediators at follow up
3. Difference between follow up and baseline levels of inflammatory markers.

Levels of biomarkers at baseline and follow up were also compared.

6.3.5 Statistical analysis

Continuous variables are presented as mean (± standard deviation) if normally distributed and median (interquartile range [IQR]) when not normally distributed. Discrete data is presented as percentage (count). Test for normality was performed

with the Shapiro-Wilk test. The distribution of inflammatory biomarker levels was non-normal and thus comparison between baseline and follow up levels were made using the Wilcoxon signed rank test. Correlation between levels of inflammatory markers and neointimal burden was made using the Spearman rank correlation coefficient.

6.4 Results

6.4.1 Population characteristics

Our study population consisted of 12 patients who had paired baseline and follow up data by June 2017. Table 16 summarises the patient and procedural characteristics at baseline. 9 patients (75%) were male and mean age was 64.8 years. All patients had stable angina. None of the patients had a pre-existing inflammatory condition, renal or liver dysfunction. Procedural success was 92% with one case of periprocedural MI. Mean follow up period was 269 days. One patient had early angiography and blood sampling (6 months after PCI) for investigation of atypical chest pain. No significant issue was identified on coronary angiogram and his symptom was deemed to be unrelated to the PCI procedure. In view of this, we included his data in our analysis.

Patient characteristics	
Age	64.8 (± 6.4)
Gender (male)	75 (9)
BMI	28.9 (± 5.5)
Hypertension	41.7 (5)
Hyperlipidaemia	41.7 (5)
Current smoker	8.3 (1)
Diabetes Mellitus	8.3 (1)
Family History	58.3 (7)
Renal Impairment	0
Creatinine (μmol/l)	84 (± 13.1)
Previous PCI	0
Previous CABG	0
Inflammatory condition	0
Stable angina	100 (12)
CCS 3/4	8.3 (1)
B2/C lesion	66.7 (8)
Mod/severe calcification	41.7 (5)
Procedural characteristics	

BVS Diameter (mm)	3.1 (± 0.4)
BVS Length (mm)	23 (± 5.8)
Number of BVS	1.2 (± 0.4)
Procedural success	91.7 (11)
TIMI III flow in MV	100 (12)
TIMI III flow in SB	100 (12)

Data expressed as Frequency (no of patients) or Mean (± sd)

Table 16: Clinical and procedural characteristics of patients in the ABC-1 substudy on inflammation.

6.4.2 Imaging results at 9 months

There were no cases of either inscaffold restenosis or inscaffold thrombosis. The mean inscaffold diameter stenosis on follow up was essentially unchanged compared to post procedural levels on QCA (18% on follow up versus 17% post PCI). All stented main vessels and side branches were widely patent.

Table 17 compares OCT parameters post BVS implantation and at follow up. Two patients did not have OCT imaging after their BVS insertion due to difficulty in getting the imaging probe past the scaffold. Vascular response was fairly benign with an average neointimal burden of 18%.

OCT parameters	Post PCI	Fup	p value
In segment Min luminal diameter (mm)	2.19 (± 0.29)	2.17 (± 0.38)	0.58
In segment Min luminal area (mm^2)	3.83 (± 1.01)	3.78 (± 1.34)	0.65
In segment Mean luminal diameter (mm)	2.85 (± 0.29)	2.69 (± 0.32)	0.03
In segment Mean luminal area (mm^2)	6.58 (± 1.41)	5.86 (± 1.42)	0.02
In scaffold Min luminal diameter (mm)	2.44 (± 0.31)	2.25 (± 0.36)	0.03
In scaffold Min luminal area (mm^2)	4.75 (± 1.30)	4.08 (± 1.27)	0.03
In scaffold Mean luminal diameter (mm)	2.88 (± 0.34)	2.67 (± 0.32)	0.02
In scaffold Mean luminal area (mm^2)	6.69 (± 1.68)	5.75 (± 1.39)	0.01
Mean scaffold area (mm^2)	7.47 (± 1.70)	7.35 (± 1.60)	0.29
Minimum scaffold area (mm^2)	5.45 (± 1.17)	5.61 (± 1.62)	0.61
Maximum scaffold area (mm^2)	9.16 (± 2.46)	9.01 (± 2.12)	0.26
Neointimal area per frame (mm^2)	n/a	1.29 (± 0.52)	n/a
Neointimal burden (%) *	n/a	18 (± 6)	n/a

Data expressed as mean (± sd)

Table 17: Comparison of measurements on OCT post BVS implantation and at follow up in the ABC-1 substudy on inflammation.

6.4.3 Relationship between baseline and fup levels of inflammatory markers

Table 18 compares the baseline and follow up levels of each marker. None of the inflammatory markers showed a significant change in serum level from baseline to follow up.

Biomarker		Baseline	Fup	p value
CRP (µg/ml)	median IQ range	1 0.6-2.5	2.1 1.3-2.9	0.53
IL-6 (pg/ml)	median IQ range	1.1 0.6-1.5	1 0.6-1.5	0.81
MCP-1 (pg/ml)	median IQ range	47.2 39.1-53.5	36.4 30.0-40.3	0.06
sCD40l (pg/ml)	median IQ range	82.6 74.1-158.2	80.6 64.9-103.9	0.53

Table 18: Levels of inflammatory markers at baseline and follow up.

6.4.4 Relationship between inflammatory markers and neointimal growth

Table 19 summarises the spearman correlation between each marker and neointimal burden on follow up OCT. We investigated levels at baseline, follow up as well as the difference in levels between the two time points (Δ). None of these parameters showed a significant association with the degree of neointimal growth at 9 months.

Marker	Spearman correlation coefficient	p value
CRP baseline	0.30	0.34
CRP fup	0.41	0.19
ΔCRP	0.14	0.67
IL-6 baseline	0.49	0.10
IL-6 fup	0.52	0.08
ΔIL-6	0.29	0.37
MCP-1 baseline	-0.22	0.48
MCP-1 fup	-0.77	0.81
ΔMCP-1	0.27	0.39
sCD40L baseline	0	0.99
sCD40L fup	-0.06	0.86
ΔScd40l	-0.27	0.39

Table 19: Correlation between levels of markers and neointimal burden.

One patient had a significantly elevated sCD40L baseline level of 2421 pg/ml compared to the cohort median of 83 pg/ml. The patient's clinical and procedural characteristics were not significantly different from those in the group. He was referred from cardiology clinic with CCS class II angina. Risk factors were hypertension and tablet controlled diabetes mellitus. Interestingly, there was a large amount of intracoronary thrombus evident on OCT shortly after BVS deployment despite pre-existing dual antiplatelet treatment (Figure 38). By 9 months, the sCD40L level had reduced to 71 pg/ml. OCT imaging at that time-point did not reveal an excessive hyperplasia with a neointimal burden of 19%.

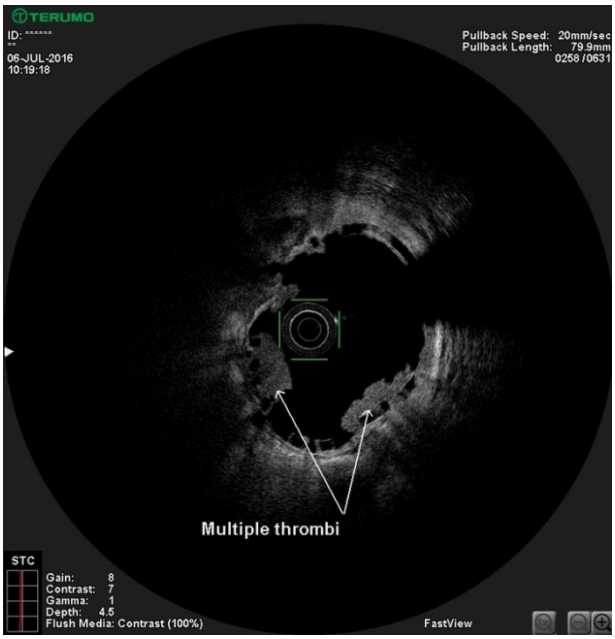

Figure 38: OCT image demonstrating multiple thrombi after deployment of BVS.

6.5 Discussion

Our study is the first to look at the influence of serum markers of inflammation in the context of PCI with the ABSORB BVS. The findings of our study can be summarised as such: 1) BVS implantation in an elective setting does not cause persistent inflammation at 9 months 2) The extent of neointimal tissue growth is independent of the inflammatory status at baseline and follow up.

BVS implantation in an elective setting does not cause a persistent rise in systemic markers of inflammation at 9 months

Based on our study, the polymer and its degradation products do not seem to evoke a systemic inflammatory response at medium term after the ABSORB BVS is implanted in an elective setting. Despite extensive published literature on the ABSORB BVS, the inflammatory response in humans is still poorly understood. Chronic low grade inflammation induced by either the polymer or its degradation products has been postulated as one possible cause for the high thrombotic rate[69]. However both PLLA[13] and PDLLA[222] polymers have used in the human coronary artery without major safety concerns. The final degradation products of the scaffold are D-lactic acid and L-lactic acid both of which naturally occur in the body. The amount of these products dispersed into the body as a result of scaffold

disintegration is far below the normal reference levels in the body [22]. It does not appear that the intermediate oligomers elicit a toxic tissue response either at least in animal studies. In swine models implanted with BVS, the inflammation score decreases progressively over 18 months[60]. This period coincides with the highest rate of mass loss and formation of degradation products. Thus, if the latter were particularly pro-inflammatory, one would expect the inflammation scores to be at their highest during that time. While the scaffold causes more inflammation than the metal stent in healthy swine arteries, giant cells suggestive of a foreign body reaction are uncommon beyond 3 months[62]. Our findings are supported by the comparable incidence of binary restenosis at 1 year between BVS and Xience DES seen in ABSORB China[223] and Japan[184].

The extent of neointimal tissue growth at 9 months is independent of the inflammatory status at baseline and follow up

The biologic response to the ABSORB BVS is probably closer to that following PCI with DES than with BMS[62]. While the predictive role of preprocedural inflammation in the development of BMS restenosis is well established, its significance in patients receiving DES is less clear. Several studies have failed to demonstrate an association between neointimal hyperplasia and either pre or post interventional biomarker levels in DES restenosis[220,224,225]. The release of potent antiproliferative agents in DES alters the biological response to vessel injury. Limus analogues have anti-inflammatory properties in addition to their inhibitory effect on the cell cycle. In particular, everolimus has been found to inhibit neutrophil activation, mitigate pro-inflammatory TNF related pathways and promote the release on the anti-inflammatory cytokines[226,227]. In addition, inhibition of the mTOR pathway in platelets prevents platelet activation and aggregation. This suppressive effect on inflammation may explain the lack of correlation we observed between baseline inflammatory status and neointimal growth.

We also did not observe any association between follow up levels of inflammatory markers and intensity of neointimal response. It is possible that the excessive hyperplastic response seen in restenosis is effected through mechanisms other than inflammation. In contrast to restenosis in BMS, a heterogeneous tissue composition is observed in most cases of BVS restenosis. In particular, restenotic

lesions that occur more than 6 month after implantation show signs suggestive of neoatherosclerosis[79]. Such systemic processes may play a more important role than locally induced inflammation in the pathology of BVS restenosis.

Finally, the case of very high preprocedural sCD40L level deserves special mention. sCD40L not only plays a role in inflammation but also in platelet activation after plaque rupture. The CD40/CD40L complex increases the expression of tissue factor while thrombomodulin expression is reduced thus creating a procoagulant state[108]. Studies using IL-6 and other markers as surrogates of inflammation have compared levels of sCD40L in both healthy subjects and cardiac patients[109]. sCD40L levels appears to be more a marker of platelet activation than inflammation in patients with coronary artery disease. The large thrombotic burden evident on OCT in conjunction with the very high pre-procedural sCD40L suggest that pre-existing thrombotic propensity may be an important factor in the development of scaffold thrombosis. The identification of such individuals may be key to the challenging issue of inscaffold thrombosis. The choice of appropriate biomarkers of platelet activation for risk stratification warrants further investigation.

6.6 Limitations

The main limitation of our study is its small sample size. This was a single centre study and our data may not be applicable to all patients. We did not measure biomarker level immediately after scaffold implantation. None of the patients in our cohort had extensive neointimal proliferation on OCT or angiographic instent restenosis. It is possible that inflammatory markers only show discriminatory power in patients with large neointimal burden. Our study design was limited to 9 months with an OCT endpoint. Thus we cannot comment on the role of inflammation in the advanced stages of the resorption process. The inflammation response may well evolve as the scaffold dissolves. Very late ISR and thrombosis may also progress through different pathological mechanisms that would not have been identified in our study. The levels of inflammatory markers especially IL-6 is known to be affected by the extent of adipose tissue and thus dependent on the weight of a patient. Since we did not routinely measure patient weight at follow up, we cannot exclude the latter as a potential confounding factor.

6.7 Conclusions

Elective implantation of the ABSORB BVS does not elicit persistent inflammation systemically when assessed by peripheral inflammatory biomarkers. The neointimal response after scaffold implantation is independent of the underlying inflammatory environment before scaffold implantation and at follow up. Thrombotic predisposition at baseline may play a part in the development of subsequent scaffold thrombosis. Future studies are needed to investigate this observation.

7 A review of wall shear stress and computational flow modelling in coronary bifurcation disease with case illustrations from the ABC-1 trial

7.1 Introduction

Atherosclerosis is a systemic disease but plaque distribution is not uniform but rather shows a predilection for particular sites such as coronary bifurcations[228]. Local perturbations to blood flow due the geometry of the vessel are responsible for the pathological vascular response seen at these locations. This mechanism also plays a role in the phenomenon of in-stent restenosis. Bifurcation stenting can significantly alter the natural configuration of the coronary artery and affect blood flow as a result.

The effect of blood flow on the vessel wall can be assessed using different haemodynamic parameters. One of the most investigated factors is the wall shear stress (WSS). This is caused by the frictional force blood exerts on the inner lining of the arterial wall. WSS exerts its influence on the endothelial cell wall via mechanotransduction mechanisms altering chemical signalling pathways, phenotypic configuration and gene expression. Under certain blood flow conditions, these processes can create a pro-atherogenic milieu leading to progression of native atherosclerosis or in-stent restenosis. WSS cannot be measured experimentally and relies on the application of computational fluid dynamics (CFD) to model its distribution within the coronary tree. Numerical modelling of haemodynamics in stented coronary arteries has gained much momentum over the recent years especially in the context of bifurcation PCI.

7.2 Aim

- To review the role of wall shear stress in the pathophysiology of native coronary disease and in-stent restenosis.
- To discuss the process by which computational fluid dynamics (CFD) is used to calculate WSS distribution in coronary arteries
- To demonstrate a novel method of assessing the haemodynamic impact of different bifurcation stenting strategies using two case studies from the ABC-1 trial.

7.3 Wall shear stress

7.3.1 General principles

Blood flowing in an artery exerts a force against the vessel wall. This force can be resolved into two orthogonal components – along the wall and perpendicular to it. When normalised with respect to surface area, the component tangential to blood flow is known as the wall shear stress. Wall shear stress is calculated as the product of blood viscosity with the velocity gradient of blood perpendicular to the wall (Figure 39). It has the dimension of force per unit area N/m^2 or Pa.

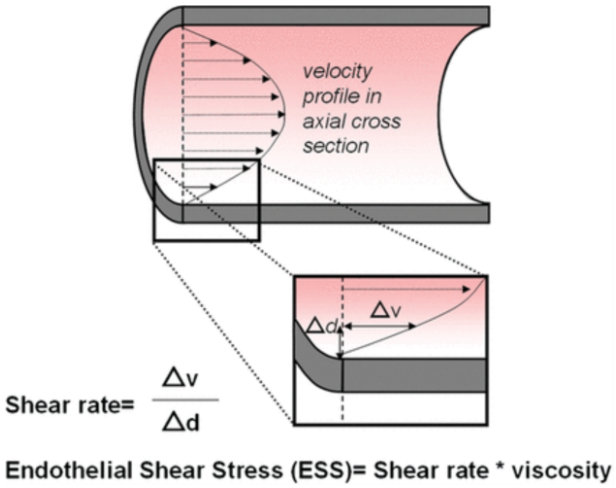

Figure 39: Diagrammatic illustration of shear stress: Shear stress is the product of velocity gradient (also known as shear rate) and viscosity of blood (Reproduced from Wentzel et al.)[229]

As blood flow varies over a cardiac cycle, the shearing force exerted on the inner wall will also fluctuate. The mean value of WSS, also known as time averaged wall shear stress (TAWSS), is commonly used to circumvent its temporal variation over the cardiac cycle. TAWSS at a location is affected by the way blood flows at that point. There are two main types of blood flow profile – laminar and disturbed flow. Laminar flow occurs when adjacent layers of blood flow in parallel and slide next to each other without mixing. In contrast, disturbed flow is a collective term encompassing any flow that does not have the streamlined characteristic of laminar flow. Flow disturbance may range from transient vortices causing flow reversal or separation to full blown turbulence

within the arterial tree. While laminar flow typically causes high shear stress, disturbed flow leads to areas of low shear stress or significant oscillations in WSS.

The endothelium forms the boundary between circulating blood and the underlying tissues of the artery. As such it is subject to the greatest variation in magnitude and direction of shearing forces. Transmission of the mechanical force is effected through the cytoskeleton and initiates a specific biological response depending on the direction and magnitude of the effector force. The relationship linking the physical deformation of the cell due to the haemodynamic external force to the resultant cellular response is known as mechanotransduction[230]. The effect of WSS on the endothelial cells has been widely studied in tissue cultures under a range of flow conditions (Figure 40).

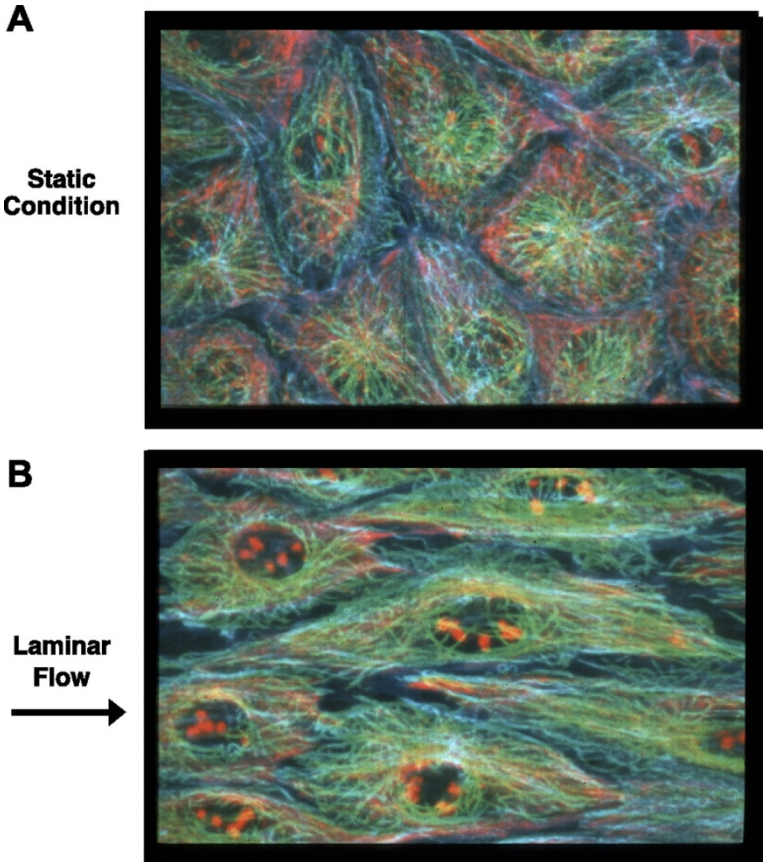

Figure 40: Effect of flow conditions on endothelial cell orientation - The cytoskeleton elements are triple stained with actin appearing as blue, microtubules as green and intermediate filaments as red..Cell arrangement under static conditions mimic those seen in disturbed flow and exhibit a more rounded configuration (top). Under laminar conditions, cells elongate in the direction of flow (bottom). (Reproduced from Chien)[230]

Mechanical forces sensed by endothelial cells can prompt a change in their morphology and function. In areas of high shear stress, endothelial cells are elongated and align themselves in the direction of flow. In contrast, cells located in regions of flow disturbance exhibit a more polygonal structure with no preferred orientation. Cell permeability to blood borne substrates is also altered while at the nuclear level, gene expression leads to the activation of pro-inflammatory pathways and molecules.

7.3.2 In atherosclerosis

Numerous studies have shown an association between regions of low or oscillatory WSS and the initiation and development of atherosclerotic plaque[228]. In contrast, exposure of endothelial cells to a normal or high shear stress confers protection against atherosclerosis[229]. The effect of local WSS distribution on plaque formation is exemplified by the distribution of plaque in coronary bifurcations and curved arteries. The lateral walls of bifurcations are typically exposed to lower shear forces compared to the flow divider or carina. As a result, plaque occurs preferentially within that location[231,232]. In non-branching vessels, the natural curvature of a vessel results differential shear stress distributions on the inner and outer curve. The inner bend is subject to a lower shear stress than the outer one and is thus more prone to atherosclerotic plaque development[233].

In early atherosclerosis, positive vessel remodelling mediated by healthy endothelium preserves the luminal size. However ongoing exposure to local areas of low shear stress causes progression of plaque disease until vessel remodelling can no longer compensate for the increasing luminal encroachment. Wall shear stress remains low downstream of the stenosis maintaining the proatherogenic environment[234]. Interestingly, high WSS may not have a benign effect in advanced atherosclerosis. High shear stress has been linked thinning of the fibrous cap through a variety of endothelial mediated processes including upregulation of matrix metalloproteinase activity and nitric oxide expression[235]. The end result is an increase in plaque vulnerability and risk of rupture precipitating an acute myocardial infarction.

7.3.3 PCI including bifurcation stenting

Percutaneous coronary intervention can affect blood flow in several ways. A stent expands and straightens the vessel altering the geometry and hence wall shear stress distribution. If the vessel is particularly curved, stenting shifts that natural bend to the edges of the stent[236]. The result is the production of sharp bends just before and after the stent. These areas are associated with low WSS. Local perturbation to blood flow leads to the accumulation of biologically active compounds which can exacerbate the neoinitimal hyperplastic response. This effect is partly responsible for the edge vascular response often seen with BMS[237]. More angulated vessels at baseline or larger changes in angulation following deployment of metal stents have been shown to be associated with greater restenosis rates and adverse clinical outcomes[238].

Device/vessel mismatch can also exert a profound effect on vessel geometry. An oversized stent causes a 'step up' and 'step down' phenomena at the proximal and distal edges respectively. The sudden expansion of the artery at the proximal stent edge can cause microrecirculation patterns resembling those typically seen after native stenosis[239]. Blood flow pattern is disrupted in those regions causing not only low WSS but also wall shear stress reversal. Growth factor expression is enhanced causing an exaggerated healing response i.e an excess of neointimal tissue. Conversely, stent underexpansion can cause malapposition. The resulting gap between the vessel wall and stent disturbs laminar flow lowering local WSS[240]. Overlapping stents are associated with a greater incidence of ISR and this may also be in part due to the adverse haemodynamic conditions resulting from multiple layers of stent protruding into the lumen.

In addition to the effect of stent placement on vessel geometry as a whole, the microenvironment around stent struts has an influence on local wall shear stress. Depending on their size and shape, struts protruding in the lumen can disrupt blood flow. Changes in the peri-strut haemodynamic environment can influence local platelet deposition and activation. Both low and high WSS have been shown to increase stent thrombogenicity - the former through its adverse effect on the endothelium and the latter through platelet activation[240].

Bifurcation stenting introduces another layer of geometrical complexity. Each of the myriad stenting techniques can change the vessel geometry and affect blood flow in its own unique way. For example, struts lying over the side branch ostium can disturb blood flow in the provisional strategy. Bench studies have demonstrated the occurrence of vortical flow structures associated with low shear stress at the carina in stented bifurcation models[241]. Histopathological analysis reveals that the carina has lower arterial healing with a greater percentage of uncovered struts and fibrin deposit compared to the lateral wall in stented bifurcation lesions. The delay in healing is further accentuated by anti-proliferative agents in drug-eluting platforms increasing the risk of thrombosis. Furthermore, bifurcation treatment is more commonly associated with adverse mechanical features such as proximal malapposition, underexpansion, distorted geometry, strut fracture following SB dilatation and distal vessel dissection. All of these factors can adversely affect WSS distribution and increase the risk of both instent restenosis and thrombosis.

7.3.4 BVS

The effect of BVS implantation on WSS has been investigated in a few studies. In the ABSORB A cohort, Karanasos et al. analysed coronary segments scaffolded with the first version of the ABSORB BVS[242]. The distribution of WSS two years after BVS implantation was computed in 7 patients and the result was compared to intracoronary tissue morphology at 5 years on OCT in order to assess the impact of WSS on long term vessel morphology. The authors found that regions with low shear stress were associated with thinner fibrous caps thereby highlighting the importance of local haemodynamics on the healing response after BVS implantation. In 12 patients from the ABSORB B cohort, Bourantas et al. investigated the effect of WSS immediately after BVS implantation on neointimal growth at 1 year[191]. Areas that were exposed to low WSS showed more intimal thickening at follow up. Analysis of the peri-strut flow distribution showed regions of low shear stress as well as recirculation zones adjacent to the struts and regions of high WSS at the top. This type of flow disturbance may be responsible for scaffold thrombosis. High WSS on top of struts can activate platelets which are then captured in the low recirculation zones adjacent to struts causing thrombus formation[70](Figure 41). Tenekecioglu et al. investigated the effect of

protruding struts had on WSS and found an inverse relationship highlighting the importance of good embedment within the arterial wall to minimise adverse haemodynamic impact[243].

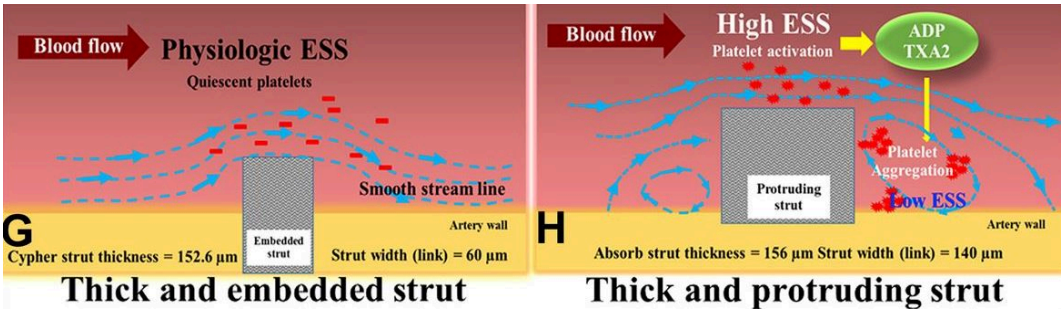

Figure 41: Schematic representation of the effect of strut embedment on shear stress (ESS): G - Laminar flow after good strut embedment. H - Significant strut protrusion causing regions of low and high shear stress generating a prothrombotic environment (Modified from Serruys et al.)[70]

The ABSORB III trial has an imaging sub study (RESTORATION) where the haemodynamic effect of the ABSORB BVS will be compared to Xience DES at 3 years[244]. This study will evaluate the distribution of WSS after stenting and at 3 year follow-up. The relationship between post procedural WSS levels will be compared to long term neointimal tissue healing. This will hopefully increase our understanding of the vascular response following scaffold implantation and its relationship to local blood flow.

7.4 Computational Fluid Dynamics

7.4.1 Rationale for CFD in calculating WSS

Calculating wall shear stress requires knowledge of the precise variation of the blood velocity close to the arterial wall. The small size of a coronary artery coupled with cardiac motion makes it impossible to measure this experimentally with any reliable degree of accuracy. Current devices used to measure blood velocity such as the intracoronary doppler wire can only give the maximum velocity of blood in the lumen. Since the spatial distribution of velocity cannot be measured experimentally, we have to rely on alternate methods to establish the velocity profile. The motion of blood can be modelled using computational fluid

dynamics (CFD). Computer simulation of blood flow is obtained by solving the equations of fluid flow also known as the Navier-Stokes equations. It is not possible to obtain exact or analytical solutions to these complex partial differential equations when modelling complex flows. Instead, we have to rely on software packages to provide solutions that are close to the exact values. Various numerical methods can be used to give approximate solutions to these differential equations including finite volume method, finite difference method and finite element analysis. All these methods essentially approximate the complicated differential equations to a system of simple linear algebraic equations which are easier to solve. A detailed description of these methods is outside the scope of this thesis but essentially a CFD solver uses one of these techniques to solve the equations governing fluid flow.

7.4.2 Principles of CFD in coronary flow modelling

To be able to conduct a CFD simulation to study intracoronary blood flow, the vessel geometry first needs to be defined. Reconstructing the three dimensional shape of the vessel consists of a number of steps:

1. Extraction of the luminal contour and centroids of the stent struts separately from the intracoronary imaging data (e.g. IVUS, OCT) with an algorithm for image segmentation.

2. Determination of the vessel orientation from 3-D imaging data (e.g. angiography, CT or MRI) to identify the lumen centreline in space.

3. Alignment of the lumen contours and stent centroids along this centreline.

4. Reconstruction of the 3D geometry of the main branch with a surface that fits the lumen contours (lofting).

5. Reconstruction of the stent from the extracted imaging data by morphing the skeleton of the stent on the aligned centroids and then positioning cross sections of the stent on the morphed skeleton and fitting a surface on these.

Once the three dimensional anatomy is available, we can then model the motion of blood flow within that geometry. First, the domain of blood to be analysed is divided into discrete cells or ‘meshed’. The size and shape of the elements can vary. Common shapes include hexahedrons, tetrahedrons and prism. The

equations of blood flow are solved in each grid. A finer mesh with more elements will give a more accurate and detailed description of the fluid dynamics in that region. However the finer the mesh is, the more expensive the simulation will be, both in terms of computation time and memory. In order to find an optimised mesh size, which ensures reliable solutions at a reasonable cost, a sensitivity study is commonly carried out by increasing the number of elements and comparing the results. In general, the mesh size depends on the geometry of the domain and on the phenomenon under study. For instance, in the region of the stent the mesh is typically finer than in the rest of the vessel lumen. This captures local flow patterns within the vicinity of the struts.

Next, the values that the solution needs to take along the boundary of the domain need to be specified. These boundary conditions define the behaviour of blood at each surface of the fluid domain. For example, it is common to define the blood velocity to be zero at the point of contact with vessel wall (the 'no slip' condition). Similarly, the blood velocity profile entering the artery can be defined to be pulsatile and not to exceed a maximum value derived from experimental data.

Finally, the characteristics of the blood are defined. The viscosity of blood can be assumed to either obey Newton's law of viscosity (Newtonian fluid) or not (Non-Newtonian fluid).

Once all the above parameters have been prescribed, the simulation is started in a CFD package and the algebraic equations are solved iteratively to find solutions that satisfy the boundary conditions defining the flow domain. The output is a set of flow variables at the mesh elements and need to be represented in a user friendly way. All CFD packages have graphic capabilities including domain geometry and vector plots which allow easy visualisation of the solutions.

7.4.3 Application in bifurcation PCI

Computer simulations have been used to assess coronary haemodynamics in bifurcation procedures for over a decade. Initial studies employed simple idealised geometries. Deplano et al. published the first CFD study on stented bifurcations showing that in a two-stent strategy, protruding struts near the inner and outer wall of the SB generated areas of low WSS[245]. Since then, several studies have

investigated the effect of different stenting techniques on coronary blood flow. Williams et al. investigated the effect of main vessel stenting followed by SB dilatation and found that SB angioplasty did not significantly improve WSS distribution[246]. Chiastra et al. found that performing KBI through the distal cell across side branch led to more favourable flow characteristics supporting current recommendations from the clinical arena[247]. Katritsis et al. showed that a provisional strategy was more advantageous from a haemodynamic perspective than a double stenting similarly confirming observations from clinical trials[248].

With advances in coronary artery imaging and computational ability, there has been an interest in the creation of patient specific bifurcation models. To allow the creation of a patient's bifurcation geometry, both invivo morphological data and the spatial orientation of the bifurcation are needed. OCT or IVUS provides the former while the 3-D configuration is obtained from CT, angiography or MRI. Various combinations of these imaging modalities have successfully been used in creating anatomically accurate reconstructions of the coronary bifurcations. Mortier et al. demonstrated the feasibility of patient specific computer modelling of bifurcation stenting in the 'John Doe' programme[249]. This project, which was endorsed by the European Bifurcation Club, demonstrated the possibility of performing virtual bifurcation stenting using the patient's coronary bifurcation anatomy and computational modelling.

7.5 Case studies from ABC1 trial

7.5.1 Methods

The wall shear stress distribution was computed using the sequence outlined in chapter 2. Neointimal thickness (NIT) was measured at 1mm intervals for 5mm on either side of the side branch and at 0.125mm (individual frames) in cross sections containing the side branch.

7.5.2 Case 1 – Distal sizing

The first case was a 67 year old lady presenting with stable angina who had a LAD/D1 bifurcation disease of Medina 0,1,0 type. The side branch was free of disease and had a diameter was 1.82mm on QCA. OCT imaging was performed

after balloon dilatation showed a proximal reference diameter of 2.90mm and distal reference diameter of 2.22mm. The patient was randomized to a distal sizing strategy. A 2.5x12mm ABSORB BVS was implanted in the main vessel at 16 atm. Proximal optimization was performed with a 3.0x8mm non-compliant balloon inflated to 14atm. The ostium of the side branch had a residual stenosis of 24% on QCA. A further OCT run performed after deployment showed good apposition of the scaffold with no edge dissection.

Fluid dynamic simulation was carried out to evaluate the wall shear stress distribution and blood velocity profile after deployment of the ABSORB BVS across the side branch. Follow-up angiogram and OCT performed 9 months after implantation showed that the luminal narrowing across the ostium of the diagonal remained stable at 23% on QCA. The time averaged wall shear stress distribution with representative OCT images is shown in Figure 42.

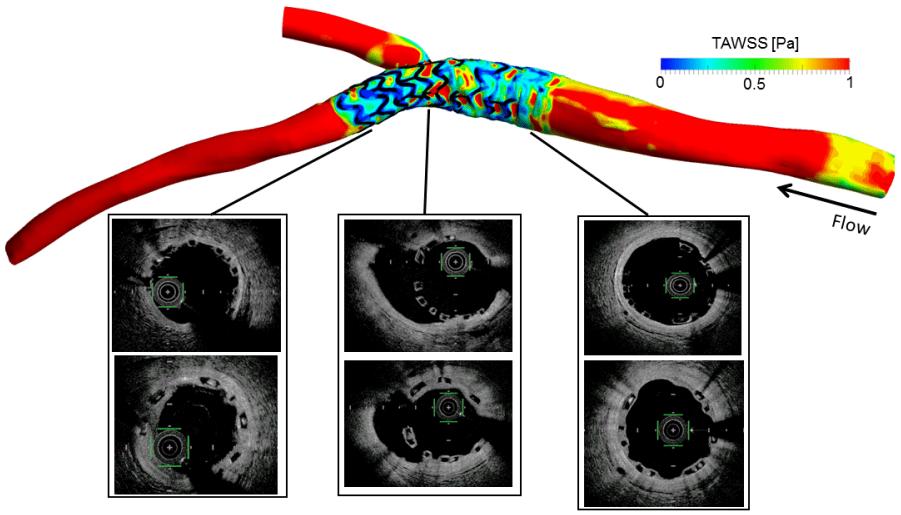

Figure 42: Case 1 - Geographical distribution of WSS along scaffolded segment

Immediately after implant, 55.8% of the scaffolded segment had a low TAWSS of ≤ 0.4 Pa. Blood flow into the diagonal was disrupted by the presence of the scaffold over the orifice (Figure 43) leading to microrecirculation and flow stasis.

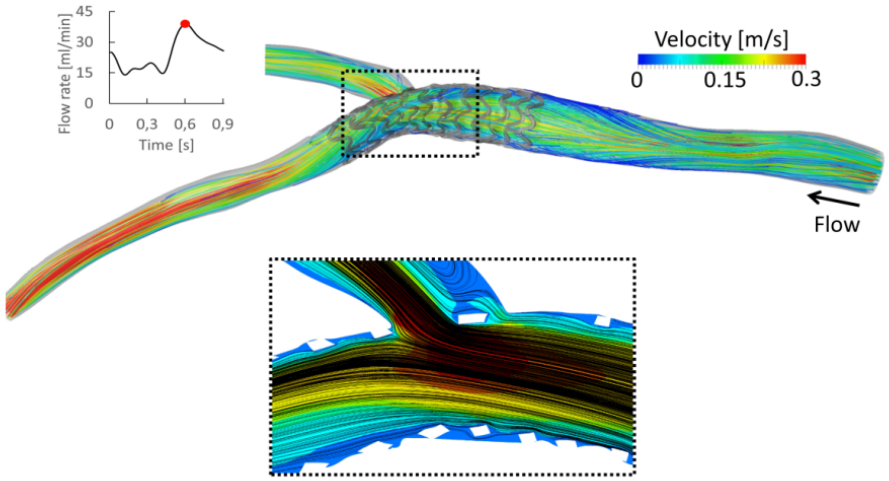

Figure 43: Case 1 - Blood velocity profile along scaffolded segment.

At follow up, there was a good healing response with complete coverage in 100% of struts (Figure 44).

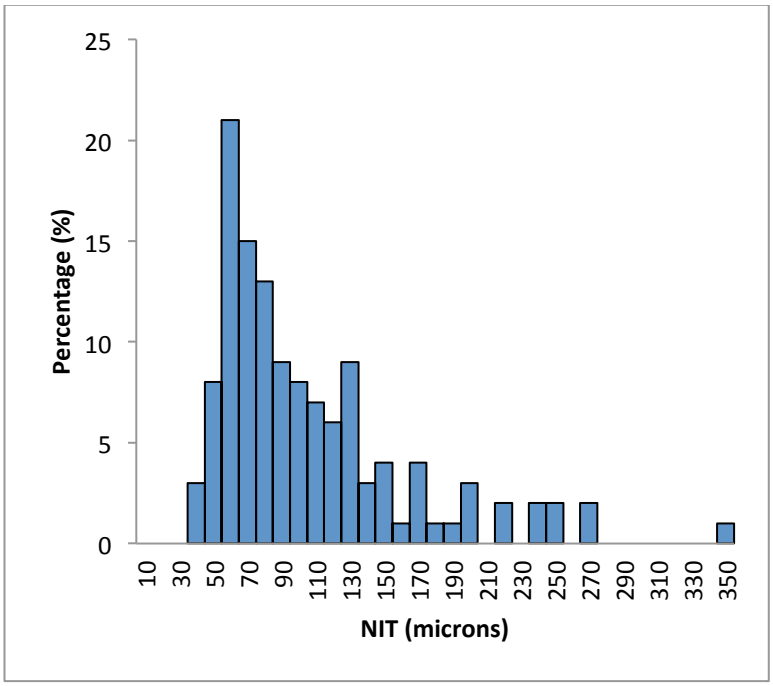

Figure 44: Case 1 - NIT distribution in scaffolded bifurcation

Neointimal growth was similar in all three bifurcation segments (Figure 45) reflecting the similar TAWSS distribution in those areas (Figure 46).

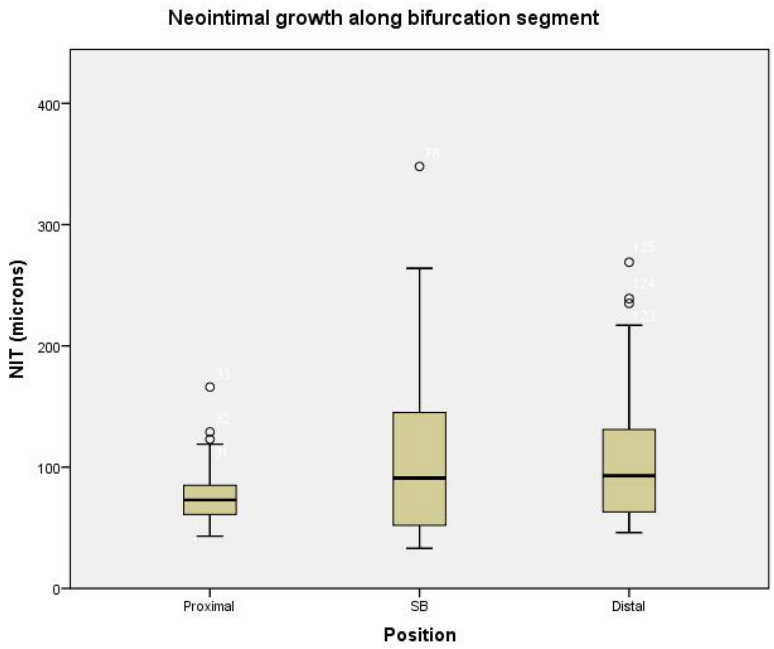

Figure 45: Case 1 - NIT grouped according to location.

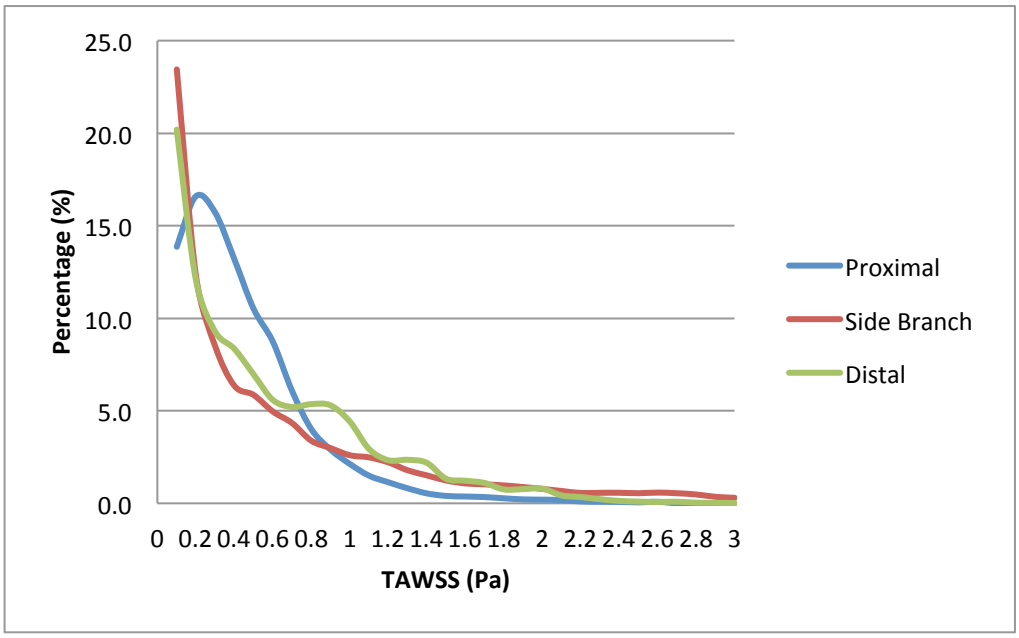

Figure 46: Case 1 - Distribution of TAWSS according to position along bifurcation segment.

7.5.3 Case 2 – Proximal sizing

The second case was a 57 year old lady presenting with stable angina who had a LAD/D1 bifurcation disease of Medina 0,1,0 type. The patient was randomised to

a proximal sizing strategy. A 3.0x28mm ABSORB BVS was implanted in the main vessel at 12 atm. Proximal optimization was performed with a 3.25x8mm non-compliant balloon inflated to 14atm. An OCT run performed after deployment showed good apposition of the scaffold with no edge dissection. Fluid dynamic simulation was carried out as previously described. Follow-up angiogram and OCT performed 9 months after implantation showed widely patent scaffold and side branch. The time averaged wall shear stress distribution is shown in Figure 47.

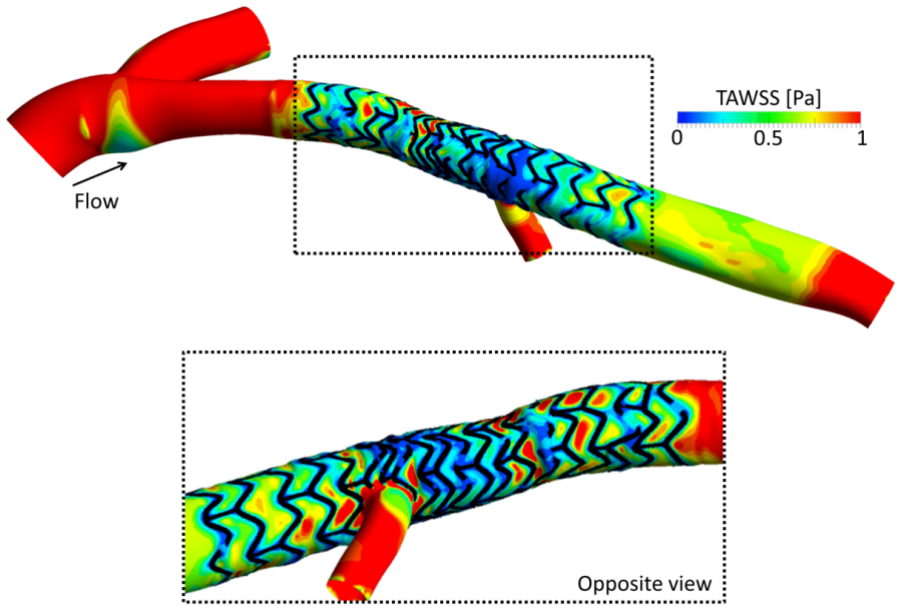

Figure 47: Case 2 - Geographical distribution of WSS along scaffolded segment

On average, the wall shear stress was highest in the distal segment. Blood flow into the diagonal was showed less blood flow disruption compared to the previous case (Figure 48).

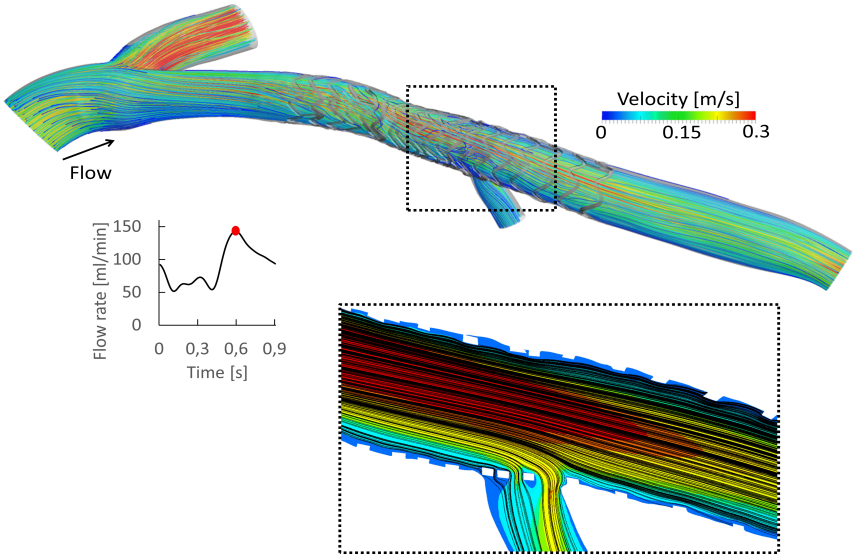

Figure 48: Case 2 - Blood velocity profile along scaffolded segment.

At follow up, there was a good healing response with complete coverage in 99% of struts in the bifurcation segment (Figure 49).

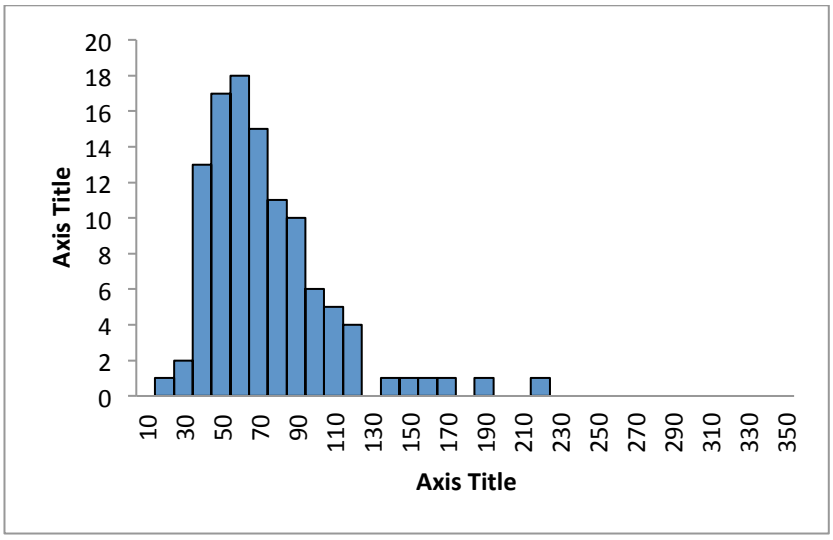

Figure 49: Case 2 - NIT distribution in scaffolded bifurcation.

Figure 50 shows the neointimal coverage along the 3 segments. While the median NIT was similar across all groups, there was a wider distribution of neointimal thickness distal to the bifurcation. Figure 51 shows that the distal segment was exposed to higher TAWSS compared to the proximal one.

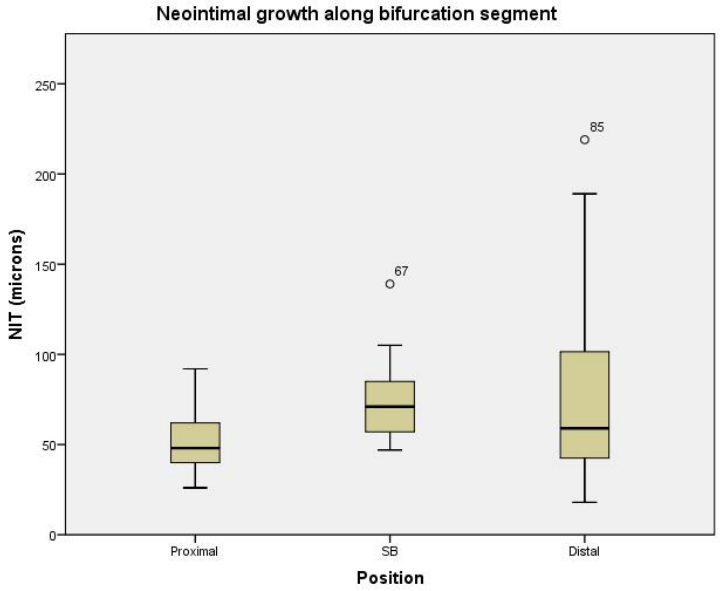

Figure 50: Case 2 - NIT grouped according to location.

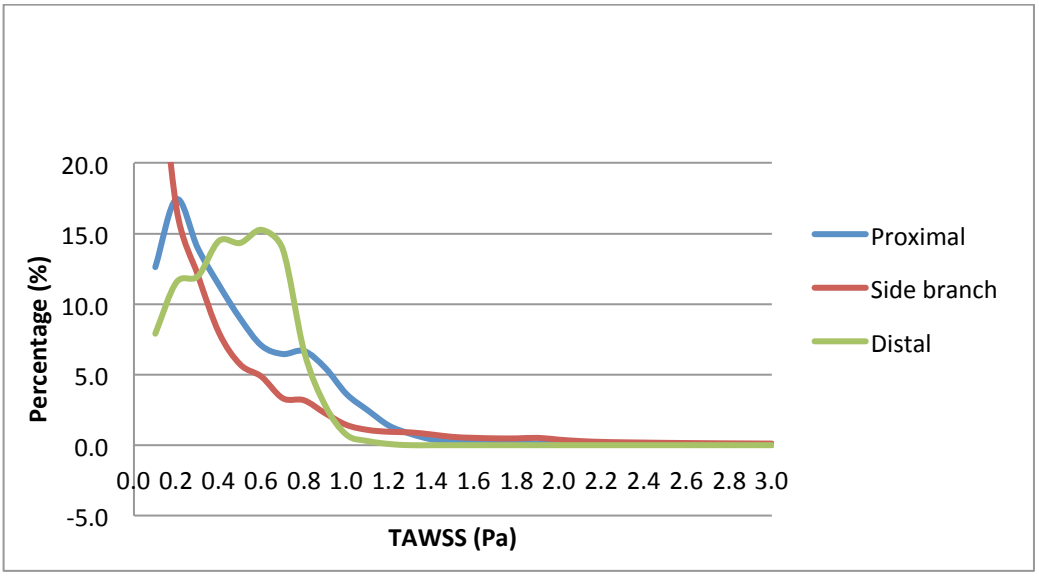

Figure 51: Case 2 - Distribution of TAWSS according to position along bifurcation segment.

7.5.4 Discussion

With the two case studies, we demonstrate 1) the possibility of calculating the WSS distribution and blood profile in bifurcation segments treated with an ABSORB BVS and 2) the potential application of such simulations in the clinical setting by matching the numerical methods with imaging or clinical outcomes in

patients. In addition, our method can be used to validate different CFD models against patient outcomes.

The effect of the ABSORB BVS on WSS has been limited to relatively straight coronary arteries. We are currently evaluating the effect of sizing strategy on WSS in patients from the ABC-1 trial. In addition, we will be investigating the influence of post procedural WSS distribution on neointimal growth. Our results will hopefully increase our understanding of the haemodynamic impact of using the ABSORB BVS to treat bifurcations.

7.6 Conclusions

The endothelium lining the coronary artery is directly subject to shearing forces induced by blood flow. Low wall shear stress typically promotes atherosclerosis and restenosis after PCI. Bifurcation stenting can cause significant geometrical changes that affect blood flow. Computational simulations can be used to evaluate which bifurcation treatment strategies confer the most favourable haemodynamic profile. We demonstrated the feasibility of performing numerical simulations on the ABSORB BVS in order to better understand the differential effects of stenting techniques on WSS. Integration of biomechanical factors in risk assessment may help identify those cases at higher risk of restenosis or thrombosis and help guide decision making in the interventional arena.

8 Summary

We assessed the use of the ABSORB BVS in coronary bifurcations and investigated its effect on inflammation, coronary microcirculation and wall shear stress. To the best of our knowledge, this is the first study to evaluate its effect on vascular biology, coronary physiology and wall shear stress in a single clinical trial. Integration of the results from each of these disciplines gave us a more comprehensive picture of the performance of this new device.

The following conclusions can be drawn from this thesis:

1. The use of the ABSORB BVS to treat 'false' bifurcations is safe and feasible. Clinical outcomes comparable to those in simpler lesions can be achieved with meticulous implantation technique and use of intracoronary imaging. Both proximal and distal sizing strategies have similar procedural complication rates when the ABSORB BVS is used to treat coronary bifurcations. While a proximal sizing strategy is associated with less significant malapposition immediately after implantation, there are fewer uncovered struts with a distal sizing strategy at medium term follow up. Longer imaging after complete scaffold bioresorption is needed.
2. The implementation of a specific BVS implantation protocol does not adversely affect the coronary microvasculature in an elective setting.
3. In patients with chronic stable angina treated with the ABSORB BVS, systemic plasma biomarker levels are not elevated at 9 months compared to pre-procedural values. The extent of neointimal proliferation is independent of either baseline or follow up inflammatory status.
4. Wall shear stress (WSS) plays an important role in the aetiology and treatment of coronary bifurcation disease. We demonstrated the application of a novel method of assessing WSS distribution when using the ABSORB BVS in a provisional strategy.

9 Final remarks

Our idea of testing the ABSORB BVS in bifurcations arose in 2014. It was a time of unbridled enthusiasm and optimism for bioresorbable technology. Operators were pushing the boundaries of this device using them in increasingly complex lesions such as CTO and true bifurcations. It seemed that it was only a matter of time before the ABSORB BVS would supplant DES and establish itself as the new standard of care in the treatment of coronary artery disease. However, they have not proven to be the panacea interventionalists were hoping for. Both trial and registry data have demonstrated worse clinical and angiographic outcomes with the ABSORB device including scaffold thrombosis. There is hope that better patient selection, refinement of the implantation techniques and further iterations of the device will improve outcomes. Longer term data from the currently ongoing ABSORB III and IV trials should provide us with a clearer picture.

Deciphering the reasons behind restenosis and thrombosis is going to be key for the future of this device. The search for a solution will require an interdisciplinary approach. Computational flow modelling, evaluation of the vascular response to stenting and assessment of coronary physiology are some of the tools that will be needed in this quest. Larger trials with a similar design to our study will significantly improve our understanding of the performance of this device.

With regards to bifurcation disease, the current iteration of the ABSORB BVS has limitations which will need to be overcome. The following changes in design are ideally needed:

- A more robust backbone that will allow the BVS to be safely expanded beyond the 0.5mm threshold that is currently advocated.
- Thinner struts to improve deliverability, reduce the risk of side branch occlusion and reduce the adverse effect of strut protrusion on blood flow.

The second generation of the ABSORB BVS will hopefully be available in the near future. Preliminary information provided by the manufacturing company (Abbott Vascular) indicates that it will have a strut thickness of 100 μm compared to the 150 μm of the BVS 1.1. The backbone and coating will remain unchanged. The reduction in strut thickness may improve outcomes. But it is important to understand the interdependence that exists among the factors that determine the final mechanical properties of the scaffold. Changing one parameter may

adversely affect another and merely shift the problem. Thus it is possible that the haemodynamic advantage conferred by thinner struts is offset by a lower tensile strength resulting in more scaffold fractures. Careful evaluation of the newer generation ABSORB BVS in the setting of large RCTs will be needed and indiscriminate 'off label' use should be discouraged.

Any new technology goes through a series of phases from inception to maturity. Amara's 'law' probably sums it best and states that[250]:

"*We tend to overestimate the effect of a technology in the short run and underestimate the effect in the long run*"

Bioresorbable technology will hopefully continue to progress mirroring the evolution of metal stents. But there is a danger that further exploration into this area is cut short. In the current era of third generation metal stents, it is becoming increasingly difficult for new contenders to demonstrate meaningful improvement in outcomes. The substantial financial investment required in return for uncertain gains may discourage future endeavours in this promising technology.

The shortcomings of metal stents that BVS were meant to address still remain. Late luminal loss, very late thrombosis and persistent abnormal vessel physiology still need to be resolved. Newer generation metal devices may be the answer but the concept of a device that disappears when it is not needed remains intuitively attractive. The outcomes of other bioresorbable devices currently under investigation will probably determine the fate of this technology. In the end, our goal as clinicians is to improve patient care. Any technology that fails to meet this goal should be abandoned. But in the pursuit of better outcomes for our patients, it is our duty to cautiously but resolutely explore any avenue that can take us there.

Bibliography

1. Roth GA, Huffman MD, Moran AE, et al. Global and Regional Patterns in Cardiovascular Mortality From 1990 to 2013. *Circulation.* 2015;132(17):1667.
2. Willis Hurst J. The first coronary angioplasty as described by Andreas Gruentzig. *American Journal of Cardiology.*57(1):185-186.
3. Serruys PW, Kutryk MJB, Ong ATL. Coronary-Artery Stents. *New England Journal of Medicine.* 2006;354(5):483-495.
4. Puel, J., Joffre, et al. *Endo-protheses coronariennes auto-expansives dans la prevention des restenoses apres angioplastie transluminale: etude clinique preliminaire.* Vol 80. Neuilly sur Seine, FRANCE: Huveaux; 1987.
5. Serruys PW, de Jaegere P, Kiemeneij F, et al. A Comparison of Balloon-Expandable-Stent Implantation with Balloon Angioplasty in Patients with Coronary Artery Disease. *New England Journal of Medicine.* 1994;331(8):489-495.
6. Sousa JE, Costa MA, Abizaid AC, et al. Sustained Suppression of Neointimal Proliferation by Sirolimus-Eluting Stents. *Circulation.* 2001;104(17):2007.
7. Windecker S, Kolh P, Alfonso F, et al. 2014 ESC/EACTS Guidelines on myocardial revascularizationThe Task Force on Myocardial Revascularization of the European Society of Cardiology (ESC) and the European Association for Cardio-Thoracic Surgery (EACTS)Developed with the special contribution of the European Association of Percutaneous Cardiovascular Interventions (EAPCI). *European Heart Journal.* 2014;35(37):2541-2619.
8. Camenzind E. Do drug-eluting stent increase death? Paper presented at: European Society of Cardiology2006; Barcelona, Spain.
9. Finn AV, Nakazawa G, Joner M, et al. Vascular Responses to Drug Eluting Stents. *Arteriosclerosis, Thrombosis, and Vascular Biology.* 2007;27(7):1500.
10. Byrne RA, Joner M, Kastrati A. Stent thrombosis and restenosis: what have we learned and where are we going? The Andreas Grüntzig Lecture ESC 2014. *European Heart Journal.* 2015;36(47):3320-3331.
11. Serruys PW, Luijten HE, Beatt KJ, et al. Incidence of restenosis after successful coronary angioplasty: a time-related phenomenon. A quantitative angiographic study in 342 consecutive patients at 1, 2, 3, and 4 months. *Circulation.* 1988;77(2):361.
12. Garg S, Serruys P. Biodegradable and non-biodegradable stents. *Minerva Cardioangiologica.* 2009;57(5):537-565.
13. Tamai H, Igaki K, Kyo E, et al. Initial and 6-Month Results of Biodegradable Poy-l-Lactic Acid Coronary Stents in Humans. *Circulation.* 2000;102(4):399.
14. Erbel R, Di Mario C, Bartunek J, et al. Temporary scaffolding of coronary arteries with bioabsorbable magnesium stents: a prospective, non-randomised multicentre trial. *The Lancet.*369(9576):1869-1875.
15. Pollman M. Engineering a bioresorbable stent: REVA programme update. *EuroIntervention.* 2009;5(F):F54-F57.

16. Ormiston JA, Webster MWI, Armstrong G. First-in-human implantation of a fully bioabsorbable drug-eluting stent: The BVS poly-L-lactic acid everolimus-eluting coronary stent. *Catheterization and Cardiovascular Interventions.* 2007;69(1):128-131.
17. Ormiston JA, Serruys PW, Regar E, et al. A bioabsorbable everolimus-eluting coronary stent system for patients with single de-novo coronary artery lesions (ABSORB): a prospective open-label trial. *The Lancet.*371(9616):899-907.
18. Serruys PW, Ormiston J, van Geuns R-J, et al. A Polylactide Bioresorbable Scaffold Eluting Everolimus for Treatment of Coronary Stenosis: 5-Year Follow-Up. *Journal of the American College of Cardiology.* 2016;67(7):766-776.
19. Morice M-C, Serruys PW, Sousa JE, et al. A Randomized Comparison of a Sirolimus-Eluting Stent with a Standard Stent for Coronary Revascularization. *New England Journal of Medicine.* 2002;346(23):1773-1780.
20. Kastrati A, Mehilli J, Pache J, et al. Analysis of 14 Trials Comparing Sirolimus-Eluting Stents with Bare-Metal Stents. *New England Journal of Medicine.* 2007;356(10):1030-1039.
21. Onuma Y, Piazza N, Ormiston JA, Serruys PW. Everolimus-eluting bioabsorbable stent – Abbot Vascular programme. *EuroIntervention.* 2009;5(F):F98-F102.
22. Oberhauser J, Hossainy S, Rapoza R. Design principles and performance of bioresorbable polymeric vascular scaffolds. *EuroIntervention.* 2009;5(F):F15-F22.
23. Onuma Y, Ormiston J, Serruys PW. Bioresorbable Scaffold Technologies. *Circulation Journal.* 2011;75(3):509-520.
24. Capodanno D, Gori T, Nef HM, et al. Percutaneous coronary intervention with everolimus-eluting bioresorbable vascular scaffolds in routine clinical practice: early and midterm outcomes from the European multicentre GHOST-EU registry. *EuroIntervention.* 2015;10(10):1144-1153.
25. Felix CM, Fam JM, Diletti R, et al. Mid- to Long-Term Clinical Outcomes of Patients Treated With the Everolimus-Eluting Bioresorbable Vascular Scaffold: The BVS Expand Registry. *JACC: Cardiovascular Interventions.* 2016;9(16):1652-1663.
26. Baumbach A, Zaman A, West NEJ, et al. Acute and one-year clinical outcomes following implantation of bioresorbable vascular scaffolds: the ABSORB UK Registry. *EuroIntervention.* 2018;13(13):1554-1560.
27. Puricel S, Cuculi F, Weissner M, et al. Bioresorbable Coronary Scaffold Thrombosis: Multicenter Comprehensive Analysis of Clinical Presentation, Mechanisms, and Predictors. *Journal of the American College of Cardiology.* 2016;67(8):921-931.
28. Medina A, Suárez de Lezo J, Pan M. A New Classification of Coronary Bifurcation Lesions. *Revista Española de Cardiología (English Edition).* 2006;59(02):183-183.
29. Steigen TK, Maeng M, Wiseth R, et al. Randomized Study on Simple Versus Complex Stenting of Coronary Artery Bifurcation Lesions. *Circulation.* 2006;114(18):1955.

30. Sheiban I, Albiero R, Marsico F, et al. Immediate and long-term results of "T" stenting for bifurcation coronary lesions. *The American Journal of Cardiology.* 2000;85(9):1141-1144.
31. Chevalier B, Glatt B, Royer T, Guyon P. Placement of coronary stents in bifurcation lesions by the "culotte" technique. *The American Journal of Cardiology.* 1998;82(8):943-949.
32. Chen S-L, Santoso T, Zhang J-J, et al. A Randomized Clinical Study Comparing Double Kissing Crush With Provisional Stenting for Treatment of Coronary Bifurcation Lesions: Results From the DKCRUSH-II (Double Kissing Crush versus Provisional Stenting Technique for Treatment of Coronary Bifurcation Lesions) Trial. *Journal of the American College of Cardiology.* 2011;57(8):914-920.
33. Lefèvre T, Darremont O, Albiero R. Provisional side branch stenting for the treatment of bifurcation lesions. *EuroIntervention.* 2011;6(J):J65-J71.
34. Louvard Y, Thomas M, Dzavik V, et al. Classification of coronary artery bifurcation lesions and treatments: Time for a consensus! *Catheterization and Cardiovascular Interventions.* 2007;71(2):175-183.
35. Al Suwaidi J, Berger PB, Rihal CS, et al. Immediate and long-term outcome of intracoronary stent implantation for true bifurcation lesions. *Journal of the American College of Cardiology.* 2000;35(4):929-936.
36. Nairooz R, Saad M, Elgendy IY, et al. Long-term outcomes of provisional stenting compared with a two-stent strategy for bifurcation lesions: a meta-analysis of randomised trials. *Heart.* 2017;103(18):1427.
37. Behan MW, Holm NR, Curzen NP, et al. Simple or complex stenting for bifurcation coronary lesions: a patient-level pooled-analysis of the Nordic Bifurcation Study and the British Bifurcation Coronary Study. *Circ Cardiovasc Interv.* 2011;4(1):57-64.
38. Ormiston JA, Webber B, Ubod B, Webster MWI, White JM. Absorb everolimus-eluting bioresorbable scaffolds in coronary bifurcations: a bench study of deployment, side branch dilatation and post-dilatation strategies. *EuroIntervention.* 2015;10(10):1169-1177.
39. Džavík V, Colombo A. The absorb bioresorbable vascular scaffold in coronary bifurcations: insights from bench testing. *JACC Cardiovasc Interv.* 2014;7(1):81-88.
40. Hildick-Smith D, de Belder AJ, Cooter N, et al. Randomized Trial of Simple Versus Complex Drug-Eluting Stenting for Bifurcation Lesions. *Circulation.* 2010;121(10):1235.
41. Toyota T, Morimoto T, Shiomi H, et al. Very Late Scaffold Thrombosis of Bioresorbable Vascular Scaffold: Systematic Review and a Meta-Analysis. *JACC: Cardiovascular Interventions.* 2017;10(1):27-37.
42. Kawamoto H, Latib A, Ruparelia N, et al. Clinical outcomes following bioresorbable scaffold implantation for bifurcation lesions: Overall outcomes and comparison between provisional and planned double stenting strategy. *Catheterization and Cardiovascular Interventions.* 2015;86(4):644-652.
43. De Paolis M, Felix C, van Ditzhuijzen N, et al. Everolimus-eluting bioresorbable vascular scaffolds implanted in coronary bifurcation lesions. *International Journal of Cardiology.*221:656-664.
44. Suarez dJ, Pedro M, Manuel P, et al. Bioresorbable Vascular Scaffold for the Treatment of Coronary Bifurcation Lesions: Immediate Results and 1-year Follow-up. *Revista Espanola de Cardiologica.* 2016;69(6):554.

45. Wiebe J, Dörr O, Bauer T, et al. Everolimus-eluting bioresorbable scaffold implantation for the treatment of bifurcation lesions — Implications from early clinical experience during daily practice. *Cardiovascular Revascularization Medicine.*17(5):313-317.
46. Naganuma T, Colombo A, Lesiak M, et al. Bioresorbable vascular scaffold use for coronary bifurcation lesions: A substudy from GHOST EU registry. *Catheterization and Cardiovascular Interventions.* 2016:n/a-n/a.
47. Tanaka A, Jabbour RJ, Kawamoto H, et al. Preliminary Report of Clinical Outcomes After Single Crossover Bioresorbable Scaffold Implantation Without Routine Side Branch Strut Dilation. *Catheterization and Cardiovascular Interventions.* 2016;88(6):865-870.
48. Maciej L. Poznan BRS registry: Long-term clinical outcome. Paper presented at: European Bifurcation Club2016; Rotterdam.
49. Alessio LM. BRS in bifurcations: mid and long-term clinical outcomes GHOST Ferrarotto Registry. Paper presented at: European Bifurcation Club2016; Rotterdam.
50. Kassab GS, Finet G. Anatomy and function relation in the coronary tree: from bifurcations to myocardial flow and mass. *EuroIntervention.* 2015;11(V):V13-V17.
51. Murray CD. The Physiological Principle of Minimum Work: I. The Vascular System and the Cost of Blood Volume. *Proceedings of the National Academy of Sciences of the United States of America.* 1926;12(3):207-214.
52. Finet G, Huo Y, Rioufol G, Ohayon J, Guerin P, Kassab GS. Structure-function relation in the coronary artery tree: from fluid dynamics to arterial bifurcations. *EuroIntervention.* 2011;6(J):J10-J15.
53. Koo B-K, de Bruyne B. FFR in bifurcation stenting: what have we learned? *EuroIntervention.* 2011;6(J):J94-J98.
54. Stankovic G, Darremont O, Ferenc M, et al. Percutaneous coronary intervention for bifurcation lesions: 2008 consensus document from the fourth meeting of the European Bifurcation Club. *EuroIntervention.* 2009;5(1):39-49 - DOI10.42.
55. Waksman R, Ormiston JA. *Bifurcation Stenting.* Wiley-Blackwell; 2012.
56. Forrester JS, Fishbein M, Helfant R, Fagin J. A paradigm for restenosis based on cell biology: Clues for the development of new preventive therapies. *Journal of the American College of Cardiology.* 1991;17(3):758-769.
57. Chaabane C, Otsuka F, Virmani R, Bochaton-Piallat M-L. Biological responses in stented arteries. *Cardiovascular Research.* 2013;99(2):353-363.
58. Brancati MF, Burzotta F, Trani C, Leonzi O, Cuccia C, Crea F. Coronary stents and vascular response to implantation: literature review. *Pragmatic and Observational Research.* 2017;8:137-148.
59. Joner M, Finn AV, Farb A, et al. Pathology of Drug-Eluting Stents in Humans. *Journal of the American College of Cardiology.* 2006;48(1):193.
60. Onuma Y, Serruys PW, Perkins LEL, et al. Intracoronary Optical Coherence Tomography and Histology at 1 Month and 2, 3, and 4 Years After Implantation of Everolimus-Eluting Bioresorbable Vascular Scaffolds in a Porcine Coronary Artery Model. *Circulation.* 2010;122(22):2288.
61. Serruys PW, Garcia-Garcia HM, Onuma Y. From metallic cages to transient bioresorbable scaffolds: change in paradigm of coronary revascularization in the upcoming decade? *European Heart Journal.* 2012;33(1):16-25.

62. Otsuka F, Pacheco E, Perkins LEL, et al. Long-Term Safety of an Everolimus-Eluting Bioresorbable Vascular Scaffold and the Cobalt-Chromium XIENCE V Stent in a Porcine Coronary Artery Model. *Circulation: Cardiovascular Interventions.* 2014;7(3):330.
63. Ormiston JA, Serruys PW, Onuma Y, et al. First Serial Assessment at 6 Months and 2 Years of the Second Generation of Absorb Everolimus-Eluting Bioresorbable Vascular Scaffold. *Circulation: Cardiovascular Interventions.* 2012;5(5):620.
64. Shin E-S, Garcia-Garcia HM, Garg S, et al. Assessment of the serial changes of vessel wall contents in atherosclerotic coronary lesion with bioresorbable everolimus-eluting vascular scaffolds using Shin's method: an IVUS study. *The International Journal of Cardiovascular Imaging.* 2011;27(7):931-937.
65. Giblett J, Brown AJ, Keevil H, Jaworski C, Hoole SP, West NEJ. Implantation of bioresorbable vascular scaffolds following acute coronary syndrome is associated with reduced early neointimal growth and strut coverage. *EuroIntervention.* 2016;12(6):724-733.
66. Sabaté M, Windecker S, Iñiguez A, et al. Everolimus-eluting bioresorbable stent vs. durable polymer everolimus-eluting metallic stent in patients with ST-segment elevation myocardial infarction: results of the randomized ABSORB ST-segment elevation myocardial infarction—TROFI II trial. *European Heart Journal.* 2016;37(3):229-240.
67. Brugaletta S, Heo JH, Garcia-Garcia HM, et al. Endothelial-dependent vasomotion in a coronary segment treated by ABSORB everolimus-eluting bioresorbable vascular scaffold system is related to plaque composition at the time of bioresorption of the polymer: indirect finding of vascular reparative therapy? *European Heart Journal.* 2012;33(11):1325-1333.
68. Kraak RP, Hassell MECJ, Grundeken MJ, et al. Initial experience and clinical evaluation of the Absorb bioresorbable vascular scaffold (BVS) in real-world practice: the AMC Single Centre Real World PCI Registry. *EuroIntervention.* 2015;10(10):1160-1168.
69. Sotomi Y, Suwannasom P, Serruys PW, Onuma Y. Possible mechanical causes of scaffold thrombosis: insights from case reports with intracoronary imaging. *EuroIntervention.* 2017;12(14):1747-1756.
70. Serruys PW, Suwannasom P, Nakatani S, Onuma Y. Snowshoe Versus Ice Skate for Scaffolding of Disrupted Vessel Wall. *JACC: Cardiovascular Interventions.* 2015;8(7):910.
71. Chan CY, Wu EB, Yan BP. Very Late Bioresorbable Scaffold Thrombosis Caused by Intraluminal Scaffold Dismantling. *JACC: Cardiovascular Interventions.* 2016;9(17):1844.
72. Mitomo S, Naganuma T, Fujino Y, et al. Bioresorbable Vascular Scaffolds for the Treatment of Chronic Total Occlusions. *Circulation: Cardiovascular Interventions.* 2017;10(1).
73. Wykrzykowska JJ, Kraak RP, Hofma SH, et al. Bioresorbable Scaffolds versus Metallic Stents in Routine PCI. *New England Journal of Medicine.* 2017;376(24):2319-2328.
74. Lafont A, Mennuni MG. Effect on death of scaffold thrombosis versus stent thrombosis. *The Lancet.* 2016;387(10034):2198.
75. Windecker S, Koskinas KC, Siontis GCM. Bioresorbable Scaffolds Versus Metallic Drug-Eluting Stents. *Journal of the American College of Cardiology.* 2015;66(21):2310-2314.

76. Serruys PW, Chevalier B, Sotomi Y, et al. Comparison of an everolimus-eluting bioresorbable scaffold with an everolimus-eluting metallic stent for the treatment of coronary artery stenosis (ABSORB II): a 3 year, randomised, controlled, single-blind, multicentre clinical trial. *The Lancet.*388(10059):2479-2491.
77. Longo G, Granata F, Capodanno D, et al. Anatomical features and management of bioresorbable vascular scaffolds failure: A case series from the GHOST registry. *Catheterization and Cardiovascular Interventions.* 2015;85(7):1150-1161.
78. Dommasch M, Langwieser N, Laugwitz K-L, Ibrahim T. Malabsorption of a Bioresorbable Vascular Scaffold System Leading to Very Late In-Scaffold Restenosis More Than 3.5 Years After Implantation. *JACC: Cardiovascular Interventions.* 2016;9(24):2571-2572.
79. Chavarría J, Suárez de Lezo J, Ojeda S, et al. Restenosis After Everolimus-eluting Vascular Scaffolding. Angiographic and Optical Coherence Tomography Characterization. *Revista Española de Cardiología (English Edition).* 2017;70(7):543-550.
80. Toutouzas K, Colombo A, Stefanadis C. Inflammation and restenosis after percutaneous coronary interventions. *European Heart Journal.* 2004;25(19):1679-1687.
81. Scheller J, Chalaris A, Schmidt-Arras D, Rose-John S. The pro- and anti-inflammatory properties of the cytokine interleukin-6. *Biochimica et Biophysica Acta (BBA) - Molecular Cell Research.* 2011;1813(5):878-888.
82. Mahinda YA, Wayne RL, Kirsty EW, Jose NVaRJH. Cardiovascular Biology of Interleukin-6. *Current Pharmaceutical Design.* 2009;15(15):1809-1821.
83. Danesh J, Kaptoge S, Mann AG, et al. Long-Term Interleukin-6 Levels and Subsequent Risk of Coronary Heart Disease: Two New Prospective Studies and a Systematic Review. *PLoS Medicine.* 2008;5(4):e78.
84. Fontes JA, Rose NR, Čihák ová D. The varying faces of IL-6: from cardiac protection to cardiac failure. *Cytokine.* 2015;74(1):62-68.
85. Hojo Y, Ikeda U, Katsuki T, et al. Interleukin 6 expression in coronary circulation after coronary angioplasty as a risk factor for restenosis. *Heart.* 2000;84(1):83.
86. Kazmierczak E, Grajek S, Kowal J, et al. Prognostic usefulness of IL-6 and VEGF for the occurrence of changes in the coronary arteries of patients with stable angina and implanted stents. In. Vol 18. Eur Rev Med Pharmacol Sci2014:2169-2175.
87. Zurakowski A, Wojakowski W, Dzeilski T, et al. Plasma levels of C-reactive protein and interleukin-10 predict late coronary in-stent restenosis 6 months after elective stenting. In. Vol 67. Kardiologica Polska2009:623-630.
88. Adukauskienė D, Čiginskienė A, Adukauskaitė A, Pentiokinienė D, Šlapikas R, Čeponienė I. Clinical relevance of high sensitivity C-reactive protein in cardiology. *Medicina.* 2016;52(1):1-10.
89. Ridker PM, Danielson E, Fonseca FAH, et al. Rosuvastatin to Prevent Vascular Events in Men and Women with Elevated C-Reactive Protein. *New England Journal of Medicine.* 2008;359(21):2195-2207.
90. Paffen E, deMaat MPM. C-reactive protein in atherosclerosis: A causal factor? *Cardiovascular Research.* 2006;71(1):30-39.

91. Shrivastava AK, Singh HV, Raizada A, Singh SK. C-reactive protein, inflammation and coronary heart disease. *The Egyptian Heart Journal.* 2015;67(2):89-97.
92. Mincu R-I, Jánosi RA, Vinereanu D, Rassaf T, Totzeck M. Preprocedural C-Reactive Protein Predicts Outcomes after Primary Percutaneous Coronary Intervention in Patients with ST-elevation Myocardial Infarction a systematic meta-analysis. *Scientific Reports.* 2017;7:41530.
93. Bibek S-b, Xie Y, Gao J-j, Wang Z, Wang J-f, Geng D-f. Role of Pre-procedural C-reactive Protein Level in the Prediction of Major Adverse Cardiac Events in Patients Undergoing Percutaneous Coronary Intervention: a Meta-analysisof Longitudinal Studies. *Inflammation.* 2015;38(1):159-169.
94. Hsieh IC, Chen C-C, Hsieh M-J, et al. Prognostic Impact of 9-Month High-Sensitivity C-Reactive Protein Levels on Long-Term Clinical Outcomes and In-Stent Restenosis in Patients at 9 Months after Drug-Eluting Stent Implantation. *PLoS ONE.* 2015;10(9):e0138512.
95. Lasave LI, Abizaid AAC, Paiva e Maia J, et al. Relationship Between Plasma C-Reactive Protein Level and Neointimal Hyperplasia Volume in Patients With Zotarolimus-Eluting Stents. Volumetric Analysis by Three-Dimensional Intracoronary Ultrasound. *Revista Española de Cardiología (English Edition).* 2007;60(09):923-931.
96. Kim B-K, Kim J-S, Oh C, et al. Impact of Preprocedural High-Sensitivity C-Reactive Protein Levels on Uncovered Stent Struts: An Optical Coherence Tomography Study After Drug-Eluting Stent Implantation. *Clinical Cardiology.* 2011;34(2):97-101.
97. Kuroda M, Otake H, Shinke T, et al. The impact of in-stent neoatherosclerosis on long-term clinical outcomes: an observational study from the Kobe University Hospital optical coherence tomography registry. *EuroIntervention.* 2016;12(11):e1366-e1374.
98. Niccoli G, Dato I, Imaeva AE, et al. Association between inflammatory biomarkers and in-stent restenosis tissue features: an Optical Coherence Tomography Study. *European Heart Journal - Cardiovascular Imaging.* 2014;15(8):917-925.
99. Niu J, Kolattukudy Pappachan E. Role of MCP-1 in cardiovascular disease: molecular mechanisms and clinical implications. *Clinical Science.* 2009;117(3):95.
100. Taubman MB, Rollins BJ, Poon M, et al. JE mRNA accumulates rapidly in aortic injury and in platelet-derived growth factor-stimulated vascular smooth muscle cells. *Circulation Research.* 1992;70(2):314.
101. Furukawa Y, Matsumori A, Ohashi N, et al. Anti–Monocyte Chemoattractant Protein-1/Monocyte Chemotactic and Activating Factor Antibody Inhibits Neointimal Hyperplasia in Injured Rat Carotid Arteries. *Circulation Research.* 1999;84(3):306.
102. Usui M, Egashira K, Ohtani K, et al. Anti-monocyte chemoattractant protein-1 gene therapy inhibits restenotic changes (neointimal hyperplasia) after balloon injury in rats and monkeys. *The FASEB Journal.* 2002.
103. Cipollone F, Marini M, Fazia M, et al. Elevated Circulating Levels of Monocyte Chemoattractant Protein-1 in Patients With Restenosis After Coronary Angioplasty. *Arteriosclerosis, Thrombosis, and Vascular Biology.* 2001;21(3):327-334.

104. Hokimoto S, Oike Y, Saito T, et al. Increased Expression of Monocyte Chemoattractant Protein-1 in Atherectomy Specimens From Patients With Restenosis After Percutaneous Transluminal Coronary Angioplasty. *Circulation Journal.* 2002;66(1):114-116.
105. Sako H, Miura S-i, Iwata A, et al. Changes in CCR2 Chemokine Receptor Expression and Plasma MCP-1 Concentration after the Implantation of Bare Metal Stents Versus Sirolimus-eluting Stents in Patients with Stable Angina. *Internal Medicine.* 2008;47(1):7-13.
106. Arefieva TI, Krasnikova TL, Potekhina AV, et al. Synthetic peptide fragment (65–76) of monocyte chemotactic protein-1 (MCP-1) inhibits MCP-1 binding to heparin and possesses anti-inflammatory activity in stable angina patients after coronary stenting. *Inflammation Research.* 2011;60(10):955.
107. Colombo A, Basavarajaiah S, Limbruno U, et al. A double-blind randomised study to evaluate the efficacy and safety of bindarit in preventing coronary stent restenosis. *EuroIntervention.* 2016;12(11):e1385-e1385.
108. Antoniades C, Bakogiannis C, Tousoulis D, Antonopoulos AS, Stefanadis C. The CD40/CD40 Ligand System: Linking Inflammation With Atherothrombosis. *Journal of the American College of Cardiology.* 2009;54(8):669-677.
109. Tousoulis D, Antoniades C, Nikolopoulou A, et al. Interaction between cytokines and sCD40L in patients with stable and unstable coronary syndromes. *European Journal of Clinical Investigation.* 2007;37(8):623-628.
110. Li G, Sanders JM, Bevard MH, et al. CD40 Ligand Promotes Mac-1 Expression, Leukocyte Recruitment, and Neointima Formation after Vascular Injury. *The American Journal of Pathology.* 2008;172(4):1141-1152.
111. Hristov M, Gümbel D, Lutgens E, Zernecke A, Weber C. Soluble CD40 Ligand Impairs the Function of Peripheral Blood Angiogenic Outgrowth Cells and Increases Neointimal Formation After Arterial Injury. *Circulation.* 2010.
112. Cipollone F, Ferri C, Desideri G, et al. Preprocedural Level of Soluble CD40L Is Predictive of Enhanced Inflammatory Response and Restenosis After Coronary Angioplasty. *Circulation.* 2003;108(22):2776-2782.
113. L'Allier PL, Tardif Jc Fau - Gregoire J, Gregoire J Fau - Joyal M, et al. Sustained elevation of serum CD40 ligand levels one month after coronary angioplasty predicts angiographic restenosis. *Canadian Journal of Cardiology.* 2005 May 1(0828-282X (Print)).
114. Türker S, Güneri S, Akdeniz B, et al. Usefulness of Preprocedural Soluble CD40 Ligand for Predicting Restenosis After Percutaneous Coronary Intervention in Patients With Stable Coronary Artery Disease. *The American Journal of Cardiology.* 2006;97(2):198-202.
115. Wexberg P, Jordanova N, Strehblow C, et al. Time course of prothrombotic and proinflammatory substance release after intracoronary stent implantation. *Thrombosis and Haemostasis.* 2008;99(4):739-748.
116. Westerhof N, Boer C, Lamberts RR, Sipkema P. Cross-Talk Between Cardiac Muscle and Coronary Vasculature. *Physiological Reviews.* 2006;86(4):1263.
117. Camici PG, d'Amati G, Rimoldi O. Coronary microvascular dysfunction: mechanisms and functional assessment. *Nat Rev Cardiol.* 2015;12(1):48-62.

118. Gould KL, Lipscomb K, Hamilton GW. Physiologic basis for assessing critical coronary stenosis. *The American Journal of Cardiology.* 1974;33(1):87-94.
119. Chareonthaitawee P, Kaufmann PA, Rimoldi O, Camici PG. Heterogeneity of resting and hyperemic myocardial blood flow in healthy humans. *Cardiovascular Research.* 2001;50(1):151-161.
120. Marzilli M, Capozza PG, Huqi A, Morrone D. Interactions between coronary stenoses and microcirculation. In: Escaned J, Serruys P, eds. *Coronary Stenosis: Imaging, structure and physiology.* 1st ed.
121. Sorop O, Merkus D, de Beer VJ, et al. Functional and Structural Adaptations of Coronary Microvessels Distal to a Chronic Coronary Artery Stenosis. *Circulation Research.* 2008;102(7):795-803.
122. Golino P, Piscione F, Willerson JT, et al. Divergent Effects of Serotonin on Coronary-Artery Dimensions and Blood Flow in Patients with Coronary Atherosclerosis and Control Patients. *New England Journal of Medicine.* 1991;324(10):641-648.
123. Sambuceti G, Marzilli M, Fedele S, Marini C, L'Abbate A. Paradoxical Increase in Microvascular Resistance During Tachycardia Downstream From a Severe Stenosis in Patients With Coronary Artery Disease: Reversal by Angioplasty. *Circulation.* 2001;103(19):2352-2360.
124. Marzilli M, Sambuceti G, Testa R, Fedele S. Platelet glycoprotein IIb/IIIa receptor blockade and coronary resistance in unstable angina. *Journal of the American College of Cardiology.* 2002;40(12):2102-2109.
125. Johnson NP, Kirkeeide RL, Gould KL. Is Discordance of Coronary Flow Reserve and Fractional Flow Reserve Due to Methodology or Clinically Relevant Coronary Pathophysiology? *JACC: Cardiovascular Imaging.* 2012;5(2):193-202.
126. Dupouy P, Aptecar E, Pelle G, et al. Early changes in coronary flow physiology after balloon angioplasty or stenting: A 24-hour Doppler flow velocity study. *Catheterization and Cardiovascular Interventions.* 2002;57(2):191-198.
127. Ng MKC, Yong ASC, Ho M, et al. The Index of Microcirculatory Resistance Predicts Myocardial Infarction Related to Percutaneous Coronary Intervention. *Circulation: Cardiovascular Interventions.* 2012;5(4):515.
128. Pijls NHJ, De Bruyne B. Coronary pressure measurement and fractional flow reserve. *Heart.* 1998;80(6):539.
129. Montalescot G, Sechtem U, Achenbach S, et al. 2013 ESC guidelines on the management of stable coronary artery diseaseThe Task Force on the management of stable coronary artery disease of the European Society of Cardiology. *European Heart Journal.* 2013;34(38):2949-3003.
130. Tonino PAL, De Bruyne B, Pijls NHJ, et al. Fractional Flow Reserve versus Angiography for Guiding Percutaneous Coronary Intervention. *New England Journal of Medicine.* 2009;360(3):213-224.
131. De Bruyne B, Pijls NHJ, Kalesan B, et al. Fractional Flow Reserve–Guided PCI versus Medical Therapy in Stable Coronary Disease. *New England Journal of Medicine.* 2012;367(11):991-1001.
132. AE SJ. Fundamental concepts of coronary physiology. In: Escaned J, Serruys P, eds. *Coronary Stenosis: Imaging, structure and physiology.*

133. Kern MJ, Lerman A, Bech J-W, et al. Physiological Assessment of Coronary Artery Disease in the Cardiac Catheterization Laboratory. *Circulation.* 2006;114(12):1321.
134. J. BC, Echavarria-Pinto M, Ryan N, Escaned J. Intracoronary thermodilution to assess coronary flow reserve and microcirculatory resistance. In: Escaned J, Serruys P, eds. *Coronary Stenosis: Imaging, structure and physiology.* 2nd ed.
135. Aarnoudse W, Fearon WF, Manoharan G, et al. Epicardial Stenosis Severity Does Not Affect Minimal Microcirculatory Resistance. *Circulation.* 2004;110(15):2137.
136. Fearon WF, Farouque HMO, Balsam LB, et al. Comparison of Coronary Thermodilution and Doppler Velocity for Assessing Coronary Flow Reserve. *Circulation.* 2003;108(18):2198.
137. Ng MKC, Yeung AC, Fearon WF. Invasive Assessment of the Coronary Microcirculation. *Circulation.* 2006;113(17):2054.
138. Melikian N, Vercauteren S, Fearon WF, et al. Quantitative assessment of coronary microvascular function in patients with and without epicardial atherosclerosis. *EuroIntervention.* 2010;5(8).
139. De Bruyne B, Oldroyd KG, Pijls NHJ. Microvascular (Dys)Function and Clinical Outcome in Stable Coronary Disease. *Journal of the American College of Cardiology.* 2016;67(10):1170.
140. Thygesen K, Alpert JS, Jaffe AS, Simoons ML, Chaitman BR, White HD. Third Universal Definition of Myocardial Infarction. *Circulation.* 2012;126(16):2020.
141. Cutlip DE, Windecker S, Mehran R, et al. Clinical End Points in Coronary Stent Trials. *Circulation.* 2007;115(17):2344.
142. Aarnoudse W, van den Berg P, van de Vosse F, et al. Myocardial resistance assessed by guidewire-based pressure-temperature measurement: In vitro validation. *Catheterization and Cardiovascular Interventions.* 2004;62(1):56-63.
143. Prati F, Regar E, Mintz GS, et al. Expert review document on methodology, terminology, and clinical applications of optical coherence tomography: physical principles, methodology of image acquisition, and clinical application for assessment of coronary arteries and atherosclerosis. *European Heart Journal.* 2010;31(4):401-415.
144. Brugaletta S, Gomez-Lara J, Diletti R, et al. Comparison of in vivo eccentricity and symmetry indices between metallic stents and bioresorbable vascular scaffolds: Insights from the ABSORB and SPIRIT trials. *Catheterization and Cardiovascular Interventions.* 2012;79(2):219-228.
145. Tearney GJ, Regar E, Akasaka T, et al. Consensus Standards for Acquisition, Measurement, and Reporting of Intravascular Optical Coherence Tomography Studies. *Journal of the American College of Cardiology.* 2012;59(12):1058-1072.
146. Nakatani S, Sotomi Y, Ishibashi Y, et al. Comparative analysis method of permanent metallic stents (XIENCE) and bioresorbable poly-L-lactic (PLLA) scaffolds (Absorb) on optical coherence tomography at baseline and follow-up. *EuroIntervention.* 2016;12(12):1498-1509.
147. Serruys PW, Onuma Y, Dudek D, et al. Evaluation of the Second Generation of a Bioresorbable Everolimus-Eluting Vascular Scaffold for the Treatment of De Novo Coronary Artery Stenosis12-Month Clinical and Imaging

Outcomes. *Journal of the American College of Cardiology.* 2011;58(15):1578-1588.
148. Gomez-Lara J, Radu M, Brugaletta S, et al. Serial analysis of the malapposed and uncovered struts of the new generation of everolimus-eluting bioresorbable scaffold with optical coherence tomography. *JACC Cardiovasc Interv.* 2011;4(9):992-1001.
149. Räber L, Mintz GS, Koskinas KC, et al. Clinical use of intracoronary imaging. Part 1: guidance and optimization of coronary interventions. An expert consensus document of the European Association of Percutaneous Cardiovascular Interventions. *European Heart Journal.* 2018;39(35):3281-3300.
150. Shibeshi SS, Collins WE. The Rheology of Blood Flow in a Branched Arterial System. *Applied rheology (Lappersdorf, Germany : Online).* 2005;15(6):398-405.
151. Davies JE, Whinnett ZI, Francis DP, et al. Evidence of a Dominant Backward-Propagating "Suction" Wave Responsible for Diastolic Coronary Filling in Humans, Attenuated in Left Ventricular Hypertrophy. *Circulation.* 2006;113(14):1768.
152. van der Giessen AG, Groen HC, Doriot P-A, et al. The influence of boundary conditions on wall shear stress distribution in patients specific coronary trees. *Journal of Biomechanics.*44(6):1089-1095.
153. Papafaklis MI, Bourantas CV, Theodorakis PE, et al. The Effect of Shear Stress on Neointimal Response Following Sirolimus- and Paclitaxel-Eluting Stent Implantation Compared With Bare-Metal Stents in Humans. *JACC: Cardiovascular Interventions.* 2010;3(11):1181-1189.
154. Sakamoto S, Takahashi S, Coskun AU, et al. Relation of Distribution of Coronary Blood Flow Volume to Coronary Artery Dominance. *American Journal of Cardiology.*111(10):1420-1424.
155. Brar SS, Gray WA, Dangas GD, Leon MB, Aharonian V. Bifurcation stenting with drug-eluting stents: a systematic review and meta-analysis of randomised trials. *EuroIntervention.* 2009;5(4):475-484.
156. Sawaya FJ, Lefèvre T, Chevalier B, et al. Contemporary Approach to Coronary Bifurcation Lesion Treatment. *JACC: Cardiovascular Interventions.* 2016;9(18):1861.
157. Hildick-Smith D, Lassen JF, Albiero R, et al. Consensus from the 5th European Bifurcation Club meeting. *EuroIntervention.* 2010;6(1):34-38.
158. Allahwala U, Cockburn J, Shaw E, Figtree G, Hansen PS, Bhindi R. Clinical utility of optical coherence tomography (OCT) in the optimisation of Absorb bioresorbable vascular scaffold deployment during percutaneous coronary intervention. *EuroIntervention.* 2015;10(10):1154-1159.
159. Caiazzo G, Longo G, Giavarini A, et al. Optical coherence tomography guidance for percutaneous coronary intervention with bioresorbable scaffolds. *International Journal of Cardiology.* 2016;221:352-358.
160. Sotomi Y, Onuma Y, Dijkstra J, et al. Impact of Implantation Technique and Plaque Morphology on Strut Embedment and Scaffold Expansion of Polylactide Bioresorbable Scaffold －Insights From ABSORB Japan Trial－. *Circulation Journal.* 2016;80(11):2317-2326.
161. Suwannasom P, Sotomi Y, Ishibashi Y, et al. The Impact of Post-Procedural Asymmetry, Expansion, and Eccentricity of Bioresorbable Everolimus-Eluting Scaffold and Metallic Everolimus-Eluting Stent on Clinical

Outcomes in the ABSORB II Trial. *JACC: Cardiovascular Interventions.* 2016;9(12):1231-1242.
162. Zhang D, Dou K. Coronary Bifurcation Intervention: What Role Do Bifurcation Angles Play? *Journal of Interventional Cardiology.* 2015;28(3):236-248.
163. Girasis C, Farooq V, Diletti R, et al. Impact of 3-Dimensional Bifurcation Angle on 5-Year Outcome of Patients After Percutaneous Coronary Intervention for Left Main Coronary Artery Disease. *JACC: Cardiovascular Interventions.* 2013;6(12):1250-1260.
164. Godino C, Al-Lamee R, Rosa CL, et al. Coronary Left Main and Non-Left Main Bifurcation Angles: How are the Angles Modified by Different Bifurcation Stenting Techniques? *Journal of Interventional Cardiology.* 2010;23(4):382-393.
165. Gomez-Lara J, Garcia-Garcia HM, Onuma Y, et al. A Comparison of the Conformability of Everolimus-Eluting Bioresorbable Vascular Scaffolds to Metal Platform Coronary Stents. *JACC: Cardiovascular Interventions.* 2010;3(11):1190-1198.
166. Gomez-Lara J, Diletti R, Brugaletta S, et al. Angiographic maximal luminal diameter and appropriate deployment of the everolimus-eluting bioresorbable vascular scaffold as assessed by optical coherence tomography: an ABSORB cohort B trial sub-study. *EuroIntervention.* 2012;8(2):214-224.
167. Liu X, Tsujita K, Maehara A, et al. Intravascular Ultrasound Assessment of the Incidence and Predictors of Edge Dissections After Drug-Eluting Stent Implantation. *JACC: Cardiovascular Interventions.* 2009;2(10):997.
168. Gonzalo N, Serruys PW, Okamura T, et al. Optical coherence tomography assessment of the acute effects of stent implantation on the vessel wall: a systematic quantitative approach. *Heart.* 2009;95(23):1913.
169. Nishida T, Colombo A, Briguori C, et al. Outcome of nonobstructive residual dissections detected by intravascular ultrasound following percutaneous coronary intervention. *American Journal of Cardiology.*89(11):1257-1262.
170. Cheneau E, Leborgne L, Mintz GS, et al. Predictors of Subacute Stent Thrombosis. *Circulation.* 2003;108(1):43.
171. Foin N, Gutiérrez-Chico JL, Nakatani S, et al. Incomplete Stent Apposition Causes High Shear Flow Disturbances and Delay in Neointimal Coverage as a Function of Strut to Wall Detachment Distance. *Circulation: Cardiovascular Interventions.* 2014;7(2):180.
172. Gutiérrez-Chico JL, Wykrzykowska J, Nüesch E, et al. Vascular Tissue Reaction to Acute Malapposition in Human Coronary Arteries. *Circulation: Cardiovascular Interventions.* 2012;5(1):20-29.
173. Attizzani GF, Capodanno D, Ohno Y, Tamburino C. Mechanisms, Pathophysiology, and Clinical Aspects of Incomplete Stent Apposition. *Journal of the American College of Cardiology.* 2014;63(14):1355-1367.
174. Muramatsu T, Onuma Y, García-García HM, et al. Incidence and short-term clinical outcomes of small side branch occlusion after implantation of an everolimus-eluting bioresorbable vascular scaffold: an interim report of 435 patients in the ABSORB-EXTEND single-arm trial in comparison with an everolimus-eluting metallic stent in the SPIRIT first and II trials. *JACC Cardiovasc Interv.* 2013;6(3):247-257.
175. Tanaka A, Jabbour RJ, Kawamoto H, et al. Incidence and significance of side branch occlusions following bioresorbable scaffold implantation for long left

anterior descending artery lesions. *International Journal of Cardiology.*222:674-675.
176. Suarez de Lezo J, Martin P, Pan M, et al. Bioresorbable Vascular Scaffold for the Treatment of Coronary Bifurcation Lesions: Immediate Results and 1-year Follow-up. *Rev Esp Cardiol (Engl Ed).* 2016;69(6):554-562.
177. Hahn J-Y, Chun WJ, Kim J-H, et al. Predictors and Outcomes of Side Branch Occlusion After Main Vessel Stenting in Coronary Bifurcation Lesions: Results From the COBIS II Registry (COronary BIfurcation Stenting). *Journal of the American College of Cardiology.* 2013;62(18):1654-1659.
178. Park JJ, Chun EJ, Cho Y-S, et al. Potential Predictors of Side-Branch Occlusion in Bifurcation Lesions after Percutaneous Coronary Intervention: A Coronary CT Angiography Study. *Radiology.* 2014;271(3):711-720.
179. Kini AS, Yoshimura T, Vengrenyuk Y, et al. Plaque Morphology Predictors of Side Branch Occlusion After Main Vessel Stenting in Coronary Bifurcation Lesions: Optical Coherence Tomography Imaging Study. *JACC: Cardiovascular Interventions.* 2016;9(8):862-865.
180. Koo B-K, Kang H-J, Youn T-J, et al. Physiologic Assessment of Jailed Side Branch Lesions Using Fractional Flow Reserve. *Journal of the American College of Cardiology.* 2005;46(4):633.
181. Pan M, Romero M, Ojeda S, et al. Fracture of Bioresorbable Vascular Scaffold After Side-Branch Balloon Dilation in Bifurcation Coronary Narrowings. *American Journal of Cardiology.*116(7):1045-1049.
182. Serruys PW, Chevalier B, Dudek D, et al. A bioresorbable everolimus-eluting scaffold versus a metallic everolimus-eluting stent for ischaemic heart disease caused by de-novo native coronary artery lesions (ABSORB II): an interim 1-year analysis of clinical and procedural secondary outcomes from a randomised controlled trial. *The Lancet.*385(9962):43-54.
183. Ellis SG, Kereiakes DJ, Metzger DC, et al. Everolimus-Eluting Bioresorbable Scaffolds for Coronary Artery Disease. *New England Journal of Medicine.* 2015;373(20):1905-1915.
184. Kimura T, Kozuma K, Tanabe K, et al. A randomized trial evaluating everolimus-eluting Absorb bioresorbable scaffolds vs. everolimus-eluting metallic stents in patients with coronary artery disease: ABSORB Japan. *European Heart Journal.* 2015;36(47):3332-3342.
185. Tanaka A, Latib A, Kawamoto H, et al. Clinical outcomes of a real-world cohort following bioresorbable vascular scaffold implantation utilising an optimised implantation strategy. *EuroIntervention.* 2017;12(14):1730-1737.
186. Seth A. My journey with BRS: Evolution in my technique - understanding results in my center with and without imaging. Paper presented at: Complex Cardiovascular Catheter Therapeutics2017; Orlando, USA.
187. Ellis SG, J. KD, Stone GW. Everolimus-eluting Bioresorbable Vascular Scaffolds in Patients with Coronary Artery Disease; ABSORB II Trial 2 year results. Paper presented at: ACC2017.
188. Karanasos A, Li Y, Tu S, et al. Is it safe to implant bioresorbable scaffolds in ostial side-branch lesions? Impact of 'neo-carina' formation on main-branch flow pattern. Longitudinal clinical observations. *Atherosclerosis.* 2015;238(1):22-25.
189. Onuma Y, Nakatani S, Grundeken M, Van Geuns R-J, Ormiston J, Serruys P. The serial follow-up of jailed side branches after implantation of bioresorbable scaffold - Insights from the ABSORB Cohort B trial using

three-dimensional optical coherence tomography. Paper presented at: European Bifurcation Club Meeting2014; France.
190. Yoshinobu O, Maik G, Yohei S, Nicolas F, John O, Patrick S. Serial evaluation of jailed side branches by BRS. Paper presented at: European Bifurcation Club2016; Rotterdam.
191. Bourantas CV, Papafaklis MI, Kotsia A, et al. Effect of the Endothelial Shear Stress Patterns on Neointimal Proliferation Following Drug-Eluting Bioresorbable Vascular Scaffold Implantation. *JACC: Cardiovascular Interventions.* 2014;7(3):315-324.
192. Onuma Y, Sotomi Y, Shiomi H, et al. Two-year clinical, angiographic, and serial optical coherence tomographic follow-up after implantation of an everolimus-eluting bioresorbable scaffold and an everolimus-eluting metallic stent: insights from the randomised ABSORB Japan trial. *EuroIntervention.* 2016;12(9):1090-1101.
193. Mintz GS. What to Do About Late Incomplete Stent Apposition? *Circulation.* 2007;115(18):2379.
194. Timmins LH, Miller MW, Clubb FJ, Moore JE. Increased arterial wall stress post-stenting leads to greater intimal thickening. *Laboratory investigation; a journal of technical methods and pathology.* 2011;91(6):955-967.
195. Serruys PW, Onuma Y, García-García HM, et al. Dynamics of vessel wall changes following the implantation of the Absorb everolimus-eluting bioresorbable vascular scaffold: a multi-imaging modality study at 6, 12, 24 and 36 months. *EuroIntervention.* 2014;9(11):1271-1284.
196. Giblett JP, Brown AJ, Hoole SP, West NEJ. Early disarticulation of a bioresorbable vascular scaffold: an underreported consequence of repeat imaging. *Cardiovascular Intervention and Therapeutics.* 2018;33(2):175-177.
197. Imai M, Kadota K, Goto T, et al. Incidence, Risk Factors, and Clinical Sequelae of Angiographic Peri-Stent Contrast Staining After Sirolimus-Eluting Stent Implantation. *Circulation.* 2011.
198. Virmani R, Guagliumi G, Farb A, et al. Localized Hypersensitivity and Late Coronary Thrombosis Secondary to a Sirolimus-Eluting Stent: Should We Be Cautious? *Circulation.* 2004.
199. Radu MD, Räber L, Kalesan B, et al. Coronary evaginations are associated with positive vessel remodelling and are nearly absent following implantation of newer-generation drug-eluting stents: an optical coherence tomography and intravascular ultrasound study. *European Heart Journal.* 2014;35(12):795-807.
200. Gori T, Jansen T, Weissner M, et al. Coronary evaginations and peri-scaffold aneurysms following implantation of bioresorbable scaffolds: incidence, outcome, and optical coherence tomography analysis of possible mechanisms. *European Heart Journal.* 2016;37(26):2040-2049.
201. Meincke F, Reinholz C, Spangenberg T, et al. Coronary Artery Aneurysm After Bioresorbable Vascular Scaffold Implantation With Post-Dilation. *JACC: Cardiovascular Interventions.* 2017;10(1):96-97.
202. Aoki J, Kirtane A, Leon MB, Dangas G. Coronary Artery Aneurysms After Drug-Eluting Stent Implantation. *JACC: Cardiovascular Interventions.* 2008;1(1):14-21.

203. Radu MD, Pfenniger A, Räber L, et al. Flow disturbances in stent-related coronary evaginations: a computational fluid-dynamic simulation study. *EuroIntervention.* 2014;10(1):113-123.
204. Murai T, Lee T, Kanaji Y, et al. The influence of elective percutaneous coronary intervention on microvascular resistance: a serial assessment using the index of microcirculatory resistance. *American Journal of Physiology - Heart and Circulatory Physiology.* 2016;311(3):H520.
205. Murai T, Kanaji Y, Yonetsu T, et al. Preprocedural fractional flow reserve and microvascular resistance predict increased hyperaemic coronary flow after elective percutaneous coronary intervention. *Catheterization and Cardiovascular Interventions.* 2017;89(2):233-242.
206. Solberg OG, Ragnarsson A, Kvarsnes A, et al. Reference interval for the index of coronary microvascular resistance. *EuroIntervention.* 2014;9(9):1069-1075.
207. Stuijfzand WJ, Raijmakers PG, Driessen RS, et al. Evaluation of myocardial blood flow and coronary flow reserve after implantation of a bioresorbable vascular scaffold versus metal drug-eluting stent: an interim one-month analysis of the VANISH trial. *EuroIntervention.* 2016;12(5):e584-e594.
208. Hoole S, Brown A, McCormick L, West N. Implantation of bioabsorbable vascular scaffolds improve the myocardial index of microcirculatory resistance. *Journal of the American College of Cardiology.* 2014;63(12):A1885.
209. Cuisset T, Hamilos M, Melikian N, et al. Direct Stenting for Stable Angina Pectoris Is Associated With Reduced Periprocedural Microcirculatory Injury Compared With Stenting After Pre-Dilation. *Journal of the American College of Cardiology.* 2008;51(11):1060-1065.
210. Sambuceti G, Marzilli M, Mari A, et al. Coronary microcirculatory vasoconstriction is heterogeneously distributed in acutely ischemic myocardium. *American Journal of Physiology - Heart and Circulatory Physiology.* 2005;288(5):H2298.
211. van de Hoef TP, van Lavieren MA, Damman P, et al. Physiological Basis and Long-Term Clinical Outcome of Discordance Between Fractional Flow Reserve and Coronary Flow Velocity Reserve in Coronary Stenoses of Intermediate Severity. *Circulation: Cardiovascular Interventions.* 2014;7(3):301.
212. Uren NG, Crake T, Lefroy DC, De Silva R, Davies GJ, Maseri A. Delayed recovery of coronary resistive vessel function after coronary angioplasty. *Journal of the American College of Cardiology.* 1993;21(3):612-621.
213. Fujii K, Kawasaki D, Oka K, et al. The Impact of Pravastatin Pre-Treatment on Periprocedural Microcirculatory Damage in Patients Undergoing Percutaneous Coronary Intervention. *JACC: Cardiovascular Interventions.* 2011;4(5):513-520.
214. Mangiacapra F, Peace AJ, Di Serafino L, et al. Intracoronary Enalaprilat to Reduce Microvascular Damage During Percutaneous Coronary Intervention (ProMicro) Study. *Journal of the American College of Cardiology.* 2013;61(6):615.
215. De Bruyne B, Pijls NHJ, Smith L, Wievegg M, Heyndrickx GR. Coronary Thermodilution to Assess Flow Reserve. *Circulation.* 2001;104(17):2003.
216. Farb A, Kolodgie FD, Hwang J-Y, et al. Extracellular Matrix Changes in Stented Human Coronary Arteries. *Circulation.* 2004;110(8):940.

217. Finn AV, Nakazawa G, Kolodgie FD, Virmani R. Temporal Course of Neointimal Formation After Drug-Eluting Stent Placement: Is Our Understanding of Restenosis Changing?⁎. *JACC: Cardiovascular Interventions.* 2009;2(4):300-302.
218. Huang S, Houghton PJ. Mechanisms of resistance to rapamycins. *Drug Resistance Updates.* 2001;4(6):378-391.
219. Ferrante G, Niccoli G, Biasucci LM, et al. Association between C-reactive protein and angiographic restenosis after bare metal stents: an updated and comprehensive meta-analysis of 2747 patients. *Cardiovascular Revascularization Medicine.* 2008;9(3):156-165.
220. Delhaye C, Maluenda G, Wakabayashi K, et al. Long-Term Prognostic Value of Preprocedural C-Reactive Protein After Drug-Eluting Stent Implantation. *The American Journal of Cardiology.* 2010;105(6):826-832.
221. Marketou M, Kochiadakis GE, Giaouzaki A, et al. Long-term serial changes in platelet activation indices following sirolimus elution and bare metal stent implantation in patients with stable coronary artery disease. *Hellenic Journal of Cardiology.*
222. Grube E, Sonoda S, Ikeno F, et al. Six- and Twelve-Month Results From First Human Experience Using Everolimus-Eluting Stents With Bioabsorbable Polymer. *Circulation.* 2004;109(18):2168.
223. Gao R, Yang Y, Han Y, et al. Bioresorbable Vascular Scaffolds Versus Metallic Stents in Patients With Coronary Artery Disease. *Journal of the American College of Cardiology.* 2015;66(21):2298-2309.
224. Gomma AH, Hirschfield GM, Gallimore JR, Lowe GDO, Pepys MB, Fox KM. Preprocedural inflammatory markers do not predict restenosis after successful coronary stenting. *American Heart Journal.* 2004;147(6):1071-1077.
225. Gremmel T, Frelinger AL, Michelson AD. Soluble CD40 Ligand in Aspirin-Treated Patients Undergoing Cardiac Catheterization. *PLoS ONE.* 2015;10(8):e0134599.
226. Vitiello D, Neagoe P-E, Sirois MG, White M. Effect of everolimus on the immunomodulation of the human neutrophil inflammatory response and activation. *Cell Mol Immunol.* 2015;12(1):40-52.
227. Arora S, Andreassen AK, Andersson B, et al. The Effect of Everolimus Initiation and Calcineurin Inhibitor Elimination on Cardiac Allograft Vasculopathy in De Novo Recipients: One-Year Results of a Scandinavian Randomized Trial. *American Journal of Transplantation.* 2015;15(7):1967-1975.
228. Chatzizisis YS, Coskun AU, Jonas M, Edelman ER, Feldman CL, Stone PH. Role of Endothelial Shear Stress in the Natural History of Coronary Atherosclerosis and Vascular Remodeling. *Journal of the American College of Cardiology.* 2007;49(25):2379-2393.
229. Wentzel JJ, Chatzizisis YS, Gijsen FJH, Giannoglou GD, Feldman CL, Stone PH. Endothelial shear stress in the evolution of coronary atherosclerotic plaque and vascular remodelling: current understanding and remaining questions. *Cardiovascular Research.* 2012;96(2):234-243.
230. Chien S. Mechanotransduction and endothelial cell homeostasis: the wisdom of the cell. *American Journal of Physiology - Heart and Circulatory Physiology.* 2007;292(3):H1209.

231. Toggweiler S, Urbanek N, Schoenenberger AW, Erne P. Analysis of coronary bifurcations by intravascular ultrasound and virtual histology. *Atherosclerosis.*212(2):524-527.
232. Oviedo C, Maehara A, Mintz GS, et al. Intravascular Ultrasound Classification of Plaque Distribution in Left Main Coronary Artery Bifurcations. *Circulation: Cardiovascular Interventions.* 2010;3(2):105.
233. Jeremias A, Huegel H, Lee DP, et al. Spatial orientation of atherosclerotic plaque in non-branching coronary artery segments. *Atherosclerosis.*152(1):209-215.
234. Gijsen FJH, Wentzel JJ, Thury A, et al. Strain distribution over plaques in human coronary arteries relates to shear stress. *American Journal of Physiology - Heart and Circulatory Physiology.* 2008;295(4):H1608.
235. Fukumoto Y, Hiro T, Fujii T, et al. Localized Elevation of Shear Stress Is Related to Coronary Plaque Rupture. *Journal of the American College of Cardiology.* 2008;51(6):645-650.
236. Wentzel JJ, M. Whelan D, van der Giessen WJ, et al. Coronary stent implantation changes 3-D vessel geometry and 3-D shear stress distribution. *Journal of Biomechanics.*33(10):1287-1295.
237. Weissman NJ, Wilensky RL, Tanguay J-F, et al. Extent and distribution of in-stent intimal hyperplasia and edge effect in a non-radiation stent population. *American Journal of Cardiology.*88(3):248-252.
238. Gyöngyösi M, Yang P, Khorsand A, Glogar D. Longitudinal straightening effect of stents is an additional predictor for major adverse cardiac events. *Journal of the American College of Cardiology.* 2000;35(6):1580-1589.
239. Brugaletta S, Gogas BD, Garcia-Garcia HM, et al. Vascular Compliance Changes of the Coronary Vessel Wall After Bioresorbable Vascular Scaffold Implantation in the Treated and Adjacent Segments. *Circulation Journal.* 2012;76(7):1616-1623.
240. Koskinas KC, Chatzizisis YS, Antoniadis AP, Giannoglou GD. Role of endothelial shear stress in stent restenosis and thrombosis: pathophysiologic mechanisms and implications for clinical translation. *J Am Coll Cardiol.* 2012;59(15):1337-1349.
241. Sanchez O, Yahagi K, Mori H, et al. Percutaneous interventions in bifurcation stenosis: Pathological substrate and procedural guidance. In: Escaned J, Serruys P, eds. *Coronary stenosis textbook.*
242. Karanasos A, Schuurbiers JCH, Garcia-Garcia HM, et al. Association of wall shear stress with long-term vascular healing response following bioresorbable vascular scaffold implantation. *International Journal of Cardiology.*191:279-283.
243. Tenekecioglu E, Sotomi Y, Torii R, et al. Strut protrusion and shape impact on endothelial shear stress: insights from pre-clinical study comparing Mirage and Absorb bioresorbable scaffolds. *The International Journal of Cardiovascular Imaging.* 2017;33(9):1313-1322.
244. Gogas BD, Yang B, Piccinelli M, et al. Novel 3-Dimensional Vessel and Scaffold Reconstruction Methodology for the Assessment of Strut-Level Wall Shear Stress After Deployment of Bioresorbable Vascular Scaffolds From the ABSORB III Imaging Substudy. *JACC: Cardiovascular Interventions.* 2016;9(5):501-503.

245. Deplano V, Bertolotti C, Barragan P. Three-dimensional numerical simulations of physiological flows in a stented coronary bifurcation. *Medical and Biological Engineering and Computing.* 2004;42(5):650-659.
246. Williams AR, Koo B-K, Gundert TJ, Fitzgerald PJ, LaDisa JF. Local hemodynamic changes caused by main branch stent implantation and subsequent virtual side branch balloon angioplasty in a representative coronary bifurcation. *Journal of Applied Physiology.* 2010;109(2):532.
247. Chiastra C, Morlacchi S, Pereira S, Dubini G, Migliavacca F. Computational fluid dynamics of stented coronary bifurcations studied with a hybrid discretization method. *European Journal of Mechanics - B/Fluids.* 2012;35:76-84.
248. Katritsis DG, Theodorakakos A, Pantos I, Gavaises M, Karcanias N, Efstathopoulos EP. Flow Patterns at Stented Coronary Bifurcations. *Circulation: Cardiovascular Interventions.* 2012;5(4):530.
249. Mortier P, Wentzel JJ, De Santis G, et al. Patient-specific computer modelling of coronary bifurcation stenting: the John Doe programme. *EuroIntervention.* 2015;11(V):V35-V39.
250. Boucher WI, Amara R. *The Study of the future : an agenda for research.* [Washington]: [National Science Foundation] : For sale by the Supt. of Docs., U.S. G.P.O.; 1977.